กลไกการเร่งอนุภาคแบบฟันเลื่อยที่คลื่นกระแทกในสนามแม่เหล็กสุ่ม

นายพีระ พงษ์กิติวณิชกุล

วิทยานิพนธ์นี้เป็นส่วนหนึ่งของการศึกษาตามหลักสูตรปริญญาวิทยาศาสตรมหาบัณฑิต
สาขาวิชาฟิสิกส์ ภาควิชาฟิสิกส์
คณะวิทยาศาสตร์ จุฬาลงกรณ์มหาวิทยาลัย
ปีการศึกษา 2547
ISBN 974-17-6897-4

SAWTOOTH MECHANISM OF PARTICLE ACCELERATION AT SHOCKS IN RANDOM MAGNETIC FIELDS

Mr. Peera Pongkitiwanichkul

A Thesis Submitted in Partial Fulfillment of the Requirements
for the Degree of Master of Science in Physics

Department of Physics
Faculty of Science
Chulalongkorn University

Academic Year 2004

ISBN 974-17-6897-4

Thesis Title	Sawtooth Mechanism of Particle Acceleration at Shocks in Random Magnetic Fields
By	Peera Pongkitiwanichkul
Field of Study	Physics
Thesis Advisor	Rujikorn Dhanawittayapol, Ph.D.
Thesis Co-advisor	Associate Professor David Ruffolo, Ph.D.

Accepted by the Faculty of Science, Chulalongkorn University in Partial Fulfillment of the Requirements for the Master 's Degree

……..Dean of the Faculty of Science
(Professor Piamsak Menasveta, Ph.D.)

THESIS COMMITTEE

…….. Chairman
(Assistant Professor Pisistha Ratanavararaksa, Ph.D.)

……. Thesis Advisor
(Rujikorn Dhanawittayapol, Ph.D.)

…….. Thesis Co-advisor
(Associate Professor David Ruffolo, Ph.D.)

…….. Member
(Nuttakorn Thubthong, Ph.D.)

…….. Member
(Somrit Wongmanerod, Ph.D.)

พีระ พงษ์กิติวณิชกุล : กลไกการเร่งอนุภาคแบบฟันเลื่อยที่คลื่นกระแทกในสนามแม่เหล็กสุ่ม. (SAWTOOTH MECHANISM OF PARTICLE ACCELERATION AT SHOCKS IN RANDOM MAGNETIC FIELDS) อ. ที่ปรึกษา : อ.ดร.รุจิกร ธนวิทยาพล, อ.ที่ปรึกษาร่วม : รศ.ดร.เดวิด รูฟโฟโล 169 หน้า. ISBN 974-17-6897-4.

เนื่องจากความไม่ต่อเนื่องของสนามแม่เหล็กบริเวณคลื่นกระแทก ทำให้อนุภาคที่มีประจุที่ผ่านคลื่นกระแทกนั้นถูกเร่งให้มีพลังงานสูงขึ้น อนุภาคที่มีประจุจะเคลื่อนที่ตามเส้นสนามแม่เหล็กเป็นหลัก ถ้าเส้นสนามแม่เหล็กสุ่มในอวกาศข้ามคลื่นกระแทกไปหลายครั้งเหมือนกับฟันเลื่อย จะทำให้อนุภาคที่เคลื่อนตามเส้นสนามสุ่มนั้นพบกับคลื่นกระแทกหลายครั้งและถูกเร่งหลายครั้ง และเนื่องจากผลของการฟุ้งในมุมพิชทำให้อนุภาคสามารถพบคลื่นกระแทกได้มากกว่าจำนวนการตัดกันของเส้นสนามแม่เหล็กกับคลื่นกระแทก สถิติในการตัดกันของเส้นสนามแม่เหล็กสุ่มกับคลื่นกระแทกสามารถพัฒนาทฤษฎีกลไกการเร่งอนุภาคแบบฟันเลื่อยให้ได้อย่างสมบูรณ์ ซึ่งจะเป็นประโยชน์ในการอธิบายการเร่งอนุภาครังสีคอสมิกในหลายสถานการณ์ทางดาราศาสตร์

ภาควิชา..... ลายมือชื่อนิสิต.....
สาขาวิชา..... ลายมือชื่ออาจารย์ที่ปรึกษา.....
ปีการศึกษา 2547 ลายมือชื่ออาจารย์ที่ปรึกษาร่วม.....

4572424923 : MAJOR PHYSICS

KEY WORDS: ASTROPHYSICS / COSMIC RAYS / PARTICLE ACCELERATION / TURBULENCE / SHOCKS

PEERA PONGKITIWANICHKUL : SAWTOOTH MECHANISM OF PARTICLE ACCELERATION AT SHOCKS IN RANDOM MAGNETIC FIELDS. THESIS ADVISOR : RUJIKORN DHANAWITTAYAPOL, Ph.D. , THESIS CO-ADVISOR : ASSOC. PROF. DAVID RUFFOLO, Ph.D. , 169 pp. ISBN 974-17-6897-4.

Since there is a discontinuity in the magnetic field and plasma speed at the shock in a space plasma, the charged particles that pass the shock are accelerated and gain energy. The charged particles are known to move mainly along magnetic field lines. If the magnetic field line crosses the shock many times like a sawtooth, the particles that follow the magnetic field lines can cross the shock many times. The diffusion in pitch angle can cause the particles to encounter the shock several times at each magnetic field-shock crossing. The statistics of the magnetic field–shock crossings can be used to develop the sawtooth mechanism of particle acceleration, including the resulting particle spectrum.

Department.....Student's signature.....

Field of study.....Advisor's signature.....

Academic year 2004 Co-advisor's signature.....

Acknowledgements

Foremost, I would really like to express my gratitude to my co-advisor, Assoc. Prof. Dr. David Ruffolo, very much for his attention, guidance, and encouragement throughout the time I was his advisee. Apart from physics knowledge I have learnt from him, I have also developed myself a great deal, such as extending my vision, improving thinking skills, improving working skills, and developing English skills by both directly and indirectly learning from him.

I am also grateful to the thesis advisor, Dr. Rujikorn Dhanawittayapol, and thesis committee, Assist. Prof. Dr.Pisistha Ratanavararaksa, Dr. Nuttakorn Thubthong, and Dr. Somrit Wongmanerod, for reading and offering suggestions for this thesis.

Furthermore, I would like to thank Miss Piyanate Chuychai for providing me as much help and guidance as she could, Mr. Paisan Tooprakai, and Miss Chanoknan Banglieng for computer-system administration, Mr. Chanruangrit Channok for his discussion on the shock acceleration, Mr. Nimit Kimpraphan for his discussion on the magnetic turbulence, Miss Kanokporn Leerungnavarat who also offered many suggestions to me.

Finally, I am extremely grateful to my father and my mother who are my inspiration and always support me to do good things. I am very proud to be their son and I hope to make them proud of me also; at least I have been trying.

This work was supported by the Thailand Research Fund.

Contents

Page

Page

List of Figures

Page

Page

Page

Page

Page

Page

Page

Page

Page

Page

Page

List of Tables

Page

Chapter 1
Introduction

1.1 Introduction

This chapter provides the overview of this thesis and its objectives, to help readers to understand this thesis more easily. The readers will also learn the purpose and scope of this work.

Cosmic rays are energetic particles or gamma rays from space. These particles can be accelerated at shocks. A shock, or a discontinuity in fluid parameters, appears when two fluids collide with a relative velocity greater the speed of sound. The acceleration of particles at a shock was first explained by Fermi (1958). The modern understanding is that collisions between the particles and the magnetic field irregularities keep the particles at the shock and assist the acceleration. The cause of acceleration is not only the collisions but also the drift motion of the particles along an electric field. The details of this process will be explained in chapter 2. At a nearly perpendicular shock, the drift motion of the particle yields a very large energy gain. In previous analytic theory work on the acceleration at a nearly perpendicular shock, the multiple magnetic field-shock crossing were not considered. We expect that these have a significant effect on the particle acceleration at the shock.

1.2 Objectives

• Develop the computer programs and methodology for tracing magnetic field lines.

• Study the effects of magnetic turbulence on the distribution of 1) the angle between the magnetic field and the shock normal at the crossing position, 2) the number of magnetic field-shock crossings per magnetic field line, and 3) the distance between two crossing positions when the mean magnetic field is nearly perpendicular to the shock normal.

• Study the effects of magnetic turbulence on particle acceleration at nearly perpendicular shocks.

1.3 Thesis Outline

In chapter 1, an introduction to and the objectives of this work are provided. Chapter 2 provides some background information about cosmic rays, shocks, shock acceleration, and magnetic turbulence. In chapter 3, the magnetic field model, the magnetic field line tracing method, and the model of shock acceleration are explained. In this chapter, we develop a new method for tracing magnetic field lines in two-component turbulence and a new model of shock acceleration at nearly perpendicular shocks. Chapter 4 will provide the statistics of magnetic field line-shock crossings. Chapter 5 will show the effects of non-turbulent and turbulent magnetic fields on charged particles. Chapter 6 will provide a summary and the conclusions of this work.

Chapter 2

Cosmic Rays and Shock Acceleration

2.1 Cosmic rays

Cosmic rays are energetic particles and gamma rays from space. The first discovery of cosmic rays was in 1912 when Victor Hess found the ionizing radiation to increase higher in the atmosphere. The conclusion of Hess's experiment is that the source of radiation is outside the earth. At that time, "cosmic rays" were defined as the extraterrestrial radiation, later identified as particles and gamma rays. From the 1930s to the 1950s, cosmic rays played an important role as a source of high energy particles for research when no high energy particle accelerators had been made. In the space age, a wider range of data are available because cosmic rays can be detected outside the Earth's atmosphere. We can measure their energy, intensity, direction, type of particle and time of arrival. Modern cosmic ray research is about where cosmic rays originate, how they gain high energies, what they tell us about the history of the universe, what are the components of galaxies, etc. Cosmic rays can be any particles, charged or neutral, and most of them that strike the Earth's atmosphere are protons. In fact, cosmic rays include all elements in the periodic table and electrons from space. Cosmic rays originate at the Sun, shocks, supernovae, stars, etc. The energy of cosmic rays varies from 10^5 to 10^{20} eV depending on their source. If cosmic rays originate within the solar system, their energy can be up to 10 GeV for some strong events

Sources	Species	Energy
Sun and Shocks	p, α, ^{12}c, ^{16}o, ... e, γ, μ	~ 100 keV up to 80 GeV
Jupiter	e	1 - 25 MeV
Termination Shock	p, α, ^{12}c, ^{16}o, ...	1 - 100 MeV
Our galaxy	p, α, ^{12}c, ^{16}o, ... e, γ	~ 100 MeV to 10^{19}eV
Other galaxies	p e	$< 10^{20}$ eV $< 10^{14}$ eV

Table 2.1: The sources of cosmic rays

at the Sun, and if any cosmic rays come from outside the solar system, their energy must be greater than about 100 MeV to come inward against the flow of the solar wind. There are many sources of cosmic rays as shown in Table 2.1.

Cosmic rays are separated into 3 types by their origin.

1. Solar energetic particles or SEP

The Sun is a source of cosmic rays. These cosmic rays can originate directly at the Sun from occasional solar storms, or from the interplanetary medium, where they are accelerated by the shock waves from solar storms. Solar energetic particles can be used to measure the elemental and composition of the Sun.

2. Galactic cosmic rays or GCR

These cosmic rays come from outside the solar system but generally from

within our Milky Way galaxy. GCRs are atomic nuclei without surrounding electrons because these electrons have been stripped away during passage through the galaxy. They have been accelerated to nearly the speed of light, probably by supernova remnants.

3. Anomalous cosmic rays or ACR

ACRs are mostly produced by neutral atoms in the interstellar medium which come into the heliosphere and become ionized by either solar UV radiation or by charge exchange with the solar wind. They are then picked up by the solar wind and carried back to the outer heliosphere. Then they are accelerated by the solar wind termination shock, and these so-called anomalous cosmic rays drift into the inner heliosphere as shown in Figure 2.1.

2.2 Spectrum of cosmic rays

We are interested in the spectrum of cosmic rays, especially the spectrum of ACRs, because this will relate to our work. The flux of cosmic rays per unit energy or cosmic ray energy spectra are known to have the power-law distributions over a wide range in energy as shown in Figure 2.2. Over such a range, the energy spectrum can be fit to

$$j(E) \propto E^{-\gamma_e}, \tag{2.1}$$

where for ionic species $j(E)$ is (particle flux)/(time $\cdot$ area $\cdot$ solid angle $\cdot$ kinetic energy/nucleon), and γ_e is a constant called the spectral index. The spectra can also be fit in terms of momentum as

$$j(p) \propto p^{-\gamma}, \tag{2.2}$$

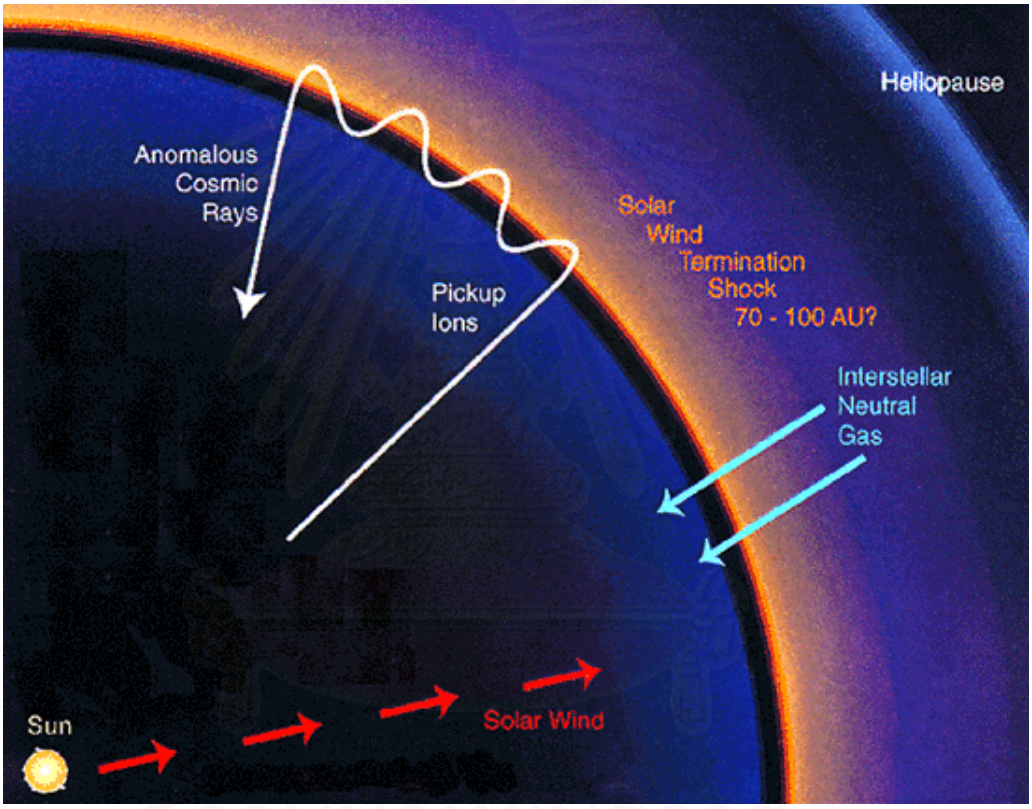

Figure 2.1: Neutral atoms from the interstellar medium are ionized and accelerated to become anomalous cosmic rays

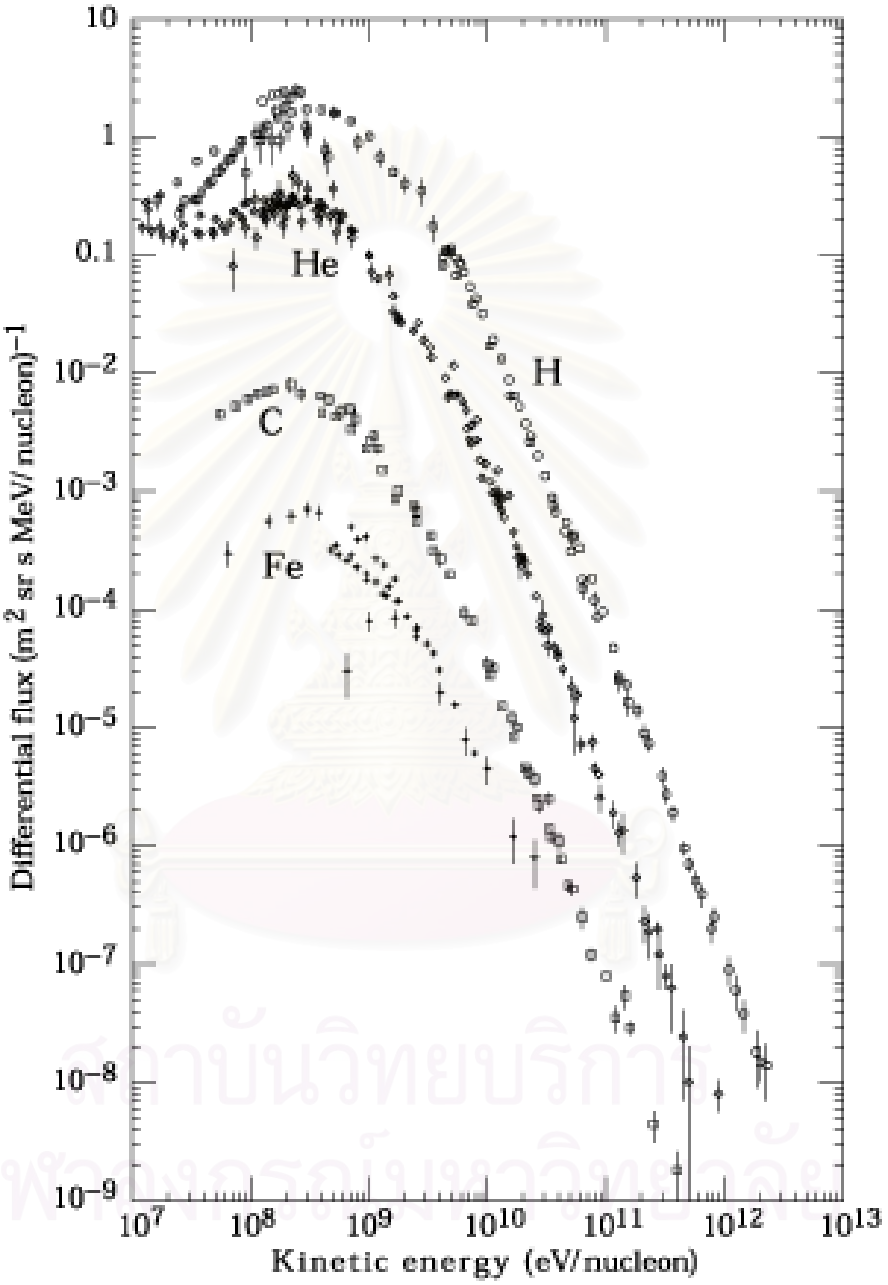

Figure 2.2: Cosmic ray spectra in the energy range from 10^7 eV to 10^{13} eV (Picture credit: Simpson 1983).

where $j(p)$ is (particle flux)/(time · area · solid angle · momentum/nucleon). For non-relativistic particles, $2\gamma_e = \gamma$ because $E \propto p^2$. If the particles have a very high energy, $E \propto p$ so $\gamma_e \approx \gamma$.

The galactic cosmic rays require an energy more than 10^8 eV to come into the solar system. The all-particle spectral index is not constant over the whole range of energy. From 10^8 eV to 10^{15} eV, γ_e is about 2.5-2.7. From 10^{15} eV to 10^{19} eV, γ_e is about 3.1. The change in spectral index at the energy of about 10^{15} eV is called the "knee." Beyond the energy of 10^{19} eV, the energy spectra become flatter. This change is called the "ankle." The particles below the ankle are thought to be produced inside the galaxy. The particles beyond the ankle are expected to be produced outside the galaxy. We believe that shocks at supernova remnants can accelerate cosmic rays up to the energy of 10^{14} eV, but the origin of cosmic rays above the knee is still uncertain. Figure 2.3 shows the "knee" and "ankle" in the cosmic ray energy spectrum.

The Sun also releases many types of particles in the solar wind, solar flares, and coronal mass ejections. The solar wind is a stream of particles from the Sun to all directions with an average speed of about 400 km/s. The source of the solar wind is the Sun's corona. The type of solar wind called fast solar wind has a speed of about 800 km/s. Fast solar wind flows from coronal hole regions. The other portion is called slow solar wind which has a typical speed of 300 km/s. The particles in the solar wind are called thermal particles because they have a Maxwellian velocity distribution. They are different from cosmic rays (energetic, non-thermal particles) which have much higher energies and typically not power law spectra. Figure 2.4 shows the total time-integrated intensity of oxygen from ≈300 eV to ≈300 MeV. This figure also shows the spectrum of ACRs as a "bump"

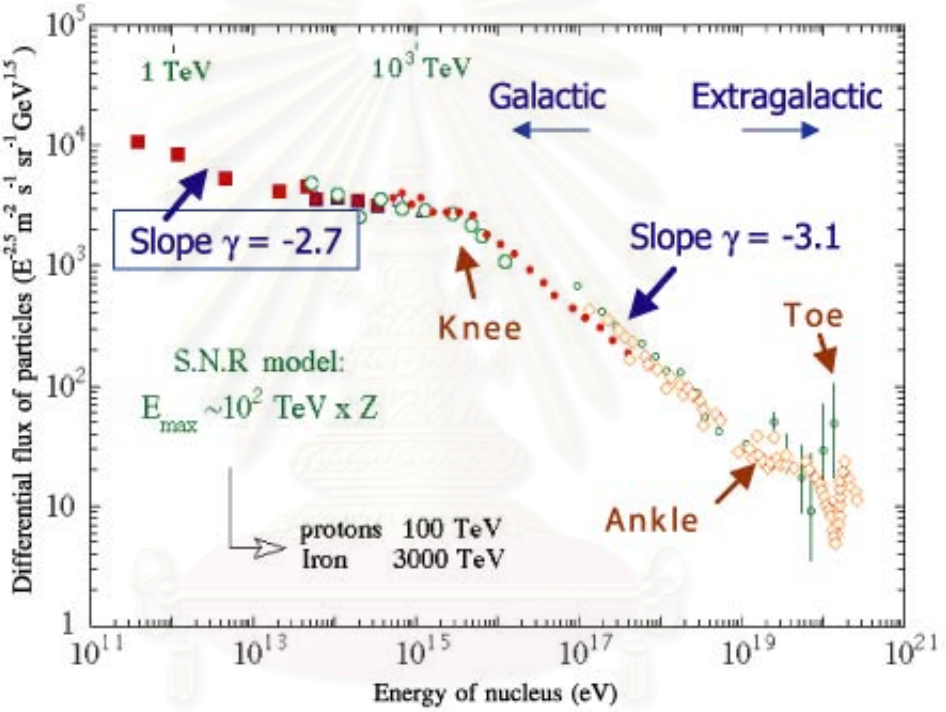

Figure 2.3: Cosmic ray spectrum in the energy range from 10^{11} eV to 10^{21} eV. Note that the spectrum is multiplied by $E^{2.5}$ to highlight spectral changes (Picture credit://seminar.kek.jp).

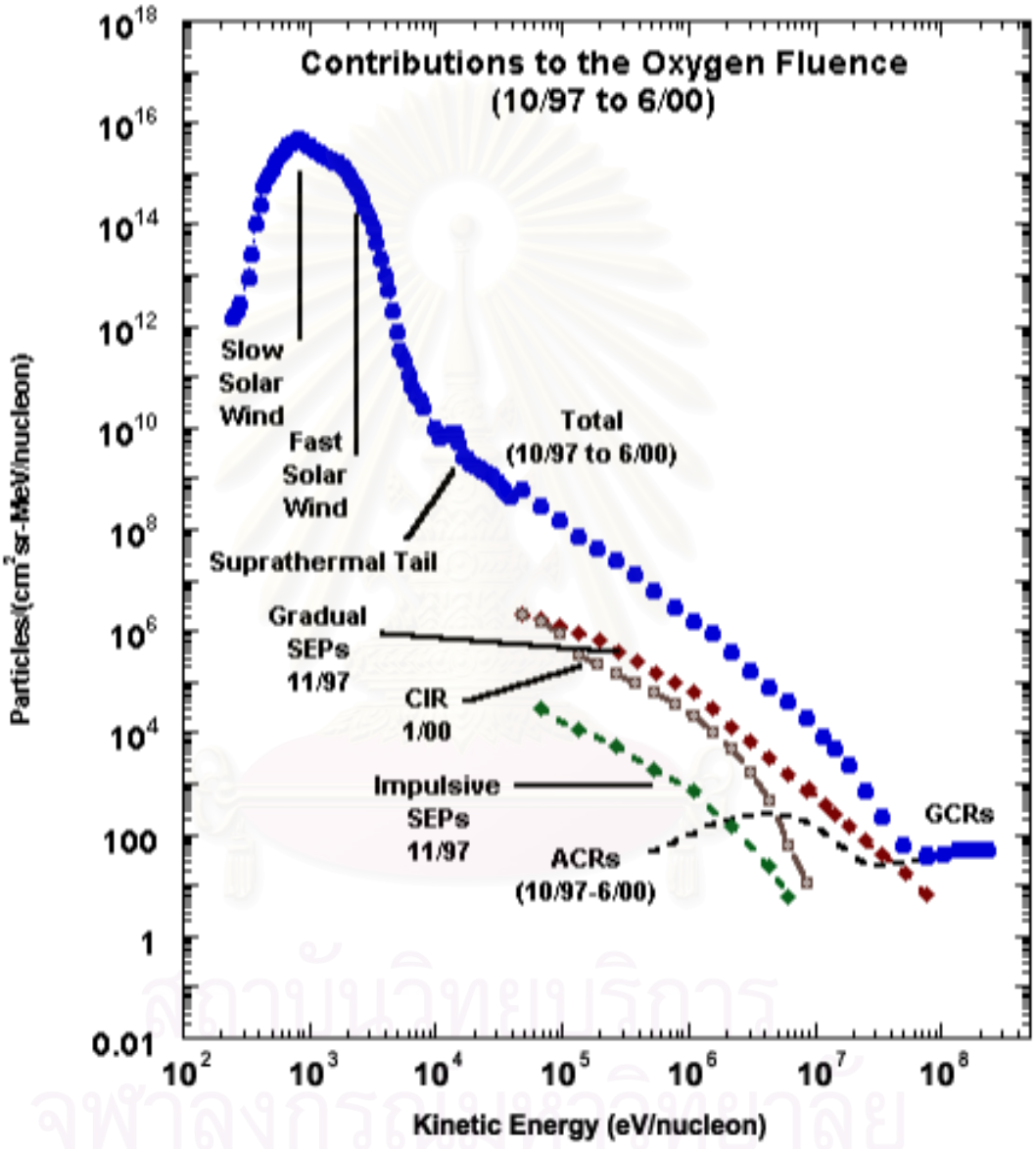

Figure 2.4: Time-integrated fluence of oxygen from ≈ 300 eV/nucleon to 300 MeV/nucleon during 10/97 to 6/00 (Picture credit: Mewaldt et al. 2001).

spectrum.

2.3 Conservation of magnetic flux and the interplanetary magnetic field

The behaviour of a magnetic field is important to the acceleration of cosmic rays at shocks because charged particles gyrate and move along the magnetic field. Different types of magnetic fields cause different types of motion of charged particles. Now we describe the shape of magnetic field lines inside the solar system. The magnetic flux is defined as

$$\Phi = \int \vec{B} \cdot d\vec{s}, \tag{2.3}$$

where $d\vec{s}$ is a vector element of area. If this area moves with the plasma velocity $\vec{U}$, the magnetic flux through this area is constant or $d\Phi/dt = 0$. To prove this, Figure 2.5 shows the change of the area with t. At time $t + \Delta t$, the flux through area B is the sum of the flux through area A and area C or

$$\Phi_A = \Phi_B - \Phi_C. \tag{2.4}$$

The total change of the magnetic flux across this area moving with the fluid over time Δt is $\Delta\Phi = \Phi_A^{t+\Delta t} - \Phi_B^t$. We can use (2.4) to write

$$\begin{aligned} \Delta\Phi &= \Phi_B^{t+\Delta t} - \Phi_B^t - \Phi_C^{t+\Delta t} \\ &= \int_B \left(\vec{B}(t+\Delta t) - \vec{B(t)}\right) \cdot d\vec{s} - \int_C \vec{B}(t+\Delta t) \cdot d\vec{s} \end{aligned} \tag{2.5}$$

At area C, $d\vec{s} = -\vec{U}\Delta t \times \vec{dl}$. Stokes's theorem and Faraday's law will be applied, and the electric field in the fixed frame is $-\vec{U} \times \vec{B}$, since there is no electric field

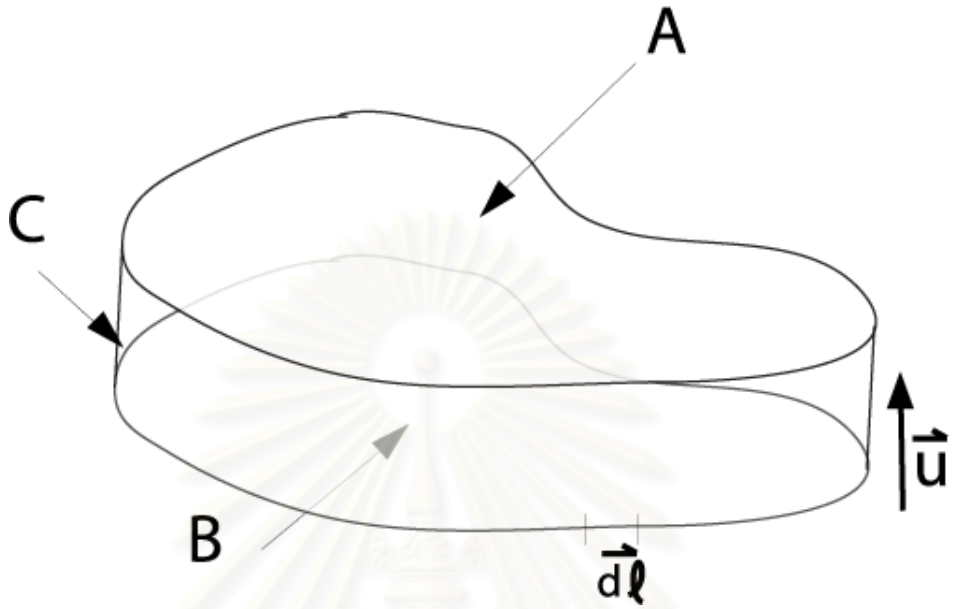

Figure 2.5: Schematic to explain the conservation of magnetic field flux. Area A, the area at time $t + \Delta t$; Area B, the area at time t; Area C, the area used to create a closed volume.

in the plasma rest frame (an electrical conductor). Then as $\Delta t \to 0$, we find

$$\begin{aligned} \frac{d\Phi}{dt} &= \int \frac{\partial \vec{B}}{\partial t} \cdot d\vec{s} + \int \vec{B} \cdot \left(\vec{U} \times d\vec{l}\right) \\ &= \int \nabla \times (\vec{U} \times \vec{B}) \cdot d\vec{s} + \int \vec{B} \cdot \left(\vec{U} \times d\vec{l}\right) \\ &= \int \left(\vec{U} \times \vec{B}\right) \cdot d\vec{l} + \int \vec{B} \cdot \left(\vec{U} \times d\vec{l}\right) \\ &= 0. \end{aligned} \tag{2.6}$$

Therefore the magnetic flux through any closed contour that moves with the plasma is constant.

Now we know the magnetic flux is constant in the plasma frame. The solar wind is also a plasma so the magnetic flux in the solar wind is constant. In other words, the magnetic field can be dragged out by the plasma. Two different volumes of the solar wind released from the same area on the Sun will define the

same magnetic field line. The solar wind moves outward from the Sun in the radial direction and drags out the magnetic field lines. The rotation of the Sun causes the curved shape of magnetic field lines (Parker 1958) as shown in Figure 2.6.

Now we will roughly calculate the shape of the magnetic field line at the solar wind termination shock, or the discontinuity of fluid parameters at the edge of the solar system. This shock occurs since the relative speed of the solar wind and the interstellar medium is greater than the speed of sound. We believe that the solar wind termination shock forms a spherical shape because the solar wind velocity is in the radial direction from the Sun. Let V_s be the speed of the solar wind, and ω be the angular velocity of the Sun. The initial solar wind velocity is $V_s\hat{r} + (\omega r_0)\hat{\phi}$ at the "corotation radius" r_0, where the plasma stops rotating rigidly with the Sun. After released from the Sun, the solar wind has $\vec{V} = V_s\hat{r} - \omega(r - r_0)\hat{\phi}$ in the frame corolating with the Sun. In this frame, the direction of the solar wind velocity is the direction of the magnetic field. The angle Ψ between $\hat{r}$ and the magnetic field can be written as

$$\tan\Psi = \frac{\omega(r - r_0)}{V_s}, \tag{2.7}$$

where ω is $2\pi/T$ for a solar rotation period T of 24.92 days. Figure 2.6 shows the interplanetary magnetic field dragged out from the Sun. At the solar wind termination shock, r is about 110 AU (M. Banaszkiewicz and J. Ziemkiewicz 1997), the shock normal is approximately along $\hat{r}$, and V_s, the solar wind speed, is about 400 km/s. Since $r_0 \ll r$, we have $\Psi \approx 89°$. The magnetic field at the solar wind termination shock is nearly perpendicular to the shock normal.

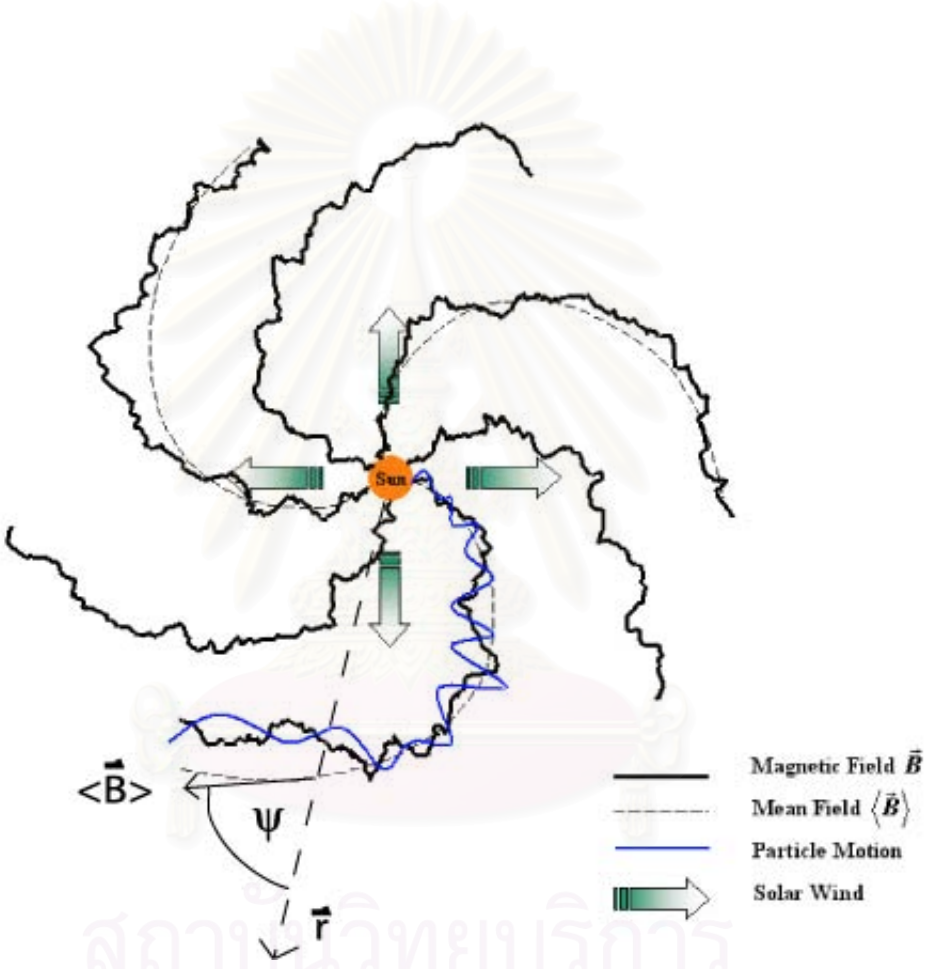

Figure 2.6: The interplanetary magnetic field and the angle ψ.

2.4 Charged particle motion in various types of magnetic fields

We are interested in cosmic rays that are charged particles. Since there is no electric field in the plasma frame, the cosmic ray motion is mainly determined by interaction with the magnetic field. To understand the accelation of particles at shocks, we must understand the particles' motion in a magnetic field (Jackson 1975; Parks 1991).

2.4.1 Charged particle in a uniform, static magnetic field

The equation of motion of a charged particle in a uniform, static magnetic field is

$$\vec{F} = m\frac{d}{dt}(\vec{v}) = q(\vec{v} \times \vec{B}), \tag{2.8}$$

where m is the rest mass of the charged particle, its charge is q, $\vec{v}$ is the particle's velocity, $\vec{B}$ is the magnetic field, and $\vec{F}$ is the force acting on the particle. Now equation 2.8 can be written as

$$\vec{F} = m\frac{d}{dt}\vec{v} = q(\vec{v} \times \vec{B}). \tag{2.9}$$

If we set the z direction to be the direction of the magnetic field, $\vec{B} = B\hat{z}$, the equation of motion becomes

$$\frac{d}{dt}v_x = \frac{q}{m}(v_y B) \tag{2.10}$$

$$\frac{d}{dt}v_y = -\frac{q}{m}(v_x B) \tag{2.11}$$

$$\frac{d}{dt}v_z = 0. \tag{2.12}$$

The solution of these equations is

$$v_x = v_\perp \cos(\omega t) \tag{2.13}$$

$$v_y = v_\perp \sin(\omega t) \tag{2.14}$$

$$v_z = v_\parallel, \tag{2.15}$$

where $\omega = qB/m$, and $v_\parallel$ and $v_\perp$ are constant. We know that $v_\parallel^2 + v_\perp^2 = v_0^2$, where v_0 is constant. Then we can write

$$v_\parallel = v_0 \cos\theta \tag{2.16}$$

$$v_\perp = v_0 \sin\theta \tag{2.17}$$

where θ is called the pitch angle. In this case, the pitch angle is constant.

This motion is called cyclotron motion or gyration. The perpendicular motion of a charged particle forms a circle. The angular frequency of the circular motion is called the gyrofrequency, and for non-relativistic particles

$$\omega = \frac{qB}{m}, \tag{2.18}$$

and the radius of the circle is called the gyroradius,

$$r_g = mv/qB. \tag{2.19}$$

The perpendicular motion makes a circulating current,

$$I = \frac{q^2 B}{2\pi m}. \tag{2.20}$$

The magnetic moment of this current is

$$\mu = I\pi r_g^2. \tag{2.21}$$

The magnetic moment can also be written in terms of the total magnetic flux within the circular path as

$$\mu = \frac{1}{2\pi}\frac{q^2}{m}\Phi, \tag{2.22}$$

where $\Phi = \pi r^2 B$. In terms of the kinetic energy of the particles moving in the direction perpendicular to B,

$$\mu = \frac{1}{2}\frac{mv_\perp^2}{B}. \tag{2.23}$$

This relation is a useful tool in the acceleration model. It will be considered again in the topic of the "adiabatic invariant" shortly.

2.4.2 Charged particle in a uniform electric field and magnetic field

Let a uniform electric field be written as $\vec{E} = \vec{E_{||}} + \vec{E_\perp}$, where $||$ and $\perp$ refer to directions parallel and perpendicular to $\vec{B}$. For convenience, we neglect the relativistic effect so the equations of motion are

$$\frac{d}{dt}mv_{||} = qE_{||} \tag{2.24}$$

$$\frac{d}{dt}m\vec{v_\perp} = q(\vec{E_\perp} + \vec{v_\perp} \times \vec{B}). \tag{2.25}$$

If the electric field is parallel to the magnetic field, the solution of (2.25) in the direction of $\vec{B}$ is

$$v_{||} = \left(\frac{qE_{||}}{m}\right)t + v_{0||} \tag{2.26}$$

and

$$z = \left(\frac{qE_{||}}{2m}\right)t^2 + v_{0||}t + z_0. \tag{2.27}$$

where $v_{0||}$ and z_0 are initial values. The particle is accelerated along the direction of $\vec{B}$. In the case of the electric field perpendicular to the magnetic field, we set the direction of $\vec{B}$ to be the z direction and the perpendicular electric field to lie in the x direction. The equations of motion are

$$\frac{d}{dt}v_x = \omega v_y + \frac{\omega E_x}{B} \tag{2.28}$$

$$\frac{d}{dt}v_y = -\omega v_x \tag{2.29}$$

$$\frac{d}{dt}v_z = 0. \tag{2.30}$$

The components of velocity of the particle from these equation are

$$v_x = v_{x0}\cos(\omega t) + (v_{y0} + \frac{E_x}{B})\sin(\omega t) \tag{2.31}$$

$$v_y = (v_{y0} + \frac{E_x}{B})\cos(\omega t) - v_{x0}\sin(\omega t) - \frac{E_x}{B} \tag{2.32}$$

$$v_z = v_{z0}. \tag{2.33}$$

We can see that the particle drifts in the y direction while it is gyrating around B. The drift direction is perpendicular to both the constant electric field and magnetic field. Thus the general velocity of the particle motion in constant electric and magnetic fields is

$$\vec{v} = \vec{u} + \frac{\vec{E}\times\vec{B}}{B^2}, \tag{2.34}$$

where $\vec{u}$ satisfies the equation $d\vec{u}/dt = (q/m)\vec{u}\times\vec{B}$ (Parks 1991).

2.4.3 Guiding center drift

A guiding center is the point defined by

$$\vec{r}_{GC} = \vec{r} - \vec{\rho} \tag{2.35}$$

where $\vec{r}$ is the position vector of the particle and ρ is the radius of curvature defined by

$$m\omega^2\vec{\rho} = q\vec{v}\times\vec{B}. \tag{2.36}$$

From (2.18), we can write

$$\vec{\rho} = \frac{\vec{p}\times\vec{B}}{qB^2}, \tag{2.37}$$

where $\vec{p}$ is the momentum of the particle. Then (2.35) becomes

$$\vec{r}_{GC} = \vec{r} - \frac{\vec{p} \times \vec{B}}{qB^2}. \tag{2.38}$$

In the previous case, the components of the electric field perpendicular to the magnetic field cause the drift motion. In the general case, any force perpendicular to the magnetic field can cause a drift motion. Let a particle move under a static magnetic field and a constant non-magnetic force $\vec{F} = \vec{F_{||}} + \vec{F_{\perp}}$. The particle motion is

$$\frac{d}{dt} v_{||} = \frac{F_{||}}{m} \tag{2.39}$$

$$\frac{d}{dt} \vec{v_{\perp}} = \frac{\vec{F_{\perp}}}{m} + \frac{q}{m} \vec{v_{\perp}} \times \vec{B}. \tag{2.40}$$

From (2.40), the particle is accelerated along $\vec{B}$ by the constant force $\vec{F_{||}}$, while $\vec{F_{\perp}}$ causes the drift motion. While the particle gyrates around $\vec{B}$, the particle is accelerated over one half of the orbit since $\vec{F_{\perp}}$ is along $\vec{v}_{\perp}$ and is decelerated over the other half of the orbit. From (2.19), the change in the velocity causes a change in the gyroradius, so the gyroradius will increase when $v_{\perp}$ is higher and decrease when $v_{\perp}$ is lower. This change in the gyroradius leads to a constant net particle drift perpendicular to the magnetic field. The average drift velocity can be found by assuming $\vec{v}_{\perp} = \vec{u} + \vec{W}$, where $\vec{u}$ satisfies the equation $d\vec{u}/dt = (q/m)\vec{u} \times \vec{B}$, and $d\vec{W}/dt = 0$ (Parks 1991). Then the equation of the perpendicular motion becomes

$$\frac{d}{dt}\vec{u} = \frac{q}{m}\vec{W} \times \vec{B} + \frac{q}{m}\vec{u} \times \vec{B} + \frac{\vec{F_{\perp}}}{m}. \tag{2.41}$$

In the frame moving with $\vec{W}$, the particle motion is a purely cyclotron motion,

$$\frac{d}{dt}\vec{u} = \frac{q}{m}(\vec{u} \times \vec{B}), \tag{2.42}$$

so (2.41) requires

$$q\vec{W} \times \vec{B} + \vec{F_{\perp}} = 0. \tag{2.43}$$

Since $\vec{W}$ is perpendicular to $\vec{B}$,

$$\vec{W} = \frac{1}{q}\frac{\vec{F_{\perp}} \times \vec{B}}{B^2} \tag{2.44}$$

by using the vector identity $(\vec{a} \times \vec{b}) \times \vec{b} = (\vec{a} \cdot \vec{b})\vec{b} - b^2\vec{a}$.

From (2.38), we obtain

$$\frac{d\vec{r}_{GC}}{dt} = \frac{d\vec{r}}{dt} + \frac{d\vec{p}/dt \times \vec{B}}{qB^2}. \tag{2.45}$$

Then (2.45) becomes

$$\begin{aligned} \frac{d\vec{r}_{GC}}{dt} &= \vec{v} + \frac{\left[\vec{F}_{\perp} + q(\vec{v} \times \vec{B})\right] \times \vec{B}}{qB^2} \\ &= \vec{v} + \frac{\vec{F}_{\perp} \times \vec{B} + q(\vec{v} \times \vec{B}) \times \vec{B}}{qB^2} \\ &= \vec{v} - \vec{v}_{\perp} + \frac{\vec{F}_{\perp} \times \vec{B}}{qB^2} \\ &= \vec{v_{||}} + \frac{\vec{F}_{\perp} \times \vec{B}}{qB^2}. \end{aligned} \tag{2.46}$$

We can conclude that the particle is accelerated along the magnetic field due to $\vec{F}_{||}$ and gyrates around the magnetic field while the guiding center drifts along the direction perpendicular to both $\vec{F}_{\perp}$ and the magnetic field.

For the next step, we will consider a non-uniform magnetic field. In the non-uniform magnetic field, the pitch angle is not a constant.

2.4.4 Adiabatic invariant

The adiabatic invariant is related to the action integral of a mechanical system. The action integral is the integration of the canonical momentum over

a cycle of the corresponding canonical coordinate. This action integral remains approximately constant when the properties of the system are changed slowly compared with the relevant period of the motion. In the case of a charged particle traveling in a uniform static magnetic field, the transverse motion is periodic, and gives the action integral as

$$J = \oint \left(\vec{P}_\perp + q\vec{A}\right) \cdot d\vec{l}, \tag{2.47}$$

where $\vec{P}_\perp$ is the transverse component of momentum in real space, $\vec{A}$ is the vector potential, and $d\vec{l}$ is the line element along the circular path (parallel to the transverse momentum)(Jackson 1975). Then using Stokes's theorem and special relativity (2.47) becomes

$$\begin{aligned} J &= \oint m\vec{v}_\perp \cdot d\vec{l} + \int_s q\vec{B} \cdot \hat{n} da & (2.48)\\ &= 2\pi m\omega_B a^2 - \pi m\omega_B a^2 & (2.49)\\ &= \pi m\omega_B a^2, & (2.50) \end{aligned}$$

where S is the surface bounded by the circular path, da is the infinitesimal area on S, a is the particle's gyroradius, and the Stokes theorem is applied to the second term in (2.47). The unit vector $\vec{n}$ is anti-parallel to $\vec{B}$ since $d\vec{l}$ is in a counterclockwise direction around $\vec{B}$. Therefore, the adiabatic invariance of J means that the flux through the particle's orbit is constant. The adiabatic invariance of J also causes $p_\perp^2/B$ and the magnetic moment of the current due to the motion of the particle to remain constant. The magnetic flux through the particle's orbit is approximately conserved. This is similar to the conserved flux through an area moving with the plasma (section 2.3). If the magnetic field changes slowly over the period of the transverse motion of the particle, the

magnetic flux is also constant through the particle orbit. The constant flux gives us

$$\frac{v_\perp^2}{B} = \frac{v_{\perp 0}^2}{B_0}. \tag{2.51}$$

The speed of any particle in a static magnetic field is constant since the magnetic force is always perpendicular to a particle's velocity. If the particle comes from a weak magnetic field B_0 to a strong magnetic field B, $|v_\perp|$ becomes larger, and $|v_{||}|$ becomes smaller. If the magnetic field B is strong enough or $|v_{\perp 0}|$ is large enough, $|v_{||}|$ becomes zero, and the particle can be reflected back. If the particle comes from a strong magnetic field B_0 to a weak magnetic field B, $|v_\perp|$ becomes smaller, and $|v_{||}|$ becomes larger, so the particle's motion becomes more parallel to the magnetic field line.

2.4.5 Curvature drift of the guiding center

We know that if the magnetic field varies very slowly, the particle's orbit will conserve the magnetic flux. If the magnetic field is curved over a part of a circle as shown in Figure 2.7, the trajectory of the particle's guiding center should be curved also. Let $\vec{\rho}$ be the radial vector of the circle as shown in Figure 2.7. We consider that the curvature of the magnetic field acts like a centrifugal force written as

$$\vec{F} = m v_{||}^2 \frac{\vec{\rho}}{\rho^2}, \tag{2.52}$$

where $v_{||}$ is the gyro-averaged guiding center velocity of particles along the direction of the curved magnetic field, and $\vec{F}$ is perpendicular to $\vec{B}$ (Parks 1991). Then the guiding center drift due to $\vec{F}$ is

$$\vec{W} = \frac{m v_{||}^2}{qB^2} \frac{\vec{\rho} \times \vec{B}}{\rho^2}. \tag{2.53}$$

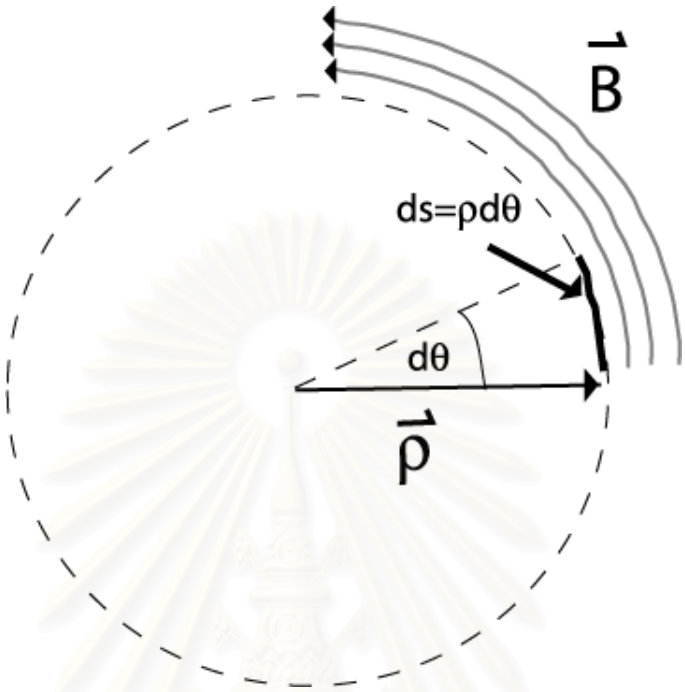

Figure 2.7: Geometry of curved magnetic field lines

The particle drifts to a direction perpendicular to both the magnetic field and the radius of curvature.

We can express ρ in terms of spatial derivatives of $\vec{B}$. Introducing spherical coordinates, let ρ be the radius and $\hat{\theta}$ be the direction of the curved magnetic field. If $ds = \rho d\theta$ is the length along the circle, then $d\vec{B}/ds$ must be in the direction of $-\vec{\rho}$. If the magnitude of the magnetic field is constant, we can write

$$\begin{aligned} \frac{\vec{\rho}}{\rho^2} &= -\frac{\partial}{\partial s}\frac{\vec{B}}{B} \\ &= -\frac{1}{B}\frac{\partial \vec{B}}{\partial s} \\ &= -\frac{1}{B^2}(\vec{B}\cdot\nabla)\vec{B}. \end{aligned} \tag{2.54}$$

Equation (2.53) becomes

$$\vec{W} = \frac{mv_{\parallel}^2}{qB^4}\vec{B}\times(\vec{B}\cdot\nabla)\vec{B}. \tag{2.55}$$

Note that

$$(\nabla \times \vec{B}) \times \vec{B} = (\vec{B} \cdot \nabla)\vec{B} - \nabla(B^2/2) \tag{2.56}$$

(Parks 1991). To show this, in index notation and using the Levi-Civita symbol, we have

$$(\nabla \times \vec{B}) \times \vec{B} = \epsilon_{ijk}\epsilon_{jml}(\partial_m B_l)B_k. \tag{2.57}$$

Using the identity

$$\epsilon_{ijk}\epsilon_{jml} = \delta_{km}\delta_{il} - \delta_{kl}\delta_{im}, \tag{2.58}$$

we have

$$(\nabla \times \vec{B}) \times \vec{B} = (\vec{B} \cdot \nabla)\vec{B} - \nabla(B^2/2). \tag{2.59}$$

After that $(\vec{B} \cdot \nabla)\vec{B} = \nabla(B^2/2)$, since $\nabla \times \vec{B} = 0$, because we consider a charged particle in a magnetic field with no current and an electric field. Therefore, the drift velocity due to the curved magnetic field can be written as

$$\vec{W} = \frac{mv_{\parallel}^2}{qB^4}\vec{B} \times \nabla(B^2/2). \tag{2.60}$$

2.4.6 Gradient drift of the guiding center

Let us define the magnetic field to only change in magnitude and to lie in the z direction. Let the magnitude of the field increase linearly along the y direction (Parks 1991). The magnetic field can be written as

$$\vec{B} = \left(B_0 + \frac{dB}{dy}y\right)\hat{z} \tag{2.61}$$

The force on the particle is

$$\begin{aligned} \vec{F} &= q\vec{v} \times \vec{B} && (2.62)\\ &= q\left(v_y\left(B_0 + \frac{dB}{dy}y\right)\right)\hat{x} - \left(v_x\left(B_0 + \frac{dB}{dy}y\right)\right)\hat{y} && (2.63)\\ &= q\left(\vec{v} \times \vec{B}_0 + \left(v_y\frac{dB}{dy}y\right)\hat{x} - \left(v_x\frac{dB}{dy}y\right)\hat{y}\right). && (2.64) \end{aligned}$$

The second and the third term in (2.64) are considered as an extra force. This force leads to the particle's drift motion. We already found the drift motion for a constant force, but this force is not constant, so we average this force over the gyromotion. Because of the small change in the magnitude of the magnetic field, the unperturbed solution dominates over a gyroperiod and gives

$$v_x = v_\perp \cos\omega t \tag{2.65}$$

$$x = \frac{v_\perp}{\omega}\sin\omega t \tag{2.66}$$

$$v_y = v_\perp \sin\omega t \tag{2.67}$$

$$y = \frac{v_\perp}{\omega}\cos\omega t, \tag{2.68}$$

where $\omega = qB_0/m$. The average of the x component in the extra force is zero, but the average of the y component is

$$\langle F_y \rangle = -\frac{qv_\perp^2}{2\omega}\frac{dB}{dy}. \tag{2.69}$$

From (2.44) and (2.69), the average gradient drift velocity is

$$\vec{W} = -\frac{v_\perp^2}{2\omega B^2}\frac{dB}{dy}(\hat{y}\times\vec{B}). \tag{2.70}$$

2.5 Shocks

In compressible fluids, if any object moving through the medium with a speed faster than the speed of sound, the properties of the fluid such as density, pressure, temperature, velocity, etc are changed suddenly. The thin region having discontinuous fluid properties is called a shock. There are shocks in space. In the solar system, a shock can be created by a coronal mass ejection (CME), a vast mass of gas filled with magnetic field lines that can be ejected from the Sun during

a solar storm. The speed of a CME is usually faster than the speed of sound and the speed of the solar wind in the interplanetary medium. At the edge of the solar system, the solar wind termination shock is expected to be found and to have a roughly spherical shape. The solar termination shock is expected to exist because the speed of the solar wind is greater than the speed of sound. There are also shocks outside the solar system. A supernova explosion can produce shocks in a supernova remnant.

2.6 Fermi acceleration

In 1949, Fermi proposed a theory of cosmic rays in which cosmic rays originate and are accelerated primarily in the interstellar space of the galaxy by collisions against moving magnetic fields. This theory provides the inverse power law spectral distribution of cosmic rays.

In the plasma frame, the average electric field is zero, but the average magnetic field is not zero. Since the plasma fluid is turbulent, the magnetic field is irregular. In the upstream plasma frame, the speed of the particle is roughly constant since the average electric field is zero. In the other frames which are not the plasma frame, if the relative velocity between that frame and the plasma frame is not parallel to the magnetic field, the electric field does not vanish and charged particles can be accelerated by the electric field. The normal incidence frame is the frame that is boosted along the average plasma velocity until the shock is stationary. Normally, the average plasma velocity is not parallel to the magnetic field so there is a nonzero eletric field. The calculation with an electric field is difficult so we will calculate the momentum changes in a frame with no electric field. There is a frame called the de Hoffman-Teller frame. This frame

has a stationary shock plane, and is boosted along the magnetic field, so there is no electric field in this frame. We will use this frame to find the momentum changes when the particles cross the shock.

The irregular magnetic field can cause the particle to change its direction with no change in the speed in the local fluid frame. If we observe the particle in the de Hoffman-Teller frame, we can imagine that the change in particle direction due to a macroscopic magnetic irregularity is like that due to an elastic collision with massive particle. If there is no shock, all irregular magnetic fields move with same average speed. The charged particle can be reflected at one magnetic field irregularity and change its direction; then it can collide with another magnetic field irregularity and change its direction back to the original direction. After two collisions the particle is back to the same direction with no change in speed.

If there is a shock (Figure 2.8), a particle initially moving with speed v can go through the shock, and after the particle passes the shock, it finds the downstream irregular magnetic field moving toward it with a speed of $U_1 - U_2$ relative to the upstream plasma, where U_1 and U_2 are the speeds of plasma upstream and downstream with respect to the de Hoffman-Teller frame, respectively. This process is shown in Figure 2.8. We can transform the particle's velocity into the rest frame of the irregular magnetic field. In this frame the particle collides with the irregular magnetic field and goes backward with no change in speed. Then we transform the particle's velocity back into the upstream plasma frame. Thus the speed becomes $v + 2(U_1 - U_2)$. This gives us

$$\frac{\langle p \rangle}{p} = \frac{2(U_1 - U_2)}{v}. \tag{2.71}$$

This is called first order Fermi acceleration.

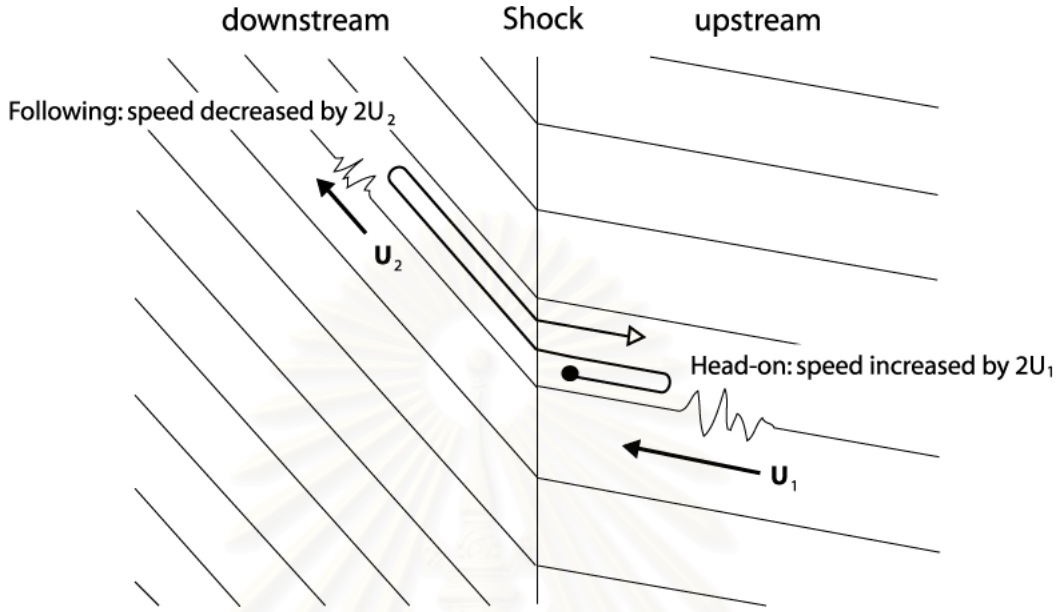

Figure 2.8: The particle collides with the irregular magnetic field in both upstream and downstream regions with different relative speeds.

2.7 Shock drift acceleration

In the solar wind frame, the average electric field is zero. Let us consider a shock frame that is called the normal incidence frame, defined as the frame where the relative velocity to the upstream plasma frame is parallel to the shock normal. In this frame, the average electric field is not zero but is equal to $-\vec{U} \times \vec{B}$, where $\vec{U}$ is the solar wind velocity with respect to shock frame and $\vec{B}$ is the average magnetic field. At a shock the magnetic field generally changes its direction and magnitude. If the magnetic field changes, charged particles will have a drift motion. In the case of an oblique shock, the magnetic field has a component along the shock plane, and the gradient of the magnetic field is in the direction of the shock normal. For positively charged particles, the drift direction is parallel to $\vec{B} \times \nabla B$. Since ∇B is parallel to the shock normal, $\vec{U} \cdot \nabla B$ is positive.

Therefore the drift direction is parallel to the direction of the electric field. In the normal incidence frame, we view that charged particles are accelerated by 1) Fermi acceleration and 2) the drift motion. If we observe the particle in the de Hoffman-Teller frame which has no electric field, the net change in the velocity of the particles after crossing the shock (Fermi acceleration) already includes the effect of the shock drift acceleration. We can easily find the momentum change since the speed of the particle remains unchanged in this frame.

2.8 Some previous work on particle acceleration at nearly perpendicular shocks

2.8.1 Adiabatic treatment (Terasawa 1979)

In this work, charged particles are set to move toward a shock. Only the particles reflected at the shock are considered. The energy gained at each crossing is shown and it depends on the pitch angle, the angle between the magnetic field and the shock, and the particle's speed. In the adiabatic treatment, the magnetic field changes slowly and smoothly at the shock, and in the kink treatment, the magnetic field changes rapidly with a discontinuity at the shock. These treatments are then compared. These two magnetic fields are shown in Figure 2.9. The kink treatment, for which the particle motion can not be solved analytically, is more realistic since the fluid parameters are discontinuous at the shock. The adiabatic treatment can be solved analytically, and is shown by Terasawa (1979) to provide a good approximation.

If there is only a magnetic field, the particle's motion can be easily approximated. Therefore, we should do all our work in the frame of a zero electric field. We know that the distribution of pitch angle is initially random in the plasma

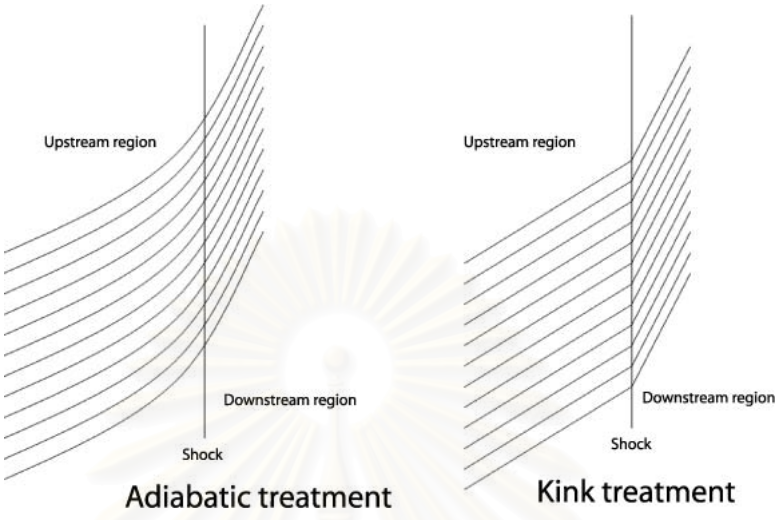

Figure 2.9: (Left) The magnetic field changes slowly at the shock in the adiabatic treatment. (Right) The magnetic field changes suddenly at the shock in the kink treatment.

frame, and there is no electric field since the plasma is a conductor. There is no electric field anywhere except at the shock since the discontinuity at a shock, the magnetic field changes in magnitude and becomes time dependent when we observe from the solar wind frame. We should transform the properties of the particles from a frame in which particles are in both a nonzero magnetic field and a nonzero electric field into a frame with a zero electric field and a static magnetic field. In the normal incidence frame, a frame that is fixed with respect to the shock in which the upstream (incident) flow is normal to the shock, the relative velocity between the plasma frame and the normal incidence frame is not in the direction of the magnetic field as in the case of a nearly perpendicular shock. Therefore the electric field is not zero in this frame. Now we will find a frame with no electric field at the shock.

In the solar wind frame the electric field is zero, since the solar wind frame is the plasma frame. The shock normal is set to be in the x direction. Let us

write the magnetic field and electric field in the solar wind frame as

$$\vec{B} = b_x\hat{x} + b_z\hat{z} \tag{2.72}$$

$$\vec{E} = 0. \tag{2.73}$$

The angle θ between the magnetic field and the shock normal is written as $\theta = \tan^{-1} b_z/b_x$ If we want to use a static magnetic field we might transform to a rest frame of the shock. If the x direction is the direction of the solar wind (if we are in the normal incidence frame), let the solar wind speed be $V_s\hat{x}$. Using the Lorentz transformation,

$$\begin{aligned} \vec{E}' &= \gamma(\vec{E} + \vec{\beta} \times \vec{B}) - \frac{\gamma^2}{\gamma+1}\vec{\beta}(\vec{\beta}\cdot\vec{E}) \\ \vec{B}' &= \gamma(\vec{B} - \vec{\beta} \times \vec{E}) - \frac{\gamma^2}{\gamma+1}\vec{\beta}(\vec{\beta}\cdot\vec{B}), \end{aligned} \tag{2.74}$$

$$\tag{2.75}$$

where $\gamma = 1/\sqrt{1 - v_s/c}$ and $\vec{\beta} = \vec{v}_s/c$, the magnetic field and electric field become

$$\vec{B}' = b_x\hat{x} + \gamma_{vs} b_z \hat{z} \tag{2.76}$$

$$\vec{E}' = (\gamma_{vs} V_s b_z/c)\,\hat{y}, \tag{2.77}$$

where $\gamma_{vs} = 1/\sqrt{1 - (V_s^2/c^2)}$. In this frame, the magnetic field is static but the electric field is not zero. We can get a frame of zero electric field and a static magnetic field by transforming the magnetic field and the electric field into the frame that moves with velocity $-u\hat{z}$ with respect to the shock frame. This is called the de Hoffmann-Teller frame. Then the magnetic field and electric field become

$$\vec{B}'' = \gamma_u(b_x - \frac{u}{c^2}\gamma_{vs} V_s b_z)\hat{x} + \gamma_{vs} b_z \hat{z} \tag{2.78}$$

$$\vec{E}'' = \gamma_u \left(\frac{\gamma_{vs} V_s b_z}{c} - \frac{u}{c} b_x\right)\hat{y}, \tag{2.79}$$

where $\gamma_u = 1/\sqrt{1-(u^2/c^2)}$. To eliminate the electric field, we need $u = \gamma_{vs} V_s b_z/b_x$. From (2.79) if $\gamma_{vs} V_s b_z/b_x \geq c$ the electric field can not be eliminated. The velocity $\vec{V_t}$ of the shock frame with no electric field is $-V_s\hat{x} - \gamma_{vs} V_s b_z/b_x \hat{z}$ with respect to the solar wind frame. The solar wind velocity is much smaller than the speed of light, so $\gamma \approx 1$. Then $|\vec{V_t}| = V_s \sec\theta$ and the direction of $\vec{V_t}$ is the direction of the magnetic field in the solar wind frame. Figure 2.10 shows the various frame we use in this section. The relation between the velocities in two frames can be written as

$$v_\perp = v_\perp^0 \tag{2.80}$$

$$v_{||} = v_{||}^0 + V_s \sec\theta, \tag{2.81}$$

where $v_\perp$ is the component of velocity perpendicular to the magnetic field, and $v_{||}$ is the component of velocity parallel to the magnetic field

In the adiabatic treatment, we imagine that the magnetic field slowly changes in magnitude so that we can use the adiabatic invariance (§2.4.4) which gives

$$\frac{v_{\perp 0}^2}{B_0} = \frac{v_\perp^2}{B}. \tag{2.82}$$

We will consider only the particles passing through the shock. In the shock frame, a particle that reaches the shock must have a pitch angle less than 90°. Thus the pitch angle cosine in the solar wind frame must be greater than $-V_s \sec\theta/v_0$ where $v_0 = v_{||0}^2 + v_{|\perp 0}^2$. Equation (2.82) tells us that only particles with some values of the pitch angle can cross the shock. The maximum pitch angle cosine in the shock frame for which a particle is reflected is

$$\mu_M = \sqrt{1 - B_1/B_2}, \tag{2.83}$$

where B_1 and B_2 are magnitudes of the magnetic field in the upstream and downstream regions, respectively. In the solar wind frame, the maximum pitch angle is written as

$$\mu_M^0 = -\frac{V_s \sec\theta}{v_0}(1-\mu_M^2) + \mu_M\sqrt{1-\left(\frac{V_s \sec\theta}{v_0}\right)^2(1-\mu_M^2)}. \tag{2.84}$$

If the particle is reflected from the shock, the magnitude of the parallel part of velocity is not changed but the direction is reversed. Then the velocity of the reflected particle in the shock frame can be written as

$$v_\perp = v_\perp^0 \tag{2.85}$$

$$v_{||} = -v_{||}^0. \tag{2.86}$$

Transforming this velocity back to the solar wind frame, we get

$$v_\perp = v_\perp^0 \tag{2.87}$$

$$v_{||} = -(v_{||}^0 + 2V_s \sec\theta). \tag{2.88}$$

Then the energy and the pitch angle of a reflected particle back in the upstream frame is

$$E = \left[1 + 4\frac{V_s \sec\theta}{v_0}\mu_0 + 4\left(\frac{V_s \sec\theta}{v_0}\right)^2\right]E_0 \tag{2.89}$$

$$\mu = -\frac{\mu_0 + 2\frac{V_s \sec\theta}{v_0}}{\sqrt{1 + 4\frac{V_s \sec\theta}{v_0}\mu_0 + 4\left(\frac{V_s \sec\theta}{v_0}\right)^2}}. \tag{2.90}$$

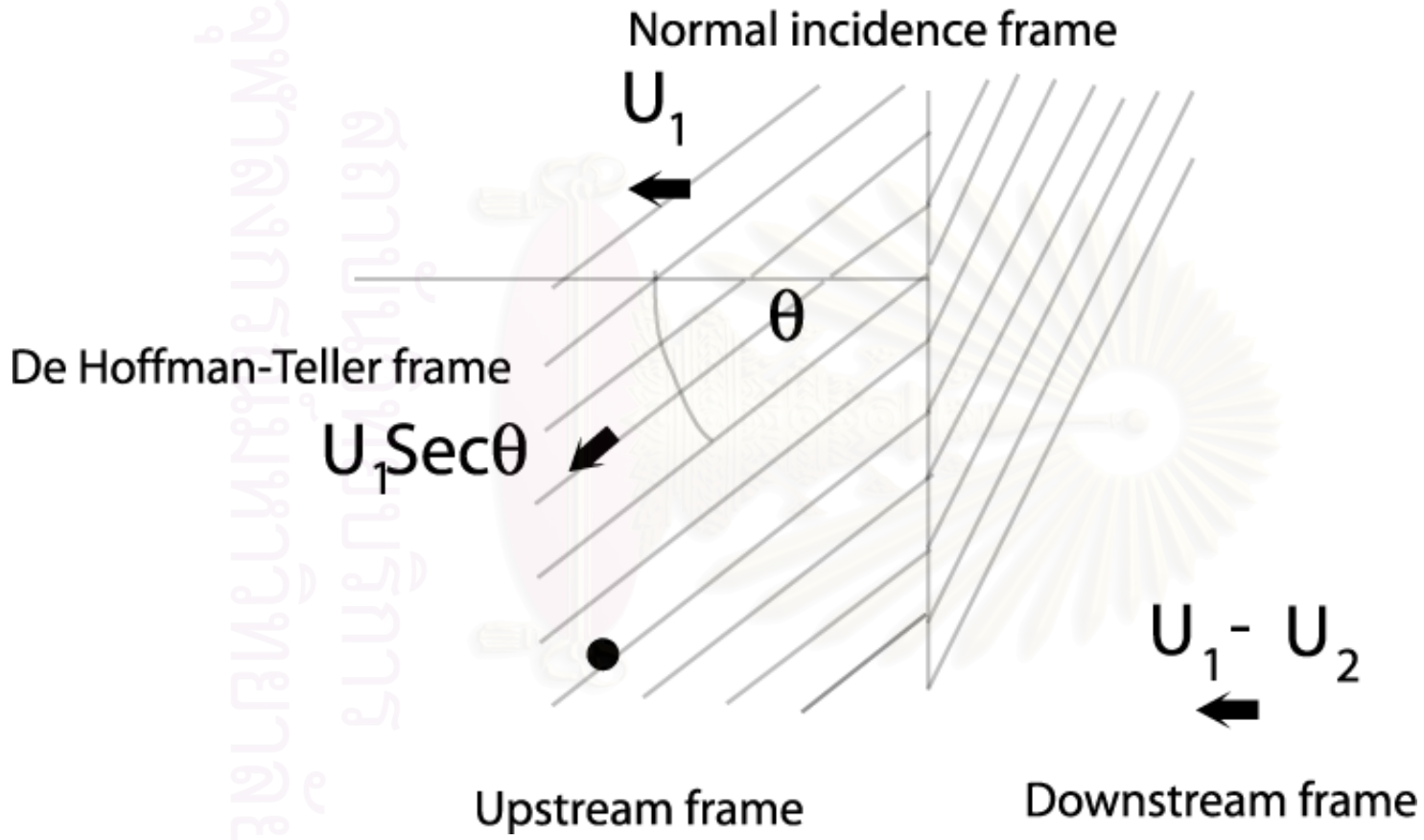

Figure 2.10: Several frames are shown in this figure. Only the normal incidence frame has an non-zero electric field.

In the kink treatment, the particle trajectories are simulated. The particle trajectory changes immediately at the shock. Some particles are reflected and some particles are transmitted at shock due to their gyrophases at the shock. In the case of the nearly perpendicular shock, the pitch angle distributions, and the energy distributions after the reflection in both treatments looked alike. The relations between the energy after the reflection and the final pitch angle are shown in Figures 2.11 to 2.14 with the crossing angles 20°, 40°, 60°, and 80°. The numbers in these figures show the number of events at that energy and that pitch angle from the kink treatment, and the dashed line is from the adiabatic treatment. The distribution of numbers is close to the dashed line when the crossing angle is 80°. The distribution of the energy after the reflection is shown in Figure 2.15, and the distribution of the pitch angle cosine after the reflection is shown in Figure 2.16 at the crossing angle 80°. Therefore we can accurately approximate the probability of reflection and the energy gained at a nearly perpendicular shock by the adiabatic treatment.

2.8.2 Microscopic derivation (Drury 1983)

From Terasawa's work, the energy gain distribution and the pitch angle distribution are considered from one crossing. In our work, the multiple crossings are taken into account. There are multiple crossings because of the magnetic turbulence. In 1983, Drury summarized how a single shock-field crossing can cause a power law spectrum of the cosmic rays. In this thesis, we will use the methods of Drury (1983) for the case of multiple crossings.

The average energy gained by crossing the shock each round, from upstream to downstream and back to upstream again, and the probability of the

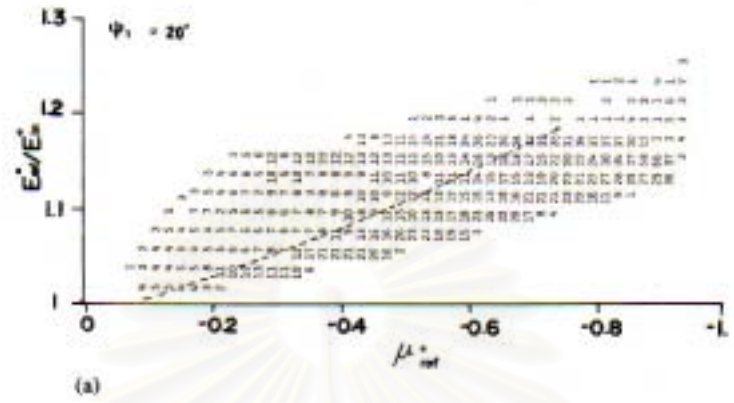

Figure 2.11: Frequency distribution in the ratio of the final energy to the initial energy and the final pitch angle for crossing angle 20°. The numbers show the number of events at that energy and that pitch angle from the kink treatment, and the dashed line is from the adiabatic treatment (Terasawa 1979).

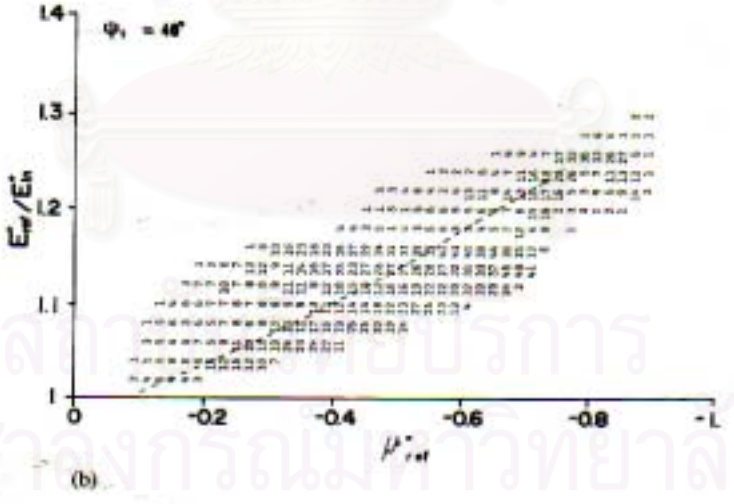

Figure 2.12: Frequency distribution in the ratio of the final energy to the initial energy and the final pitch angle for crossing angle 40°. The numbers show the number of events at that energy and that pitch angle from the kink treatment, and the dashed line is from the adiabatic treatment (Terasawa 1979).

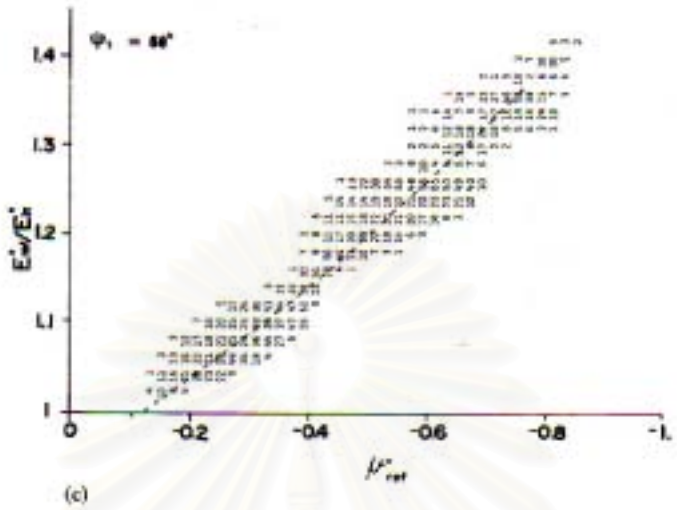

Figure 2.13: Frequency distribution in the ratio of the final energy to the initial energy and the final pitch angle for crossing angle 60°. The numbers show the number of events at that energy and that pitch angle from the kink treatment, and the dashed line is from the adiabatic treatment (Terasawa 1979).

particle's escape away from the shock are considered by Drury(1983). The average energy is calculated from the change of magnitude of the particle's speed when 1) the particle's velocity is transformed from the upstream frame into the downstream frame upon crossing the shock, 2) the particle downstream changes direction due to scattering in the irregular magnetic field, 3) returns to the shock, and 4) returns back into the upstream frame. For an oblique shock, it is also possible that in step 1 the particle immediately reflects back upstream.

First, we consider the case of a parallel shock, which has a magnetic field parallel to the shock normal. Let us set p and v to be the magnitude of the particle's momentum and velocity, respectively. In the downstream frame, the particle's momentum becomes $p[1 + \mu(U_1 - U_2)/v]$, where U_1 and U_2 are the average speed of the plasma in the upstream and downstream region, respectively,

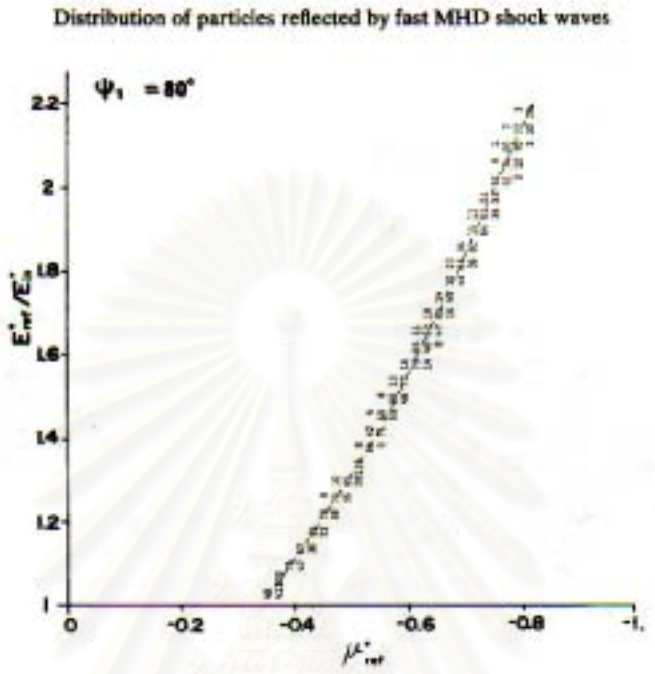

Figure 2.14: Frequency distribution in the ratio of the final energy to the initial energy and the final pitch angle for crossing angle 80°. The numbers show the number of events at that energy and that pitch angle from the kink treatment, and the dashed line is from the adiabatic treatment (Terasawa 1979).

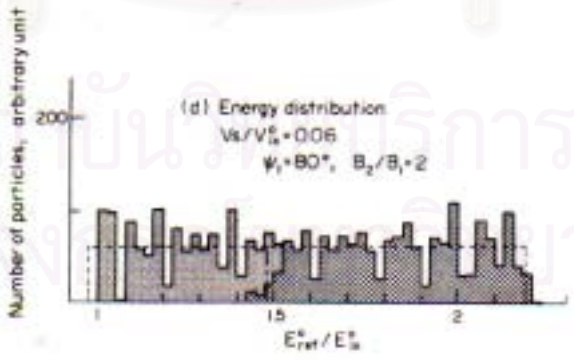

Figure 2.15: The distribution of the ratio of the final energy to the initial energy in which the histogram is from the kink treatment and the dashed line is from the adiabatic treatment (Terasawa 1979).

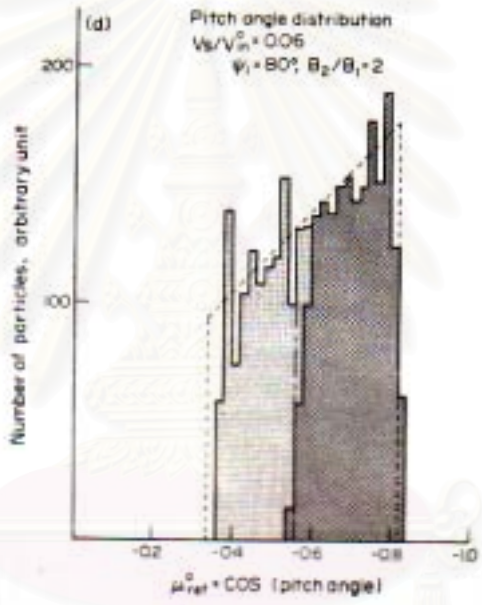

Figure 2.16: The distribution of the pitch angle cosine after reflection in which the histogram is from the kink treatment and the dashed line is from the adiabatic treatment (Terasawa 1979).

and μ is the incident particle's pitch angle. Then the particle is scattered back upstream, and its momentum becomes $p[1+\mu(U_1-U_2)/v-\mu'(U_1-U_2)/v]$, where μ' is the final pitch angle. We average the change in magnitude of the particle momentum over possible values of the initial and final pitch angle:

$$\begin{aligned}\langle p\rangle &= p\int_0^1\int_{-1}^0[\mu(U_1-U_2)/v-\mu'(U_1-U_2)/v]4\mu\mu' d\mu' d\mu \\ &= \frac{4}{3}(U_1-U_2)/v. \end{aligned} \tag{2.91}$$

The probability of escape is calculated from the flux coming to the shock from the upstream region and the flux going away from the shock into the downstream region. The flux of particles with speed v coming to the shock is $\int_0^1 \mu v n d\mu/2 = nv/4$ where n is the number of particles having the speed of v. The flux of particles escaping from the shock is nU_2. The escape probability is the ratio of the escaping flux to the incoming flux, or $nU_2/(nv/4) = 4U_2/v$. The probability that the particle comes back to the shock n times without escaping is

$$P(>n) \approx \prod_{i=1}^{n}\left(1-\frac{4U_2}{v_i}\right), \tag{2.92}$$

while its momentum becomes

$$p_n \approx \prod_{i=1}^{n}\left[1+\frac{4}{3}(U_1-U_2)/v_i\right]. \tag{2.93}$$

This means that after crossing n times, the particle has a momentum of p_n. If $v \gg U_1$, we get

$$\ln p_n/p_0 \approx \frac{4}{3}(U_1-U_2)\sum_{i=1}^{n}\frac{1}{v_i} \tag{2.94}$$

$$\ln P(>n) \approx -4U_2\sum_{i=1}^{n}\frac{1}{v_i} \tag{2.95}$$

or

$$P(>n) = \left(\frac{p_n}{p_0}\right)^{-3U_2/(U_1-U_2)}. \tag{2.96}$$

The number of particles accelerated to momentum p_n or more is

$$N(>n) = \frac{U_1}{U_2}\left(\frac{p_n}{p_0}\right)^{-3U_2/(U_1-U_2)} N_0, \tag{2.97}$$

where N_0 is the total number of particle and the factor U_1/U_2 is from the conserved flux, the number and the energy are conserved. The phase space density of particles accelerated to only momentum p_n is

$$f_p = \frac{1}{4\pi p^2}\frac{dN(>p)}{dp} = \frac{N_0}{4\pi}\frac{3U_1}{U_1-U_2}\left(\frac{p_n}{p_0}\right)^{-3U_1/(U_1-U_2)} \tag{2.98}$$

Next, we consider an oblique shock. Pitch angles and gyrophases of particles are separated into 5 sets:

1. Let μ_1 and ϕ_1 be the pitch angle and gyrophase of a particle reaching the shock from the upstream region.

2. Let μ_2 and ϕ_2 be the pitch angle and gyrophase of the particle after transmission into the downstream region (if applicable).

3. Let μ_3 and ϕ_3 be the pitch angle and gyrophase of the particle of the particle after reflection at the shock back to the upstream region (if applicable).

4. If a particle is transmitted into the downstream region, diffuses, and returns to the shock, let μ_4 and ϕ_4 be the pitch angle and gyrophase of that particle.

5. Let μ_3 and ϕ_3 be the pitch angle and gyrophase of a particle with μ_4 and ϕ_4 after transmission back to the upstream region.

Figure 2.17 shows the directions of motion and (μ,ϕ) sets in each region.

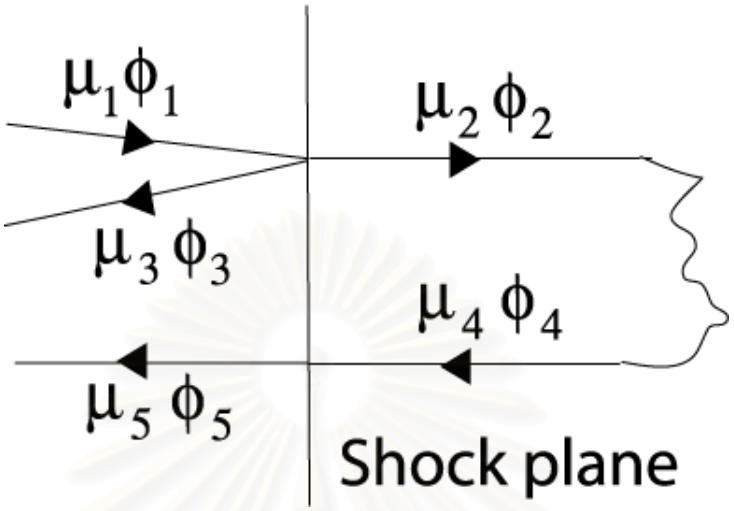

Figure 2.17: The directions of motion and (μ,ϕ) sets in each region.

Now let T_1 be the set of pitch angles and phases of the particles that are transmitted through the shock from the upstream region. Let R_1 be the set of pitch angles and phases of the particles that are reflected at the shock back into the upstream region. Let T_2 be the set of pitch angles and gyrophases of the particles that are transmitted through the shock from the downstream region. A superior bar denotes the set of reversed trajectories of that set. For example, $\bar{T}_2 = (\mu, \phi)|(-\mu, \phi) \in T_2$. The probability of transmission is the ratio of the flux in T_1 to the total incident flux or

$$P_t = \frac{\frac{1}{4\pi}\int\limits_{T_1} n\mu_1 v d\mu_1 d\phi_1}{\frac{1}{4\pi}\int\limits_{T_1 \cup R_1} n\mu_1 v d\mu_1 d\phi_1}. \tag{2.99}$$

Using Liouville's theorem, we get

$$\frac{1}{B_1}\mu_1 d\mu_1 d\phi_1 = \frac{1}{B_2}\mu_2 d\mu_2 d\phi_2. \tag{2.100}$$

The value of μ is from 0 to 1 in set $\bar{T}_2$ and $T_1 \cup R_1$. Let θ_1 be the angle at the upstream region, and θ_2 be the angle at the downstream region. Each trajectory

in T_1 (upstream) correspends to a trajectory in $\bar{T}_2$ (downstream). Therefore, using (2.100) we have

$$\begin{aligned} P_t &= \frac{\frac{B_1}{4\pi B_2}\int\limits_{\bar{T}_2} n\mu_2 v d\mu_2 d\phi_2}{\frac{1}{4\pi}\int\limits_{T_1\cup R_1} n\mu_1 v d\mu_1 d\phi_1} \\ &= \frac{B_1}{B_2} \\ &= \frac{\cos\theta_2}{\cos\theta_1} \end{aligned} \tag{2.101}$$

Therefore, the flux into the downstream region is

$$\begin{aligned} \int\limits_{T_1} \frac{nv}{4\pi}\cos\theta_1\mu_1 d\mu_1 d\phi_1 &= P_t \int_0^{2\pi}\int_0^1 \frac{nv}{4\pi}\cos\theta_2\mu_2 d\mu_2 d\phi_2 \\ &= \frac{n}{4}v\cos\theta_2 \end{aligned} \tag{2.102}$$

The flux to ∞ in the downstream region is $nU_2\cos\theta_2$. Thus the probability that the particles coming from upstream are transmitted and do not return to the shock again is $4U_2\cos\theta_2/(v\cos\theta_1)$.

On a certain area on the shock plane, the same number of the magnetic field lines passes from both the upstream region and the downstream region. At the shock, the angle between the shock normal and the magnetic fields from both sides of the shock are different. The intensity of the magnetic field is the number of magnetic field lines per normal area. The normal area is proportional to $1/\cos\theta$.

A particle crossing from any direction always gains energy. If a particle with momentum p in the upstream frame comes to the shock from the upstream region, it can be reflected at the shock, so (μ_1,ϕ_1) changes to (μ_3,ϕ_3), or transmitted into the downstream region, so (μ_1,ϕ_1) changes to (μ_2,ϕ_2). From (2.101) the probability of particle transmission into the downstream frame is B_1/B_2, and the

escape probability after the transmission is $4U_2/v$. The probability that the particle goes back to the shock from the downstream region, with (μ_4,ϕ_4) changing to (μ_5,ϕ_5), is $(B_1/B_2)(1-4U_2/v)$. We can neglect $4U_2/v$ by assuming $(4U_2/v) \ll 1$.

Let v_i be the speed of the particle at the plasma frame, and μ_i be its pitch angle in that plasma frame. Since the relative velocity between a plasma frame and the de Hoffman-Teller frame is parallel to the magnetic field, the velocity v of the particle in the de Hoffman-Teller frame becomes

$$\begin{aligned} v &= \sqrt{(\mu_i v_i + U_i)^2 + (1-\mu_i^2)v_i} \\ &= v_i \left(1 + \frac{\mu_i U_i}{v_i}\right), \end{aligned} \tag{2.103}$$

$$\tag{2.104}$$

where U_i is the relative speed between the plasma frame and the de Hoffman-Teller frame, and we work to the order U_i/v_i. If the particle is reflected back or transmitted to the plasma region with the relative speed between the plasma frame and the de Hoffman-Teller frame U_j, the speed of the particle at the next plasma frame is

$$\begin{aligned} v_j' &= \sqrt{(\mu_j v - U_j)^2 + (1-\mu_j^2)v} \\ &= v \left(1 - \frac{\mu_j U_j}{v}\right), \end{aligned} \tag{2.105}$$

$$\tag{2.106}$$

The speed change is

$$\begin{aligned} v_j' - v_i &= v \left(1 - \frac{\mu_j U_j}{v}\right) - v_i \\ &= \mu_i U_i - \mu_j U_j, \end{aligned} \tag{2.107}$$

$$\tag{2.108}$$

when we keep terms to order U/v. Now the average momentum gained in a full cycle is

$$\begin{aligned}\frac{\langle\Delta p\rangle}{p} &= \frac{1}{\pi v}\int_{R_1} U_1(\mu_1-\mu_3)\mu_1 d\mu_1 d\phi_1 + \frac{1}{\pi v}\int_{T_1}(U_1\mu_1 - U_2\mu_2)\mu_1 d\mu_1 d\phi_1 \\ &\quad + \frac{P_t}{\pi v}\int_{T_2}(U_1\mu_4 - U_2\mu_5)\mu_4 d\mu_4 d\phi_4. \end{aligned} \tag{2.109}$$

The probability of escaping is small and is ignored in this calculation. By using Liouville's theorem,

$$\begin{aligned}\int_{R_1} -\mu_3\mu_1 d\mu_1 d\phi_1 &= \int_{\tilde{R}_1} -\mu_3^2 d\mu_3 d\phi_3 \\ &= \int_{\tilde{R}_1} -\mu^2 d\mu d\phi \end{aligned} \tag{2.110}$$

and

$$\begin{aligned}\int_{T_1} -\mu_2\mu_1 d\mu_1 d\phi_1 &= \frac{B_1}{B_2}\int_{T_2} -\mu_2^2 d\mu_2 d\phi_2 \\ &= \frac{2\pi}{3}\frac{B_1}{B_2} \end{aligned} \tag{2.111}$$

and

$$\begin{aligned}\int_{T_2} -\mu_5\mu_4 d\mu_4 d\phi_4 &= \frac{B_1}{B_2}\int_{\tilde{T}_1} -\mu_5^2 d\mu_5 d\phi_5 \\ &= \frac{B_1}{B_2}\int_{T_1} -\mu^2 d\mu d\phi. \end{aligned} \tag{2.112}$$

Now, (2.109) becomes

$$\begin{aligned}\frac{\langle\Delta p\rangle}{p} &= \frac{1}{\pi v}\int_{R_1+T_1} U_1\mu_1^2 d\mu_1 d\phi_1 - \frac{1}{\pi v}\left(\int_{R_1} U_1\mu_1\mu_3 d\mu_1 d\phi_1 + \int_{T_1} U_2\mu_1\mu_2 d\mu_1 d\phi_1\right) \\ &\quad + \frac{B_1}{B_2\pi v}\int_{T_2}(U_1\mu_4 - U_2\mu_5)\mu_4 d\mu_4 d\phi_4 \end{aligned}$$

$$= \frac{2}{\pi v}\int_{R_1+T_1} U_1\mu_1^2 d\mu_1 d\phi_1 - \frac{1}{\pi v}\int_{T_1} U_1\mu_1\mu_3 d\mu_1 d\phi_1 + \frac{2U_2}{3v}\frac{B_1}{B_2}$$
$$+\frac{B_1}{B_2\pi v}\int_{T_2} U_2\mu_4^2 d\mu_4 d\phi_4 - \frac{B_1}{B_2\pi v}\int_{T_2} U_1\mu_4\mu_5 d\mu_4 d\phi_4. \quad (2.113)$$

The second term is canceled with the fifth term since

$$\frac{1}{\pi v}\int_{T_1} U_1\mu_1\mu_3 d\mu_1 d\phi_1 = \frac{B_1}{B_2\pi v}\int_{T_2} U_1\mu_2\mu_3 d\mu_2 d\phi_1$$
$$= -\frac{B_1}{B_2\pi v}\int_{T_2} U_1\mu_4\mu_5 d\mu_4 d\phi_4, \quad (2.114)$$

because $\mu_2 = -\mu_4$, $\mu_3 = -\mu_5$, and $\phi_i = \phi_j$. The third term and the fourth term give the same value. Thus,

$$\frac{\langle \Delta p\rangle}{p} = \frac{4}{3}\left(\frac{U_1}{v} - \frac{U_2\cos\theta_2}{v\cos\theta_1}\right). \quad (2.115)$$

As in the parallel shock case, $d\ln N(>p)/d\ln p$ is the power law index of the integral spectrum and the ratio of the escape probability to the mean momentum gain. In this case, the slope of the power law is

$$\frac{d\ln N(>p)}{d\ln p} = \frac{-(4U_2\cos\theta_2)/(v\cos\theta_1)}{\langle\Delta p\rangle/p} = \frac{-3U_2\cos\theta_2}{U_1\cos\theta_1 - U_2\cos\theta_2}. \quad (2.116)$$

2.9 Summary

Cosmic rays are energetic particles and gamma rays from space. The acceleration processes at shocks cause the power law spectrum of cosmic rays. From classical electrodynamics, we know that charged particles move along magnetic field lines and can be reflected by an intense magnetic field. The drift motion can happen when the particles are in a non-uniform magnetic field. At shocks, there is a discontinuity, where the magnetic field changes suddenly. There the

particles gain energy by shock drift acceleration and Fermi acceleration, which have already been developed into the theory of diffusive shock acceleration. The shock drift acceleration happens when the drift motion due to the non-uniform magnetic field is in the direction of the electric field at the shock. Fermi acceleration is due to the collisions between the particles and the irregular magnetic field with different relative velocities. In the nearly perpendicular case, the adiabatic treatment and the kink treatment give similar results for the distribution of energy gained and the distribution of reflected pitch angles. The particle motion can be considered in frames with no electric field. The frames with no electric field are the upstream frame, the downstream frame, and the de Hoffman-Teller frame. By using Liouville's theorem, we can find that the energy increases when particles cross the shock.

In our work, we see that the magnetic field at a nearly perpendicular shock probably crosses the shock more than one time. We can approximate the change in the particle's motion at the shock by using the adiabatic treatment since the adiabatic treatment can be used in the nearly perpendicular case. The frames we use are only the upstream frame, the downstream frame, and the de Hoffman-Teller frame. We can find the distribution of energy by considering the energy gained at each crossing and the probability of recrossing the shock again.

Chapter 3
Model Components

We introduce the model of the turbulent magnetic field in this chapter. We develop a new simulation method for the magnetic field line tracing. This method gives more accurate results and uses less time for the tracing simulation than the adaptive step size Runge-Kutta method does.

3.1 Turbulent magnetic field model

Fluid motions (such as the solar wind) in space are generally turbulent, so the magnetic field is also irregular. We use a two component model of the turbulent magnetic field in space (Matthaeus, Goldstein, & Roberts 1990). This model was motivated by the observation that solar wind fluctuations are concentrated at nearly parallel and nearly perpendicular wave numbers. This model provides a good explanation of the parallel transport of solar energetic particles (Bieber et al 1994; Bieber, Wanner, & Matthaeus 1996; Dröge 2000).

The total field includes a mean magnetic field and a turbulent magnetic field. The turbulent magnetic field is set to be perpendicular to the mean magnetic field. The magnetic field is written as

$$\mathbf{B} = B_0\hat{\mathbf{z}} + b_x(x, y, z)\hat{\mathbf{x}} + b_y(x, y, z)\hat{\mathbf{y}} \tag{3.1}$$

From (3.1), the mean magnetic field lies in the z direction, B_0 is a constant, and the turbulent magnetic field lies on the $x - y$ plane. The "slab" component, depending only on the z direction, and the "2D" component, depending only on

the x and y direction, are combined in the turbulent magnetic field:

$$\mathbf{b}_{slab} = b_x(z)\hat{\mathbf{x}} + b_y(z)\hat{\mathbf{y}} \tag{3.2}$$

$$\mathbf{b}_{2D} = b_x(x,y)\hat{\mathbf{x}} + b_y(x,y)\hat{\mathbf{y}} \tag{3.3}$$

From the Biot-Savart law, any magnetic field line must form a loop. This law implies that

$$\nabla \cdot \mathbf{B} = 0. \tag{3.4}$$

The slab magnetic field already follows this law by construction. The 2D component can be written as

$$\mathbf{b}^{2D}(x,y) = \nabla \times [a(x,y)\hat{\mathbf{z}}], \tag{3.5}$$

where $a(x,y)$ is related to a vector potential. It can be called the magnetic potential function for the 2D component. For any function of z for the slab field and any function of x and y for the magnetic potential function, the Biot-Savart law is not violated.

The slab and 2D magnetic fields are different. If we use only one of them, we obtain an unrealistic model of the magnetic field in space. In the case of the pure slab magnetic field, the magnetic field line generated from this field can diffuse though the space, but any position on the $x-y$ plane gives the same value of the magnetic field as shown in Figure 3.1. Thus the slab component allows diffusive behavior but a translation on $x-y$ plane gives no change in the magnetic field. In the case of the pure 2D magnetic field, the shape of the magnetic field line is periodic as shown in Figure 3.2. A combination of magnetic fields from both slab and 2D parts is much more realistic, and indeed is directly indicated by magnetic field data (Matthaeus, Goldstein, & Roberts 1990). When both slab

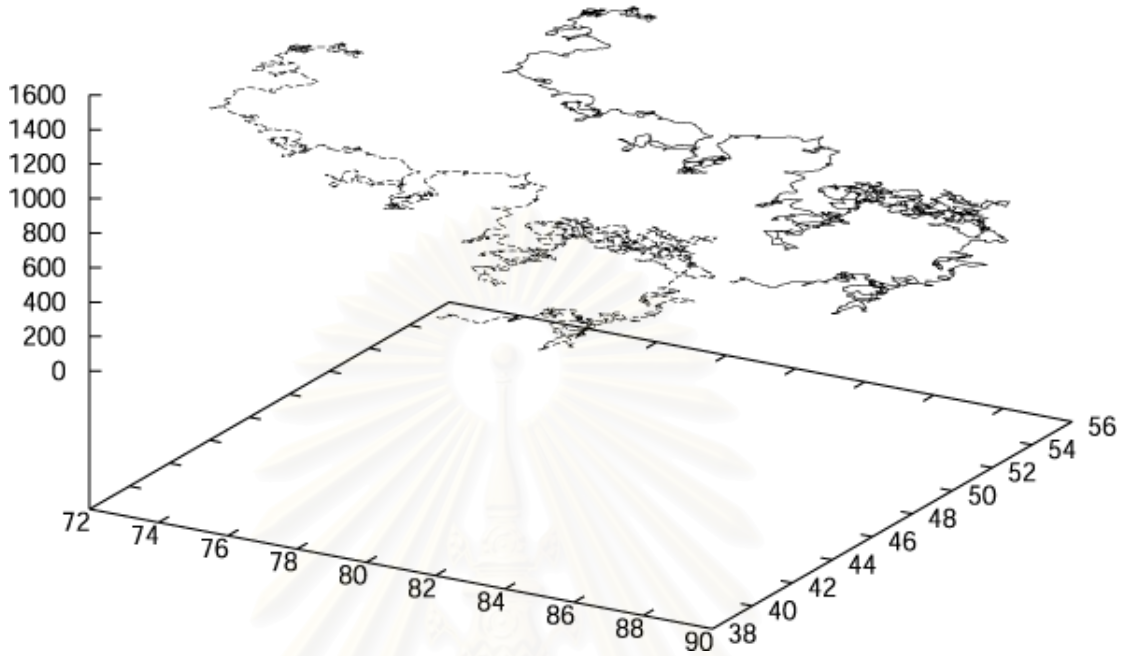

Figure 3.1: Two magnetic field lines in the pure slab case.

and 2D components are included into the model, different positions give different magnetic field lines and the magnetic field lines can diffuse as shown in Figure 3.3. Figures 3.1 to 3.3 are shown in arbitrary units.

3.2 Generating the magnetic field

Both the slab and 2D components are random functions since they are used to generate the turbulent magnetic field. These random functions are the results of the inverse Fourier transformation of a turbulent power spectrum with random phases. The same type of spectrum can be found in many turbulent phenomena.

Figure 3.4 shows a typical turbulent power spectrum in a log-log scale. The slope of -5/3 is a universal slope for intermediate wave numbers in all tur-

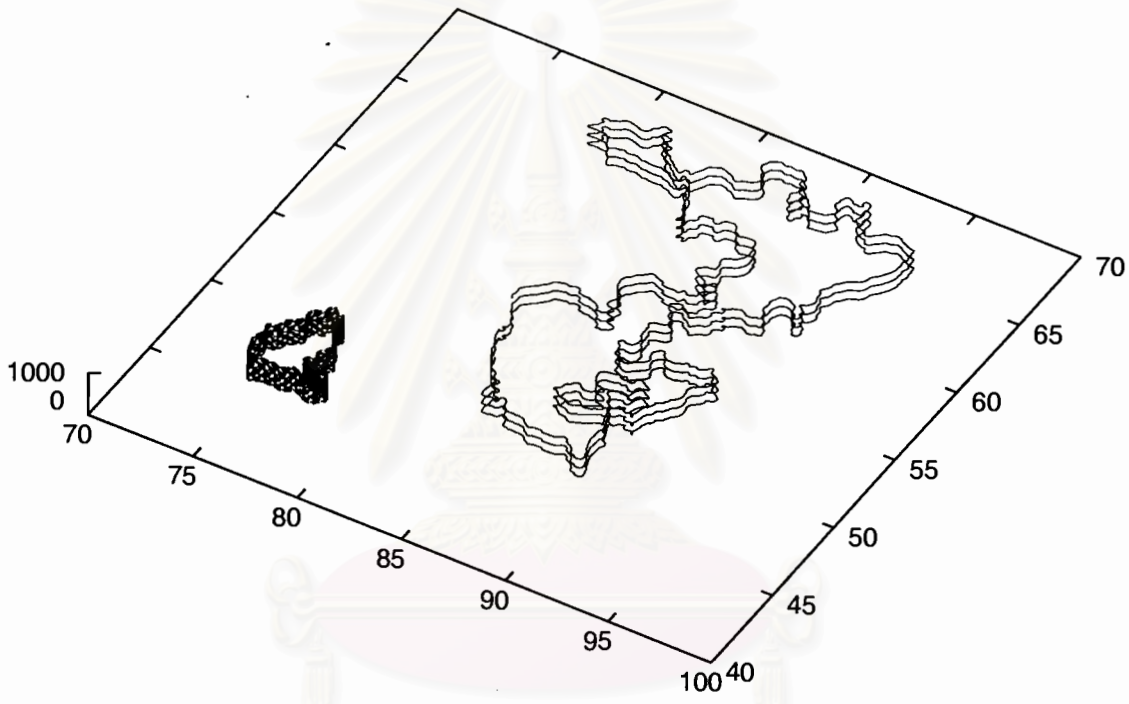

Figure 3.2: Two magnetic field lines in the pure 2D case.

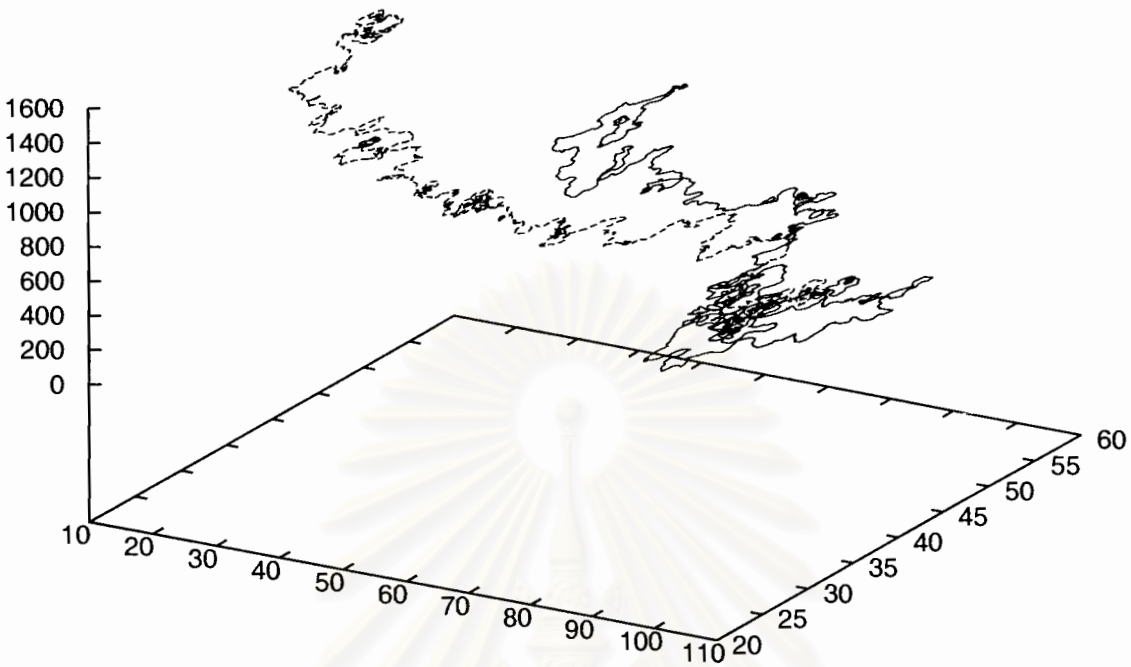

Figure 3.3: Two magnetic field lines in the composite turbulence case.

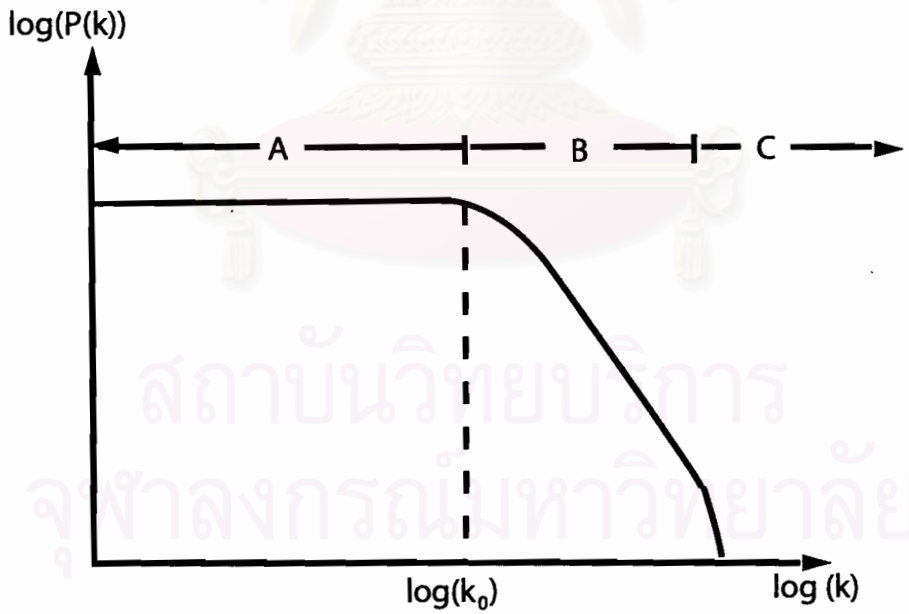

Figure 3.4: A typical turbulent spectrum that contains region A, the energy-containing range; region B, the inertial range; and region C, the dissipation range.

bulent phenomena. This is called the Kolmogorov power spectrum after the discoverer of the universal spectrum. The scale k_0 divides the wave numbers into two groups, large and small distance scales. These are visualized as eddy sizes in a turbulent flow. The large scale eddies are represented by small wave numbers in region A. These are the scales that energy is fed into. The small scale eddies are represented by large wave numbers in regions B and C. These receive energy from the large scales. This energy transfer into small scales is called an energy cascade. For the smallest eddy in region C, there is dissipation of energy since the fluid viscosity is important. The scale of k_0 corresponds to scale of the correlation length of the magnetic field. The correlation length l_c is defined as

$$l_c \equiv \frac{\int_0^\infty \langle b_x(z_0) b_x(z_0 + \Delta z)\rangle d\Delta z}{\langle b_x^2 \rangle} \tag{3.6}$$

and $k_0 = 1/l_c$

3.2.1 Generating the slab field

The slab magnetic field is a random function with

$$\langle b_x^{slab} \rangle = 0, \qquad \langle b_y^{slab} \rangle = 0, \tag{3.7}$$

since the mean magnetic field is parallel to the z direction. To express the turbulent properties, we use a power spectrum as in Figure 3.4 for regions A and B.

In fact, the power spectrum of a magnetic field is the Fourier transform of the correlation function:

$$P_{xx}(\mathbf{k}) \equiv \frac{1}{(2\pi)^{\frac{n}{2}}} \int_{-\infty}^{\infty} R_{xx}(\mathbf{r}) \exp[i(\mathbf{r}\cdot\mathbf{k})] d^n r \tag{3.8}$$

$$P_{yy}(\mathbf{k}) \equiv \frac{1}{(2\pi)^{\frac{n}{2}}} \int_{-\infty}^{\infty} R_{yy}(\mathbf{r}) \exp[i(\mathbf{r}\cdot\mathbf{k})] d^n r, \tag{3.9}$$

where n is the dimensionality of the fluctuations (slab: $n = 1$, 2D: $n = 2$) and the correlation function is defined by

$$R_{xx}(\mathbf{r}) \equiv \langle b_x(\mathbf{r}_0) b_x(\mathbf{r}_0 + \mathbf{r}) \rangle \tag{3.10}$$

$$R_{yy}(\mathbf{r}) \equiv \langle b_y(\mathbf{r}_0) b_y(\mathbf{r}_0 + \mathbf{r}) \rangle. \tag{3.11}$$

First, the power spectrum (P_{xx}^{slab} or P_{yy}^{slab}) is generated. One possible spectrum is

$$P_{xx}^{slab}(k_z) = P_{yy}^{slab}(k_z) = \frac{C_1}{[1 + (k_z l_z)^2]^{\frac{5}{6}}}, \tag{3.12}$$

where l_z is a characteristic length scale related to l_c in 3.6

$P_{xx}^{slab}(k_z)$ and $P_{yy}^{slab}(k_z)$ are also proportional to $|b_x^{slab}(k_z)|^2$ and $|b_y^{slab}(k_z)|^2$. After that, a random phase in each component is generated to form a complex number with no preferred phase in wave number space:

$$\begin{aligned} b_x^{slab}(k_z) &= \sqrt{P_{xx}^{slab}(k_z)} \exp(i\phi_x) \\ &= \sqrt{P_{xx}^{slab}(k_z)} \cos\phi_x + i\sqrt{P_{xx}^{slab}(k_z)} \sin\phi_x, \end{aligned} \tag{3.13}$$

$$\begin{aligned} b_y^{slab}(k_z) &= \sqrt{P_{yy}^{slab}(k_z)} \exp(i\phi_y) \\ &= \sqrt{P_{yy}^{slab}(k_z)} \cos\phi_y + i\sqrt{P_{yy}^{slab}(k_z)} \sin\phi_y. \end{aligned} \tag{3.14}$$

where i is $\sqrt{-1}$, and ϕ_x and ϕ_y are random phases for each k_z (varying from 0 to 2π).

Finally, we transform $\mathbf{b}^{slab}$ into real space by inverse Fourier transforms. We can write the slab magnetic field as

$$b_x^{slab}(z) = \frac{1}{\sqrt{2\pi}} \int_{-\infty}^{\infty} b_x^{slab}(k_z) \exp(-ik_z z) dk_z, \tag{3.15}$$

$$b_y^{slab}(z) = \frac{1}{\sqrt{2\pi}} \int_{-\infty}^{\infty} b_y^{slab}(k_z) \exp(-ik_z z) dk_z, \tag{3.16}$$

$$\mathbf{b}^{slab}(z) = b_x^{slab}(z)\hat{\mathbf{x}} + b_y^{slab}(z)\hat{\mathbf{y}}. \tag{3.17}$$

Note that the numerical method that we use for the inverse Fourier transform is the "fast Fourier transform" (Press et al. 1992). In the numerical method, we divided the total length of z into 2^n grid points, where we used $n = 22$.

3.2.2 Generating the 2D field

The power spectrum of the 2D magnetic field must also have the characteristics of the energy-containing range and of the Kolmogorov power spectrum. The magnetic field must be consistent with (3.4) so we start by generating the potential function $a(x, y)$ so that the inverse Fourier transform of the correlation function $\langle a(\mathbf{r}_0)a(\mathbf{r}_0 + \mathbf{r})\rangle$ is

$$A(k_\perp) = \frac{1}{[1 + (k_\perp l_\perp)^2]^{\frac{7}{3}}}, \tag{3.18}$$

where

$$k_\perp = \sqrt{k_x^2 + k_y^2}, \tag{3.19}$$

and $l_\perp$ is related to the correlation length in the $x - y$ plane.

This spectrum gives a magnetic field power spectrum proportional to $k^{-5/3}$ for large wave numbers. Then, the inverse Fourier transform of $a(x, y)$ is

$$a(k_\perp) = \sqrt{A(k_\perp)}\exp(i\phi). \tag{3.20}$$

The random phase ϕ is used to create a complex number for $a(k_\perp)$ for the same reason as for the slab part.

The relation between the magnetic field and potential function in wave number space can be written as

$$\mathbf{b}^{2D}(k_x, k_y) = -i\mathbf{k} \times [a(k_x, k_y)\hat{\mathbf{z}}]. \tag{3.21}$$

Now one way to generate the 2D magnetic field in real space is

$$b_x^{2D}(x,y) = \frac{1}{2\pi}\int_{-\infty}^{\infty}\int_{-\infty}^{\infty} b_x^{2D}(k_x,k_y)\exp[-i(\mathbf{r}\cdot\mathbf{k})]dk_xdk_y, \quad (3.22)$$

$$b_y^{2D}(x,y) = \frac{1}{2\pi}\int_{-\infty}^{\infty}\int_{-\infty}^{\infty} b_y^{2D}(k_x,k_y)\exp[-i(\mathbf{r}\cdot\mathbf{k})]dk_xdk_y. \quad (3.23)$$

We use the fast Fourier transform as the numerical technique. This yields b^{slab} and b^{2D} at equally spaced grid points. In this work, we actually generate the magnetic field by using $\vec{b_2} = \nabla \times [a(x,y)\hat{z}]$, where this magnetic field $\vec{b}_2$ is calculated after we use the inverse Fourier transform to generate the potential function. If we calculate the magnetic field $\vec{b}_1$ in wave number space and then transform into real space, using equations (3.21) to (3.23), this magnetic field is different from the magnetic field that we actually use. Let

$$\begin{aligned} a(x,y) &= \sum_{k_x}\sum_{k_y} a(k_x,k_y)\exp\left[-i(k_xx+k_yy)\right] \\ &= \sum_{k_x}\sum_{k_y} |a(k_x,k_y)|\exp\left[i(\phi-k_xx-k_yy)\right], \end{aligned} \quad (3.24)$$

where $a(k_x,k_y) = |a(k_x,k_y)|\exp(i\phi)$, and ϕ is a random phase that is different for each (k_x,k_y). Then consider the x-component of the 2D magnetic field. From (3.21), the component b_{1x} is given by

$$b_{1x}(x,y) = \sum_{k_x}\sum_{k_y} -ik_y a(k_x,k_y)\exp\left[-i(k_xx+k_yy)\right]. \quad (3.25)$$

Because the magnetic field is real, $a(-k_x,-k_y) = a(k_x,k_y)^*$. Equation (3.25) is written as

$$b_{1x} = \sum_{k_x}\sum_{k_y\geq 0} 2\mathrm{Re}\left\{-ik_y|a|\exp\left[i(\phi-k_xx-k_yy)\right]\right\}, \quad (3.26)$$

However, b_{2x} is calculated from the potential function in real space by

$$b_{2x}(x,y) = \frac{A(x,y+\Delta y)-A(x,y)}{\Delta y}$$

$$
\begin{aligned}
&= \sum_{k_x}\sum_{k_y} a(k_x,k_y)\exp\left[-i(k_x x + k_y(y+\Delta y))\right]/\Delta y \\
&\quad -a(k_x,k_y)\exp\left[-i(k_x x + k_y y)\right]/\Delta y \\
&= 2\sum_{k_x}\sum_{k_y\geq 0} \\
&\quad \mathrm{Re}\left\{-ik_y|a|\exp i(\phi - k_x x - k_y y)\left[\frac{\exp(-ik_y\Delta y)-1}{-ik_y\Delta y}\right]\right\} \qquad (3.27)
\end{aligned}
$$

Each (k_x, k_y) component in b_{2x} is that for b_{1x} multiplied by $|[1-\exp(-ik_y\Delta y)]/ik_y\Delta y|$, which is always less than or equal to one. Therefore,

$$\langle b_{1x}^2\rangle > \langle b_{2x}^2\rangle. \qquad (3.28)$$

Therefore, we need to use a small value of Δy to maintain an approximately correct variance of the turbulence in the magnetic field. We need $\Delta y \ll l_\perp$, because when $\Delta y \geq l_\perp$, the value of $|a(k_x,k_y)|$ drops very fast.

3.3 Magnetic field line tracing

The position of a magnetic field line is determined as

$$\frac{dx}{B_x} = \frac{dy}{B_y} = \frac{dz}{B_z}. \qquad (3.29)$$

This equation guarantees that at any point, the magnetic field at that point is parallel to the magnetic field line.

3.3.1 Magnetic field line tracing in the pure slab case

In the pure slab case, (3.29) becomes

$$\frac{dx}{dz} = \frac{b_x^{slab}}{B_0}, \qquad \frac{dy}{dz} = \frac{b_y^{slab}}{B_0}. \qquad (3.30)$$

The magnetic field computed from the Fourier transform is discrete and exists on the grid points of z. Therefore, to trace the field lines between grid points using

(3.29), we need to determine $\mathbf{b}^{slab}$ at intermediate points by interpolation. Here we use linear interpolation of $\mathbf{b}^{slab}$ so the magnetic field between the grid points is

$$b_x^{slab}(z) = \frac{z - i\delta z}{\delta z}(b_x^{slab})_{i+1} + \frac{(i+1)\delta z - z}{\delta z}(b_x^{slab})_i, \tag{3.31}$$

where δz is the distance between the grid points, i and $i+1$ label the grid points at $z = i\delta z$ and $(i+1)\delta z$, and z is the position between two grid points. We can rewrite the magnetic field between grid points as

$$b_x^{slab}(z) = m_x z + c_x, \tag{3.32}$$

where

$$m_x = \frac{(b_x^{slab})_{i+1} - (b_x^{slab})_i}{\delta z}, \tag{3.33}$$

and

$$c_x = (b_x^{slab})_i(i+1) - (b_x^{slab})_{i+1} i. \tag{3.34}$$

This method is also used for the y component:

$$b_y^{slab}(z) = m_y z + c_y, \tag{3.35}$$

where

$$m_y = \frac{(b_y^{slab})_{i+1} - (b_y^{slab})_i}{\delta z}, \tag{3.36}$$

and

$$c_y = (b_y^{slab})_i(i+1) - (b_y^{slab})_{i+1} i. \tag{3.37}$$

Now, (3.30) becomes

$$\frac{dx}{dz} = \frac{m_x z + c_x}{B_0} \tag{3.38}$$

$$\frac{dy}{dz} = \frac{m_y z + c_y}{B_0}. \tag{3.39}$$

And the solutions are

$$x = x_0 + \frac{1}{B_0}\left[m_x(z^2 - z_0^2) + c_x(z - z_0)\right] \tag{3.40}$$

$$y = y_0 + \frac{1}{B_0}\left[m_y(z^2 - z_0^2) + c_y(z - z_0)\right] \tag{3.41}$$

for a starting location (x_0, y_0, z_0)

3.3.2 Magnetic field line tracing in the pure 2D case

As the magnetic field is discrete and depends on x and y, bilinear interpolation is used. The potential function between four grid points can be written as

$$\begin{aligned} a(x,y) = {} & \frac{(x - i\delta x)(y - j\delta y)}{\delta x\,\delta y} a_{i+1,j+1} + \frac{[(i+1)\delta x - x](y - j\delta y)}{\delta x\,\delta y} a_{i,j+1} \\ & + \frac{(x - i\delta x)[(j+1)\delta y - y]}{\delta x\,\delta y} a_{i+1,j} + \frac{[(i+1)\delta x - x][(j+1)\delta y - y]}{\delta x\,\delta y} a_{i,j}, \end{aligned} \tag{3.42}$$

or as the simpler expression

$$a(x,y) = a_1 xy + a_2 x + a_3 y + a_4. \tag{3.43}$$

Then the magnetic field within this cell is

$$b_x^{2D} = \frac{\partial a}{\partial y} = a_1 x + a_3, \tag{3.44}$$

and

$$b_y^{2D} = -\frac{\partial a}{\partial x} = -a_1 y - a_2, \tag{3.45}$$

so (3.29) becomes

$$\frac{dx}{dz} = \frac{a_1 x + a_3}{B_0} \tag{3.46}$$

$$\frac{dy}{dz} = -\frac{a_1 y + a_2}{B_0}. \tag{3.47}$$

The solutions of (3.46) and (3.47) are

$$\frac{z-z_0}{B_0} = \frac{1}{a_1}\ln\left(\frac{a_1x+a_3}{a_1x_0+a_3}\right) \tag{3.48}$$

$$\frac{z-z_0}{B_0} = -\frac{1}{a_1}\ln\left(\frac{a_1y+a_2}{a_1y_0+a_2}\right) \tag{3.49}$$

for a starting location (x_0, y_0, z_0). These can also be expressed as

$$x = \frac{a_1x_0+a_3}{a_1}\exp\left[\frac{a_1}{B_0}(z-z_0)\right] - \frac{a_3}{a_1} \tag{3.50}$$

$$y = \frac{a_1y_0+a_2}{a_1}\exp\left[-\frac{a_1}{B_0}(z-z_0)\right] - \frac{a_2}{a_1}, \tag{3.51}$$

3.3.3 Magnetic field line tracing in composite turbulence

For composite 2D+slab turbulence, we interpolate $\mathbf{b}^{slab}$ and a within an x-y-z cell as above. Then (3.29) becomes

$$\frac{dx}{dz} = \frac{m_xz+a_1x+C_x}{B_0}, \tag{3.52}$$

where

$$C_x = c_x + a_3, \tag{3.53}$$

and

$$\frac{dy}{dz} = \frac{m_yz-a_1y+C_y}{B_0}, \tag{3.54}$$

where

$$C_y = c_y - a_2. \tag{3.55}$$

The solutions of these equations are

$$x = A_x\exp\left(\frac{a_1}{B_0}z\right) - \frac{m_x}{a_1}z - \left[\frac{m_xB_0+C_xa_1}{a_1^2}\right] \tag{3.56}$$

$$y = A_y\exp\left(\frac{-a_1}{B_0}z\right) + \frac{m_y}{a_1}z - \left[\frac{m_yB_0-C_ya_1}{a_1^2}\right], \tag{3.57}$$

where A_x and A_y are constants calculated from the initial position of the field line.

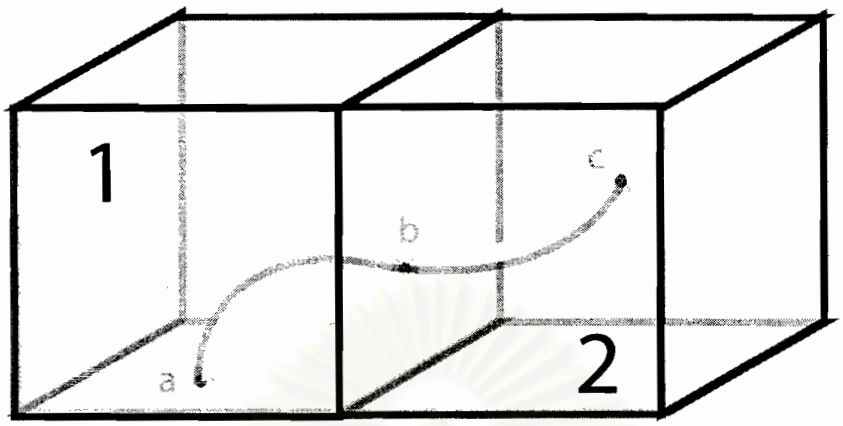

Figure 3.5: Magnetic field line passing through Box 1 and into Box 2.

3.3.4 Magnetic field line tracing across cell boundaries

All the analytic solutions we have shown so far can be used only within one cell surrounded by grid points. If we want to connect the field line across each cell the field line passes, we must find the position at the cell's wall where the field line passes through and exits the cell. Then the final position of the previous cell is the initial position of the next cell. When we find the initial and final positions in each cell, we will obtain the whole field line.

In Figure 3.5 point "a" is the initial point of the tracing in Box 1, and point "b" is the end of the field line in Box 1. Point "b" is also the initial point for tracing the field line in Box 2 and point "c" is the end of the field line in Box 2.

3.4 Shock model

A shock is a discontinuity in fluid parameters. This discontinuity always forms a sheet as shown in Figure 3.6. This sheet divides space into two parts, upstream and downstream. In the upstream part, the fluid has not yet encoun-

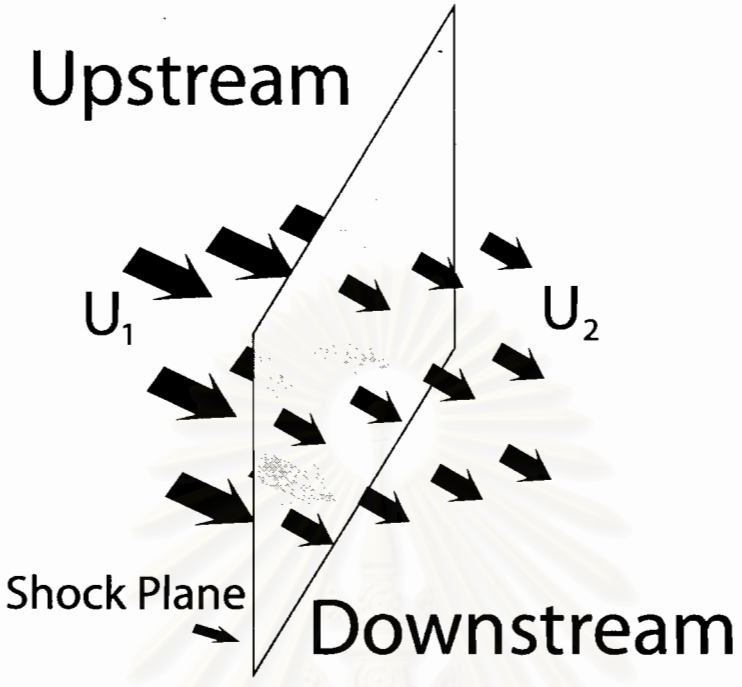

Figure 3.6: The shock plane is the border between upstream region and downstream region.

tered the shock. For the matter in this part, $\vec{U_1}$ is set to be the average velocity coming to the shock. In the downstream part, the fluid has already passed the shock. For the matter in this part, $\vec{U_2}$ is set to be the average velocity.

In the magnetic field model, we set the z direction along the average magnetic field. We will consider only the case of a nearly perpendicular shock. In this case, the average magnetic field is nearly perpendicular to the shock normal. Let the shock normal be in the $x-z$ plane as $\hat{n} = a_1\hat{x} + a_2\hat{z}$. If the angle between the mean magnetic field and the shock normal is θ, then

$$\hat{n} \cdot \hat{z} = a_2 = \cos\theta \tag{3.58}$$

and $a_1 = \sin\theta$, so the equation of the shock plane is

$$(x - x_0)\sin\theta + (z - z_0)\cos\theta = 0, \tag{3.59}$$

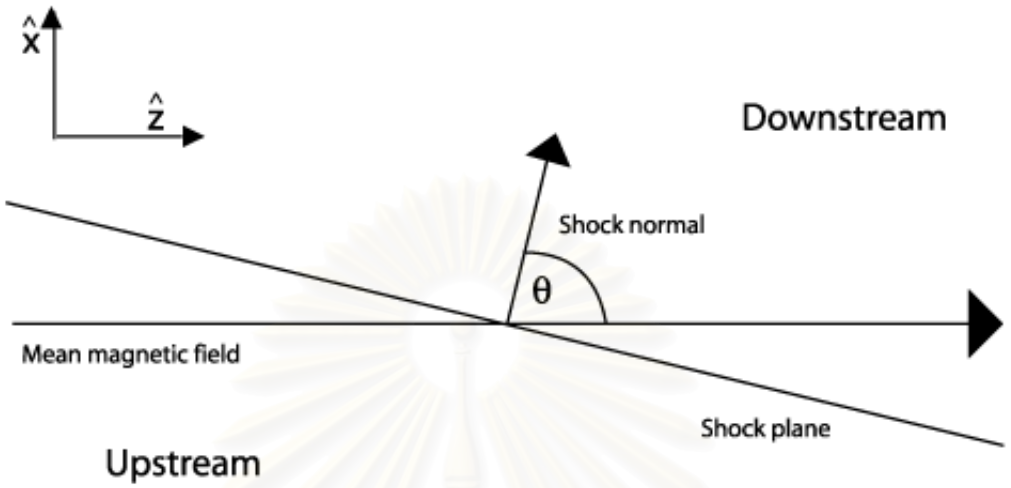

Figure 3.7: Shock plane and the mean magnetic field.

and $a_1 = \sin\theta$, so the equation of the shock plane is

$$(x - x_0)\sin\theta + (z - z_0)\cos\theta = 0, \tag{3.59}$$

where (x_0, z_0) is a point on the shock plane. If $(x - x_0)\sin\theta + (z - z_0)\cos\theta > 0$, then (x, z) is taken to be downstream. If $(x - x_0)\sin\theta + (z - z_0)\cos\theta < 0$, then (x, z) is set to be upstream. Figure 3.7 shows the shock plane, the shock normal, and the mean magnetic field.

Chapter 4

Statistics of magnetic field line-shock crossings

From Chapter 2, we know that the shape of the magnetic field affects the motion of charged particles. Since the magnetic field is turbulent, the particles can move and diffuse along the magnetic field. Therefore the particles can come back to the shock many times. The energy gained and the probability of escape from the shock depend on the number of shock-field crossings, the crossing angles, and the distance between crossings.

4.1 Parameters in the magnetic field line program

First, we describe the parameters that are used to create the power spectrum of the magnetic field. The parameter $\delta b/B_0$ is related to the energy of the turbulent magnetic field, where $\delta b = \sqrt{\langle b_x^2 \rangle + \langle b_y^2 \rangle}$, and B_0 is the average magnetic field. We set $B_0 = 1$ for convenience. Because the magnetic field has two components, slab and 2D, the parameter E_{slab} is the ratio of the energy in the "slab" component to the total energy in the turbulent magnetic field. Then the ratio of the energy of "2D" components to the total energy is $1 - E_{slab}$. From chapter 3, the slab power spectrum of the turbulent magnetic field is

$$P_{xx}^{slab}(k_z) = P_{yy}^{slab}(k_z) = \frac{C_1}{[1 + (k_z l_z)^2]^{\frac{5}{6}}}, \tag{4.1}$$

and the 2D power spectrum of the turbulent potential function is

$$A(k_\perp) = \frac{1}{[1 + (k_\perp l_\perp)^2]^{\frac{7}{3}}}. \tag{4.2}$$

The parameter l_z is proportional to the correlation length of the slab magnetic field. If we know the correlation length of the turbulent magnetic field in space, we can set the actual scale of the magnetic field in the model. The parameter $l_\perp$ is proportional to the correlation length of the 2D magnetic field

After we set the parameters for the power spectra of both slab and 2D magnetic fields, we will generate the magnetic field in wave number space. Then we transform it into real space according to methods in chapter 3. Before the transformation, we must set the size of the box and the number of grid points inside the box. We set the length along the mean magnetic field to be $100,000$ in arbitary units (au) with $2^{22} = 4,194,304$ grid points. Thus Δz between data points is $100,000/4,194,304 = 0.0238$ au. The distance Δz is not changed for all simulations. The length in x and y is 200 au with $2^{12} = 4,096$ grid points. Thus $\Delta x = \Delta y = 0.0488$ in all simulations. The last parameter is the upstream angle between the mean magnetic field and the shock normal. We set the angle to be 89° as the approximate value determined for the termination shock in Chapter 2.

The speed of the bulk plasma changes immediately after passing the shock. Let r be the ratio of the bulk plasma speed before passing the shock to that after passing the shock. Let the shock normal be $\hat{x}$. Since the magnetic field line is dragged by the plasma, in the downstream region, the component of the magnetic field in the x direction is contracted r times. We can generate the magnetic field line without being concerned with the shock. After the field line is in the downstream region we can contract its x component. This contraction has no effect on collected data, the number of crossings, the upstream angle, or the distance between crossings.

When we generate magnetic field lines, we vary the values of $\delta b/B_0$, E_{slab},

l_z, and $l_\perp$ to understand which parameters affect the number of crossings, the crossing angle, and the distance between each crossing. All magnetic field line positions are collected on the grid points along the z direction.

4.2 Number of crossings

In this section, the number of shock-field crossings per simulated magnetic field line is counted. The number of crossings can reduce the probability of particles' escape from the shock. The particles are known to follow the magnetic field line and come to the shock around the shock-field crossing position. Some of the particles are reflected back to the upstream region because their pitch angle is not low enough to be in the loss cone that enters the downstream region. Some particles can be transmitted into the downstream region, and can come back to the shock again, if the magnetic field line they follow crosses the shock again. If the distance between each crossing is further than the particle's mean free path, the pitch angle is randomly changed. The particles can diffuse back to the shock before the next crossing or are reflected back at the next crossing. If there are many shock-field crossings, we expect a low probability of particles' escape. For each crossing, the particle gains energy in both directions, upstream to downstream and downstream to upstream. If there are many crossings, the particles are accelerated many times.

In our simulations, the magnetic field line starts from one side of the shock and then crosses to the other side of the shock. If the magnetic field line crosses the shock twice, it is back to the same side as before crossing. If the magnetic field line is on the other side, the number of crossings is odd. After all crossings the magnetic field line must be on the other side so the number of crossings must

be an odd number.

Figures 4.1 to 4.3 show the effect of $\delta b/B_0$ on the number of crossings in the pure slab case. From the Figures, a field line can cross a shock more often when $\delta b/B_0$ is larger. Now we change only l_z in the pure slab case, and the distributions are shown in Figure 4.4 for $l_z = 0.5$ au and $l_z = 0.1$ au, respectively. We can see that the number of crossings does not depend on l_z in the pure slab case.

Since the compound case is more realistic, we set $E_{slab} = 0.8$ and vary the value of $\delta b/B_0$. Figures 4.5 to 4.7 show the effect of various $\delta b/B_0$ on the number of crossings at $E_{slab} = 0.8$. We also show the probability at $E_{slab} = 0.5$, in Figures 4.8 to 4.10, and $E_{slab} = 0.2$, in Figures 4.11 to 4.13. From the data, the probability does not depend on E_{slab}.

For compound turbulence, the change in the scale of the magnetic field again has no effect on the probability distribution of the number of crossings. The probability distributions of the number of crossings with $\delta b/B_0 = 0.5$ and $E_{slab} = 0.5$ are shown in Figure 4.14 with $l_z = 0.5$ au and $l_\perp = 1$ au, and Figure 4.15 with $l_z = 1$ au and $l_\perp = 0.2$ au. The probability distributions of the number of crossings with $\delta b/B_0 = 0.5$ and $E_{slab} = 0.2$ are shown in Figure 4.16 with $l_z = 0.5$ au and $l_\perp = 1$ au, and Figure 4.17 with $l_z = 1$ au and $l_\perp = 0.2$ au.

Now we consider the pure 2D case. The pure 2D case does not have diffusive properties since the magnetic field lines form periodic spiral lines because each field line follows a path at a constant value of the potential function. Therefore the distribution of the number of crossings is not like those in the pure slab and compound cases. Figures 4.18 to 4.20 show the distributions of the number of crossings for the pure 2D case with $\delta b/B_0$= 0.5, 0.3, and 0.1, respectively.

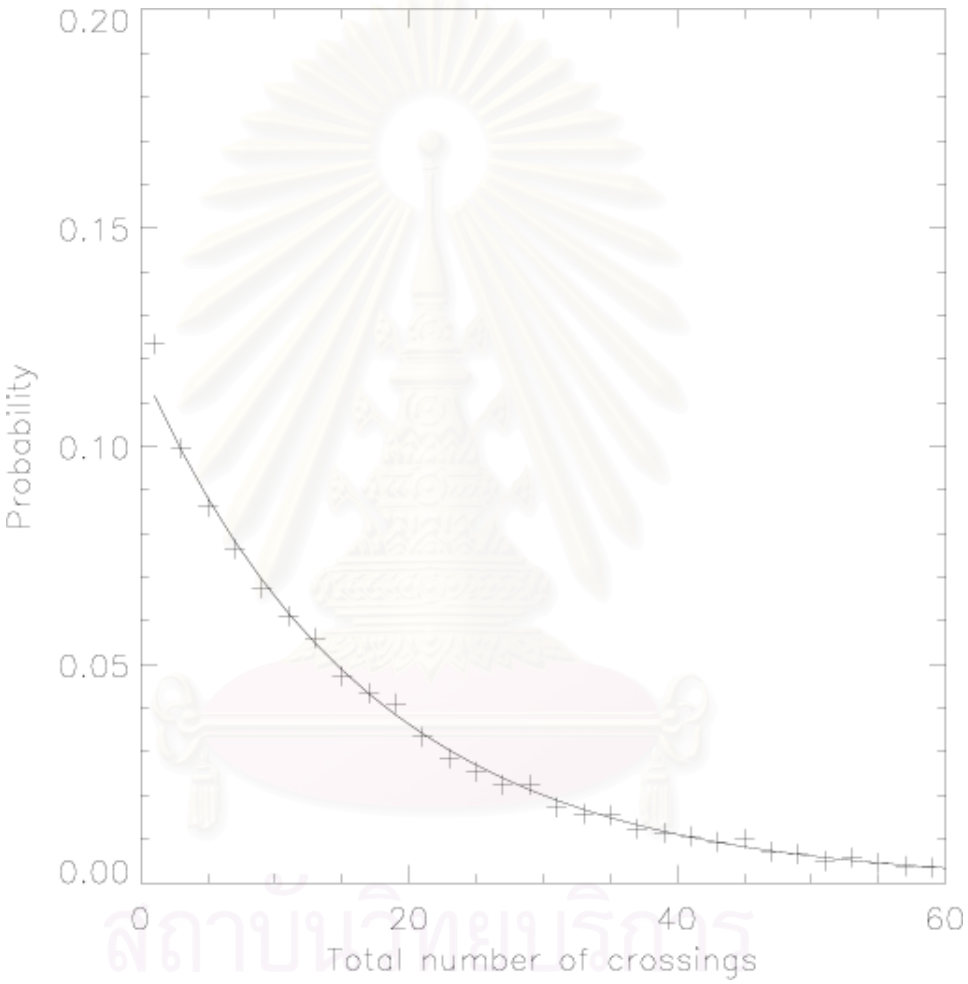

Figure 4.1: The probability distribution vs. the number of shock-field crossings of a nearly perpendicular shock at $\delta b/B_0 = 0.5$, $E_{slab} = 1$, and $l_z = 1$ is plotted with the fitted curve.

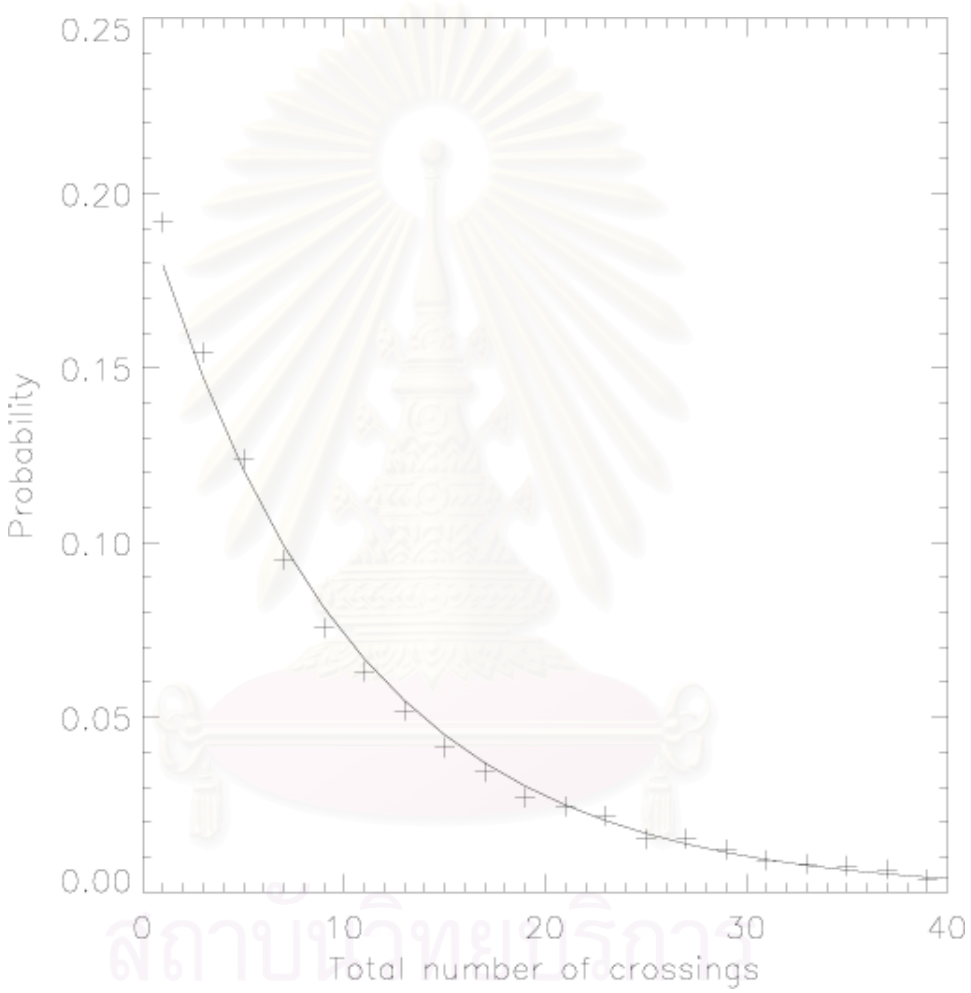

Figure 4.2: The probability distribution vs. the number of shock-field crossings of a nearly perpendicular shock at $\delta b/B_0 = 0.3$, $E_{slab} = 1$, and $l_z = 1$ is plotted with the fitted curve.

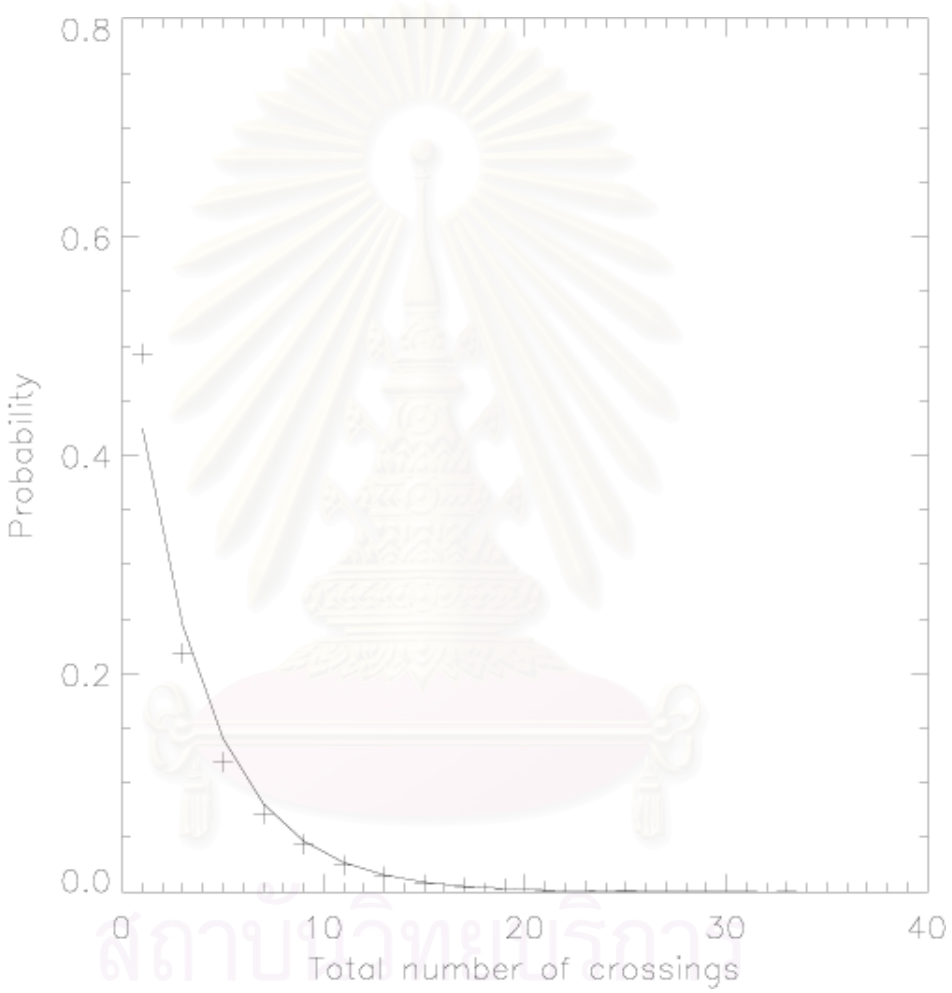

Figure 4.3: The probability distribution vs. the number of shock-field crossings of a nearly perpendicular shock at $\delta b/B_0 = 0.1$, $E_{slab} = 1$, and $l_z = 1$ is plotted with the fitted curve.

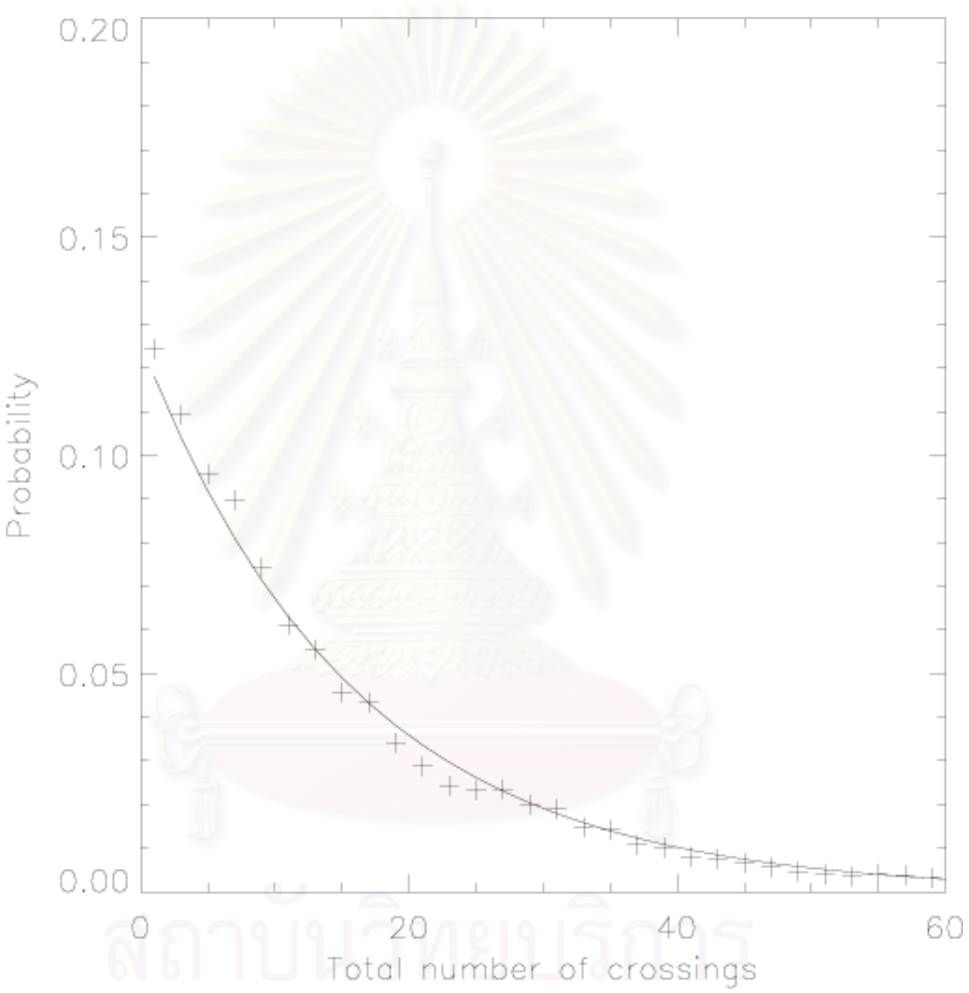

Figure 4.4: The probability distribution vs. the number of shock-field crossings of a nearly perpendicular shock at $\delta b/B_0 = 0.5$, $E_{slab} = 1$, and $l_z = 0.5$ is plotted with the fitted curve.

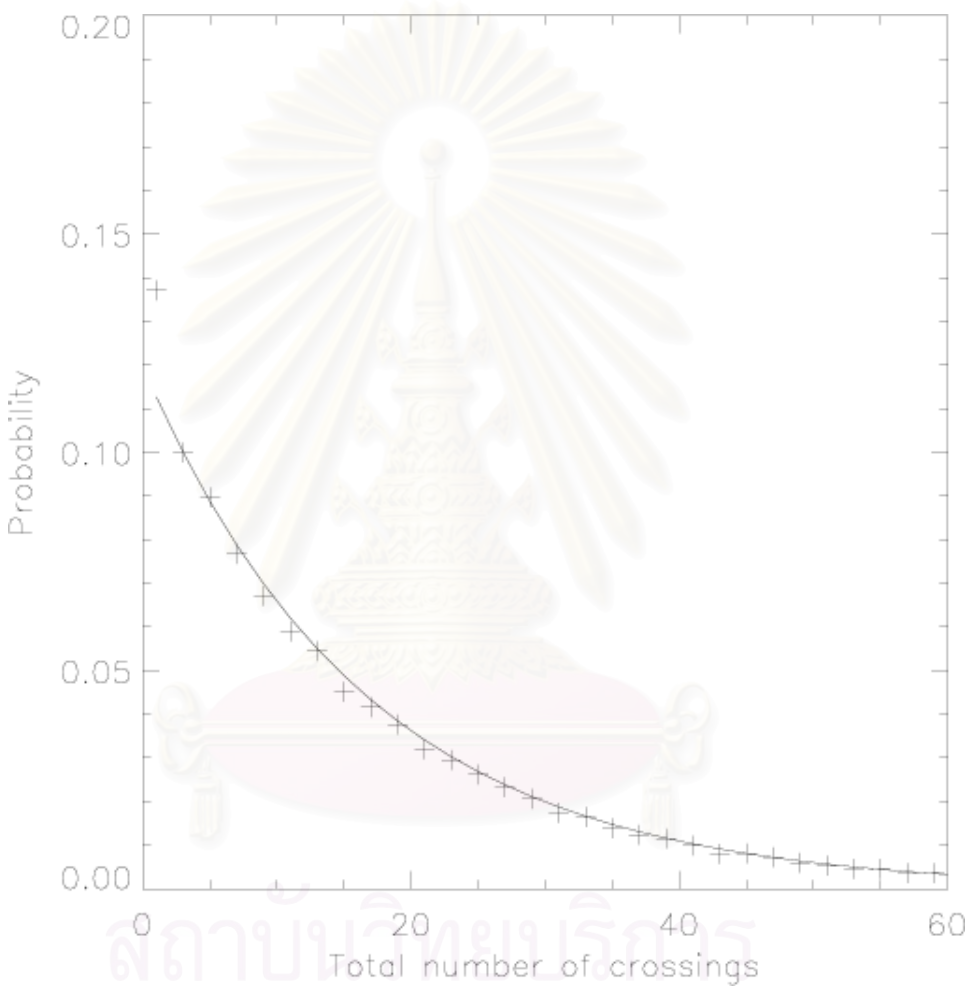

Figure 4.5: The probability distribution vs. the number of shock-field crossings of a nearly perpendicular shock is plotted with the fitted curve at $\delta b/B_0 = 0.5$, $E_{slab} = 0.8$, $l_z = 1$, and $l_\perp = 1$.

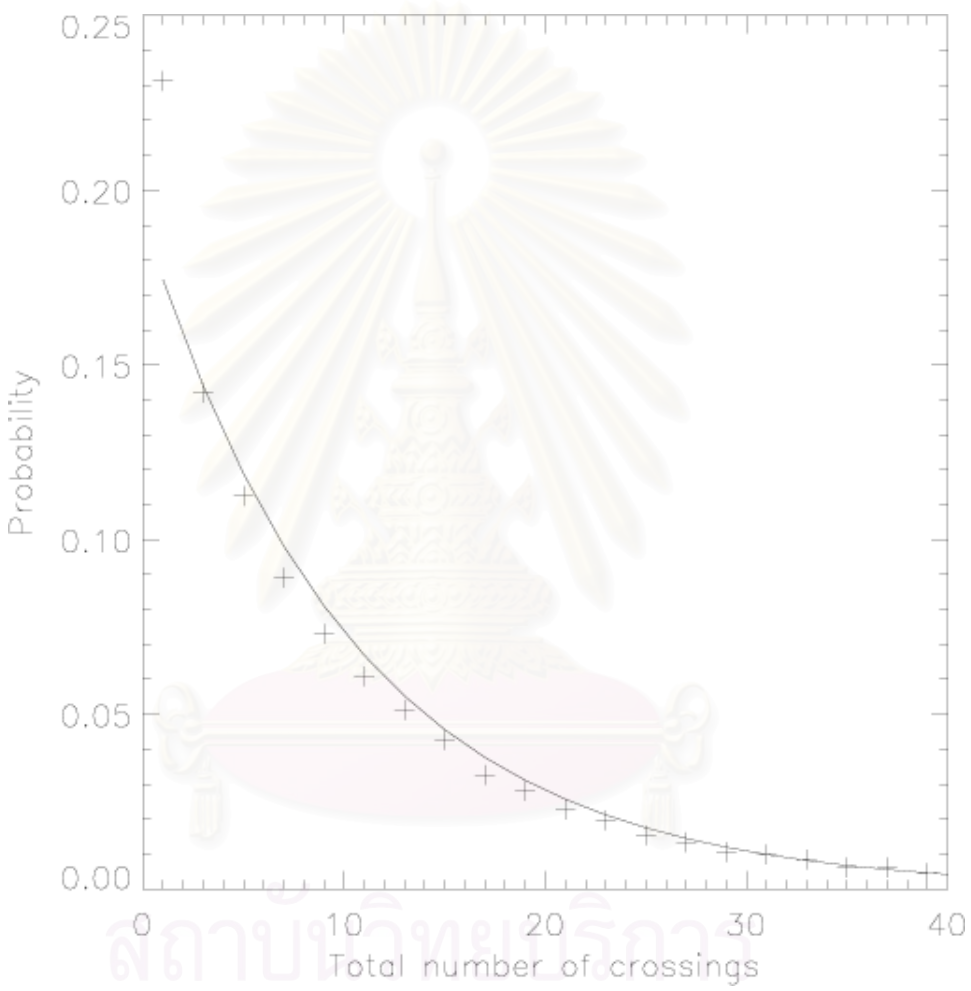

Figure 4.6: The probability distribution vs. the number of shock-field crossings of a nearly perpendicular shock is plotted with the fitted curve at $\delta b/B_0 = 0.3$, $E_{slab} = 0.8$, $l_z = 1$, and $l_\perp = 1$.

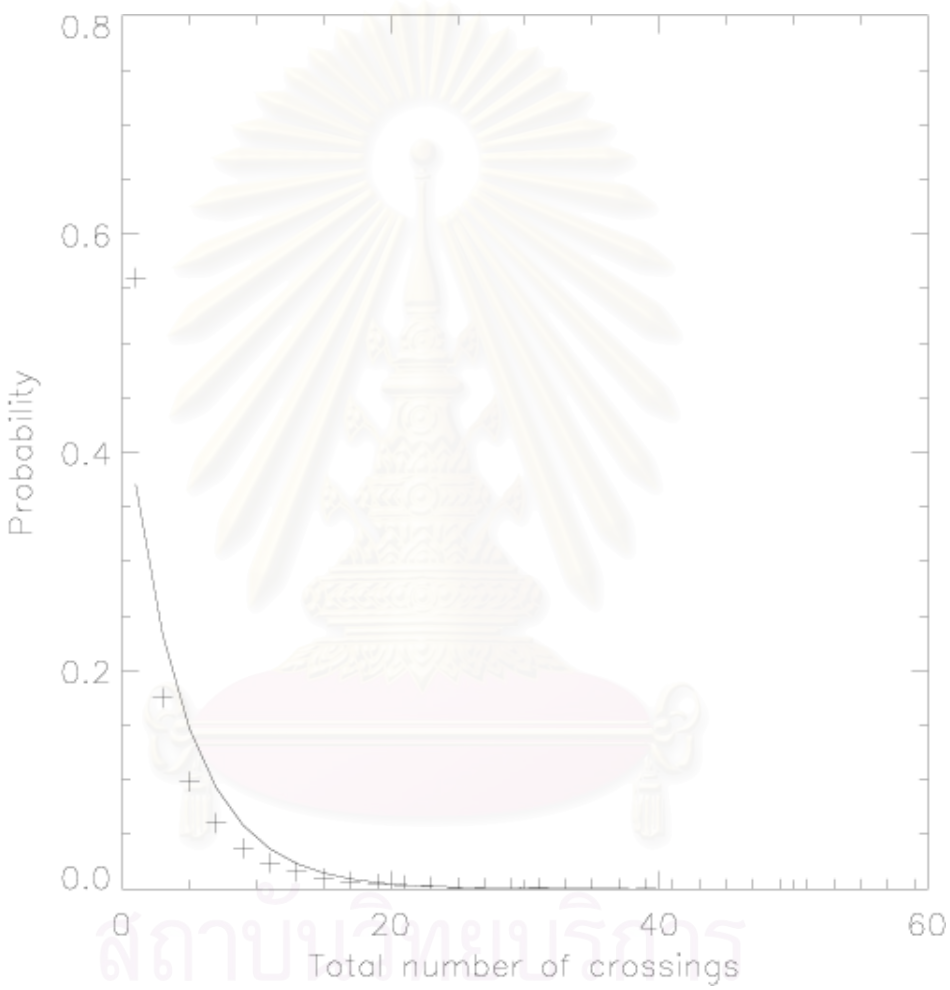

Figure 4.7: The probability distribution vs. the number of shock-field crossings of a nearly perpendicular shock is plotted with the fitted curve at $\delta b/B_0 = 0.1$, $E_{slab} = 0.8$, $l_z = 1$, and $l_\perp = 1$.

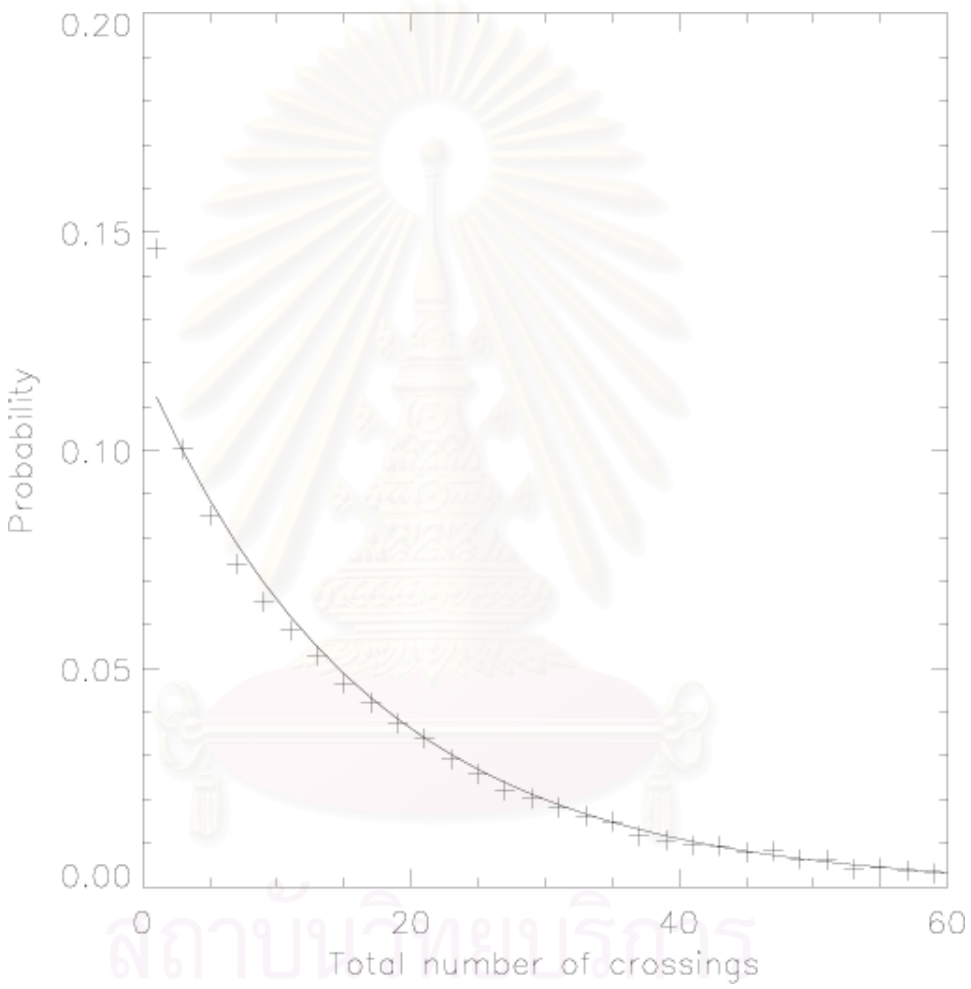

Figure 4.8: The probability distribution vs. the number of shock-field crossings of a nearly perpendicular shock is plotted with the fitted curve at $\delta b/B_0 = 0.5$, $E_{slab} = 0.5$, $l_z = 1$, and $l_\perp = 1$.

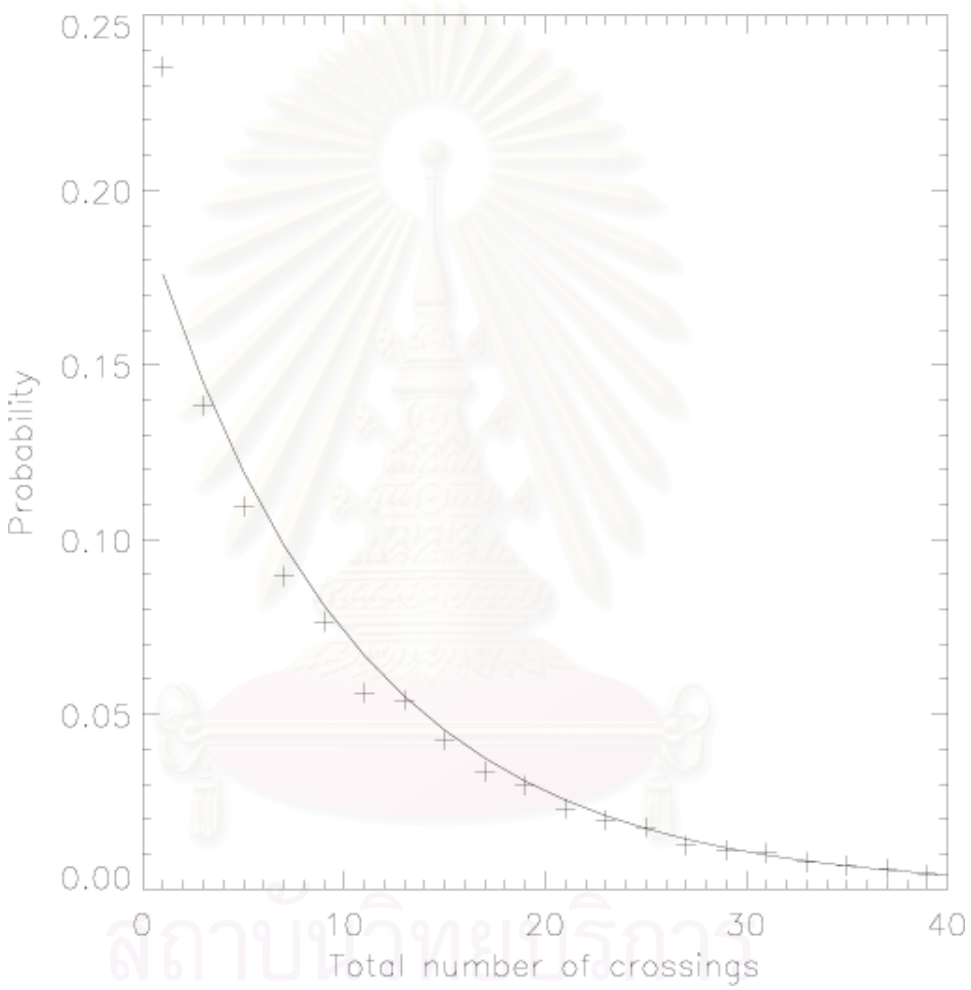

Figure 4.9: The probability distribution vs. the number of shock-field crossings of a nearly perpendicular shock is plotted with the fitted curve at $\delta b/B_0 = 0.3$, $E_{slab} = 0.5$, $l_z = 1$, and $l_\perp = 1$.

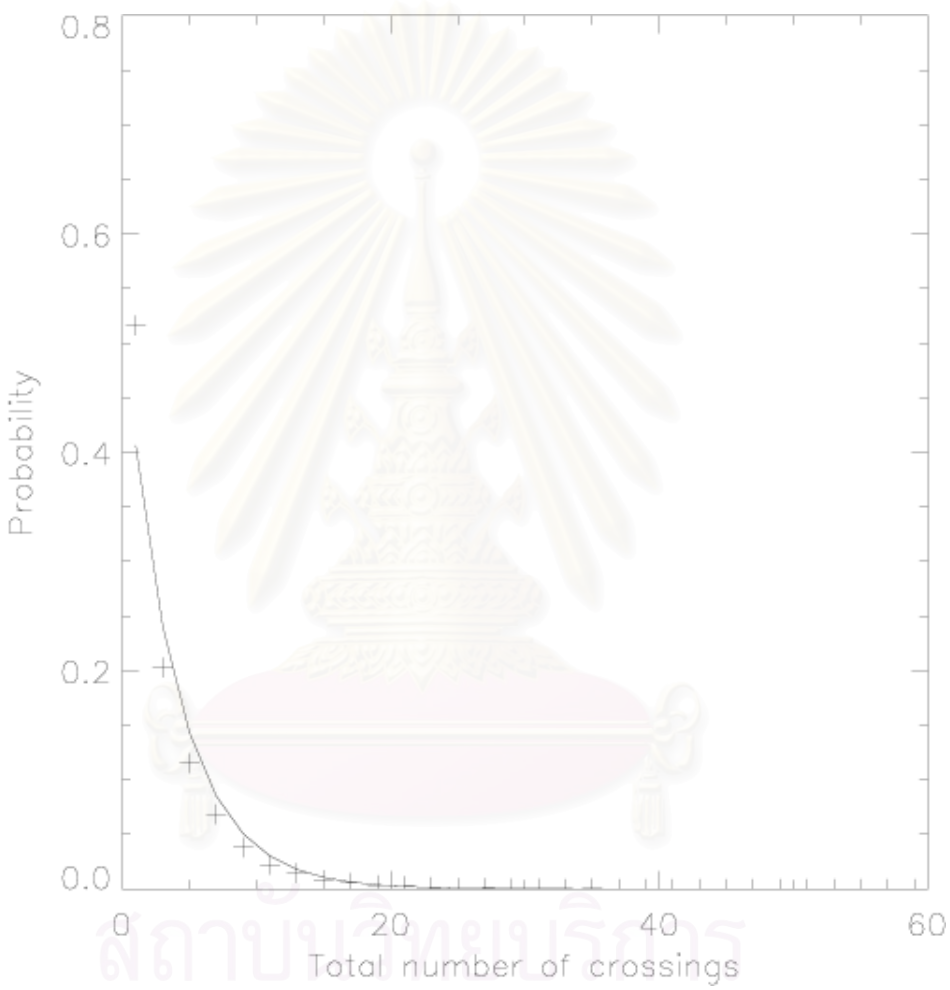

Figure 4.10: The probability distribution vs. the number of shock-field crossings of a nearly perpendicular shock is plotted with the fitted curve at $\delta b/B_0 = 0.1$, $E_{slab} = 0.5$, $l_z = 1$, and $l_\perp = 1$.

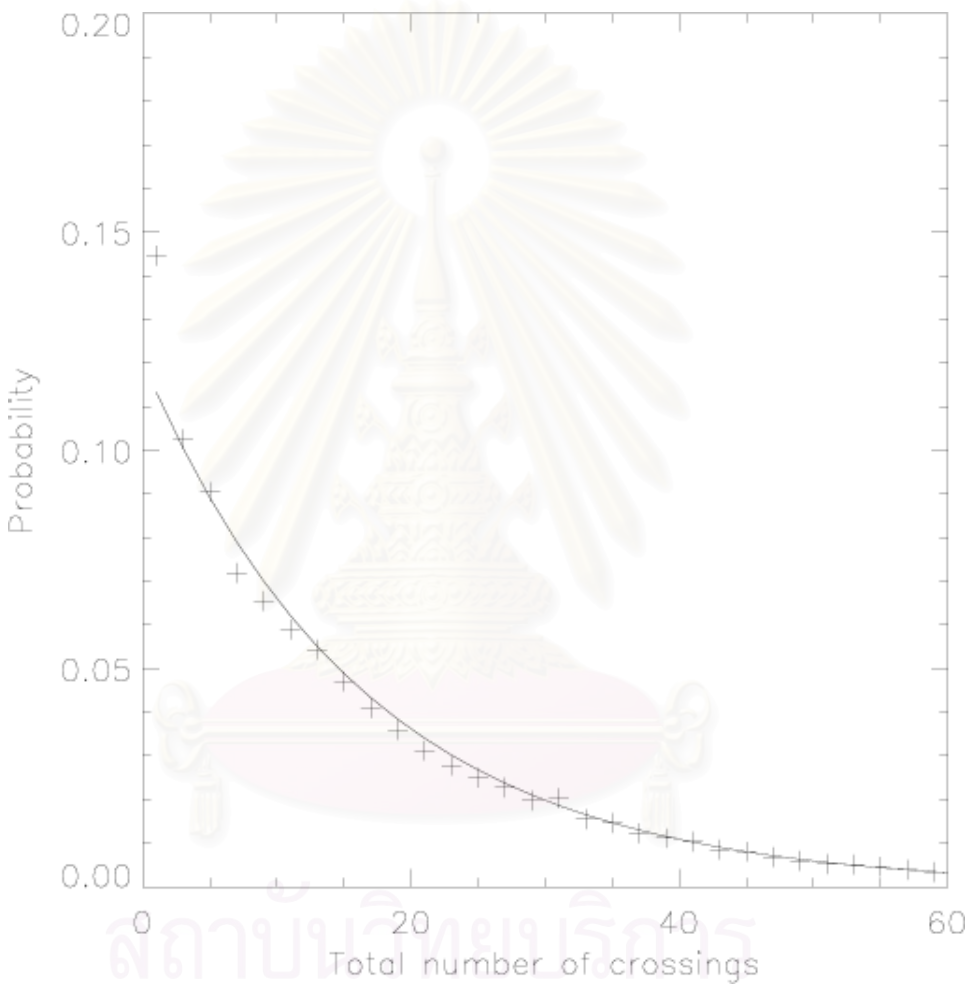

Figure 4.11: The probability distribution vs. the number of shock-field crossings of a nearly perpendicular shock is plotted with the fitted curve at $\delta b/B_0 = 0.5$, $E_{slab} = 0.2$, $l_z = 1$, and $l_\perp = 1$.

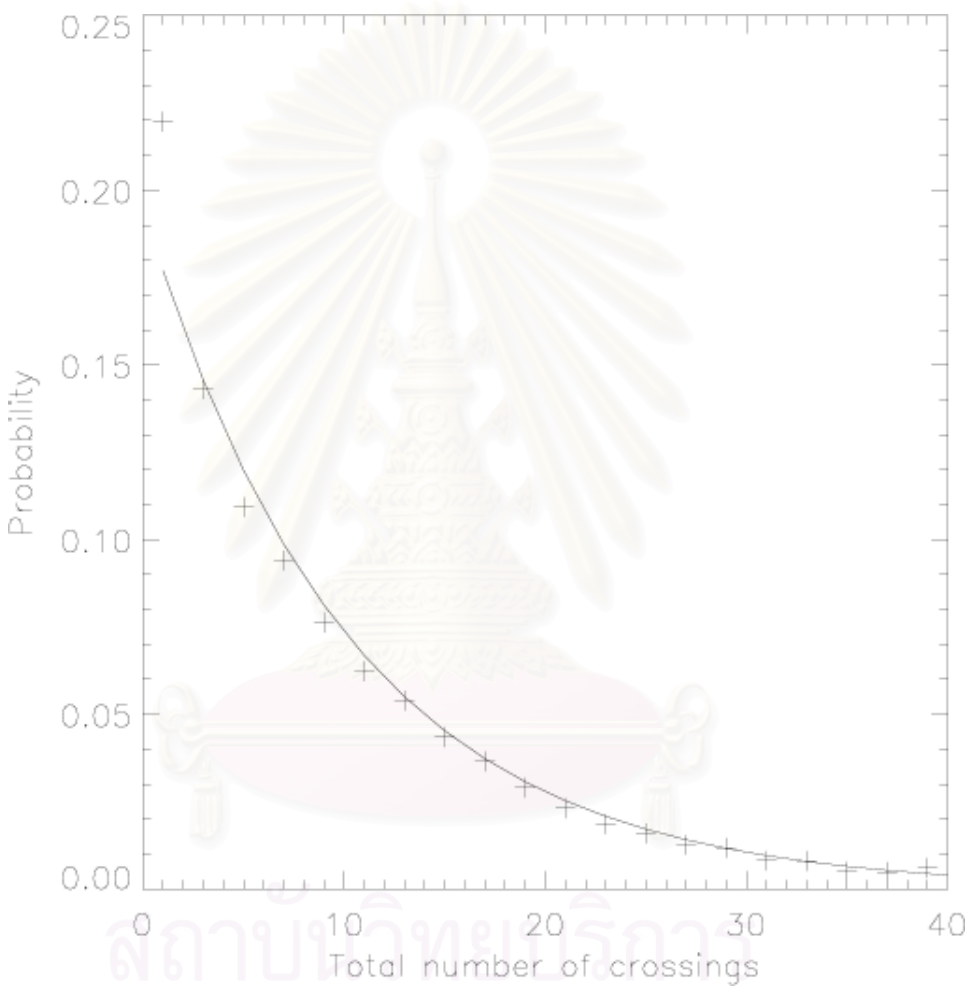

Figure 4.12: The probability distribution vs. the number of shock-field crossings of a nearly perpendicular shock is plotted with the fitted curve at $\delta b/B_0 = 0.3$, $E_{slab} = 0.2$, $l_z = 1$, and $l_\perp = 1$.

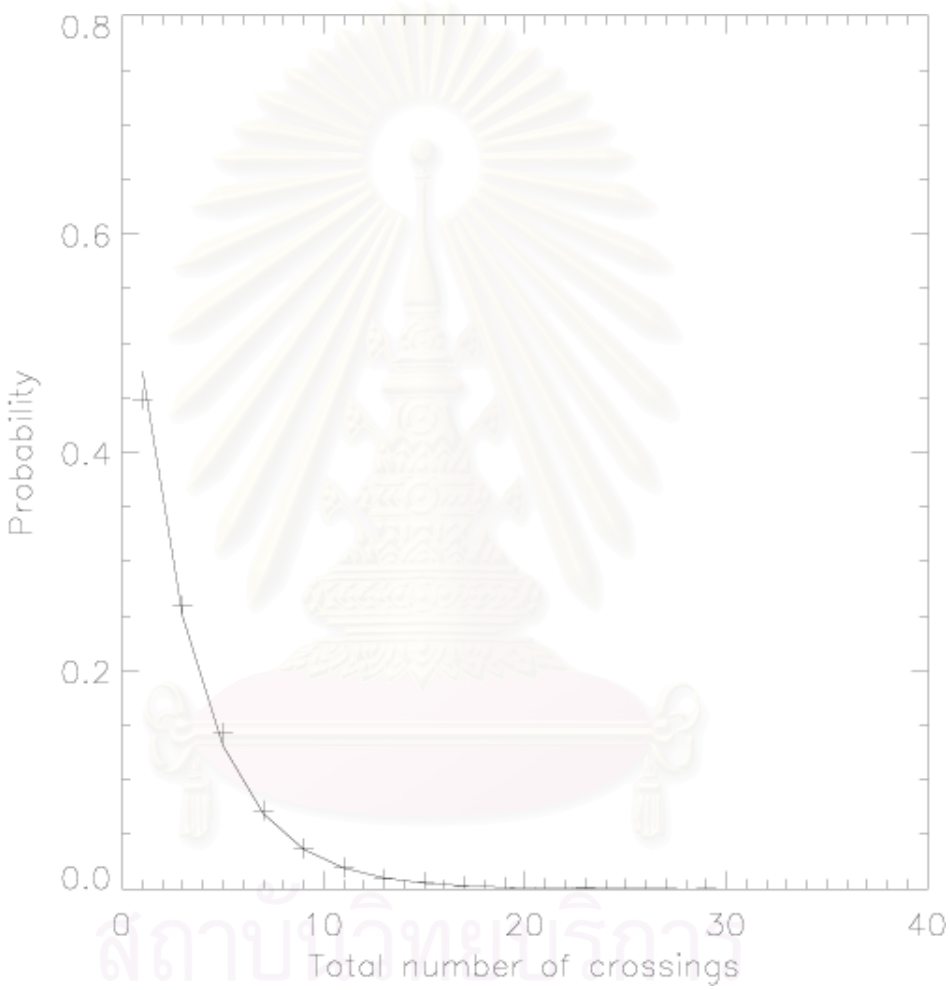

Figure 4.13: The probability distribution vs. the number of shock-field crossings of a nearly perpendicular shock is plotted with the fitted curve at $\delta b/B_0 = 0.1$, $E_{slab} = 0.2$, $l_z = 1$, and $l_\perp = 1$.

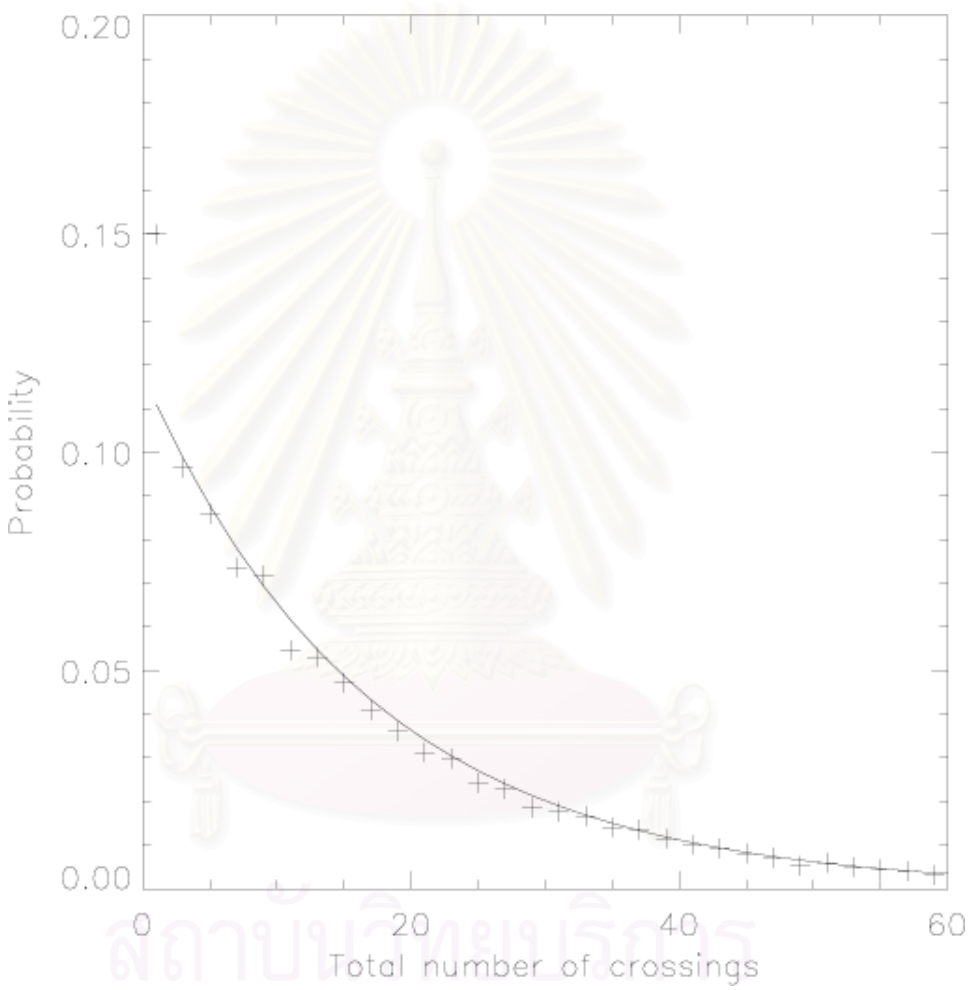

Figure 4.14: The probability distribution vs. the number of shock-field crossings of a nearly perpendicular shock is plotted with the fitted curve at $\delta b/B_0 = 0.5$, $E_{slab} = 0.5$, $l_z = 0.5$, and $l_\perp = 1$.

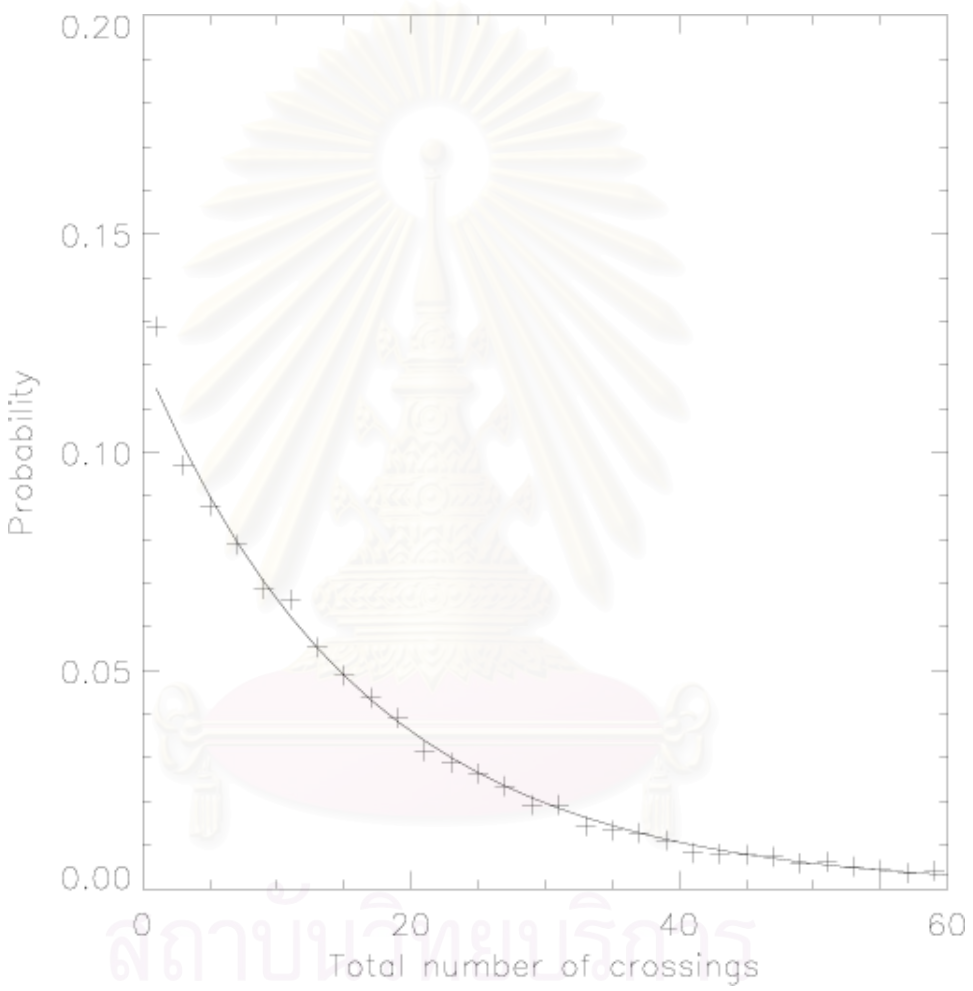

Figure 4.15: The probability distribution vs. the number of shock-field crossings of a nearly perpendicular shock is plotted with the fitted curve at $\delta b/B_0 = 0.5$, $E_{slab} = 0.5$, $l_z = 1$, and $l_\perp = 0.2$.

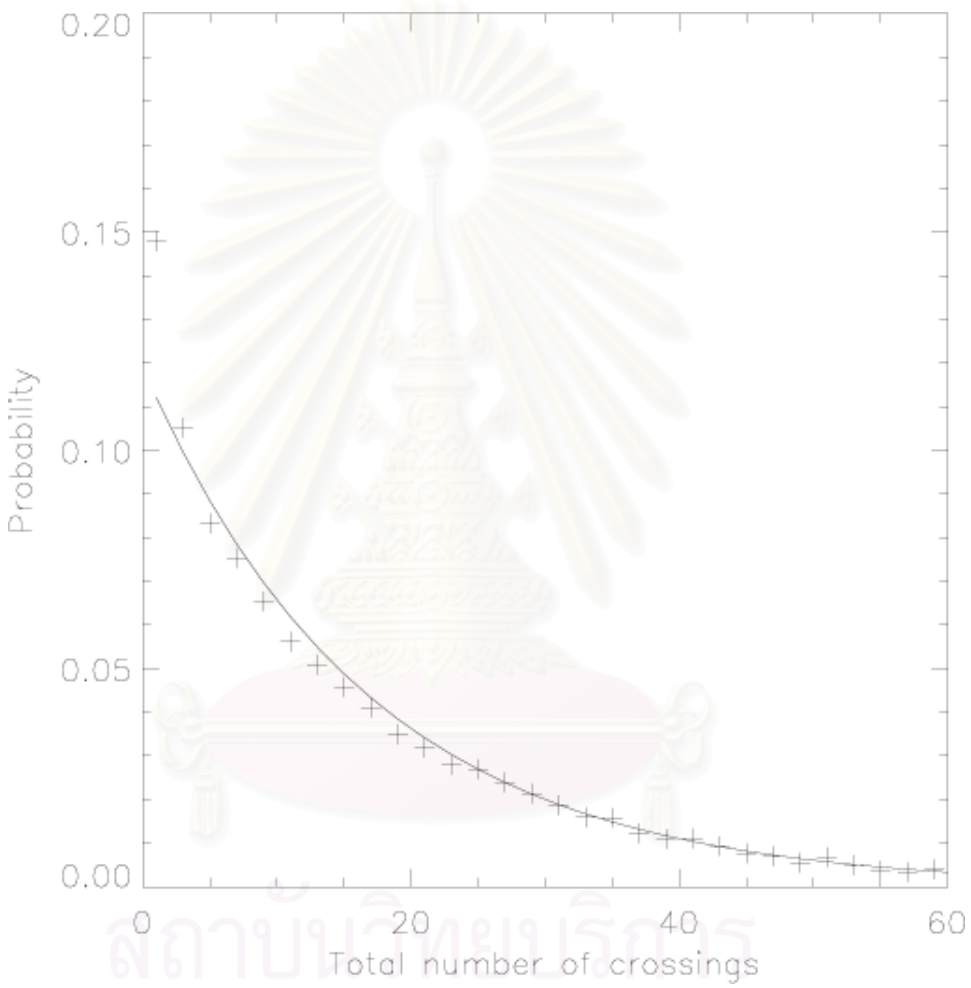

Figure 4.16: The probability distribution vs. the number of shock-field crossings of a nearly perpendicular shock is plotted with the fitted curve at $\delta b/B_0 = 0.5$, $E_{slab} = 0.2$, $l_z = 0.5$, and $l_\perp = 1$.

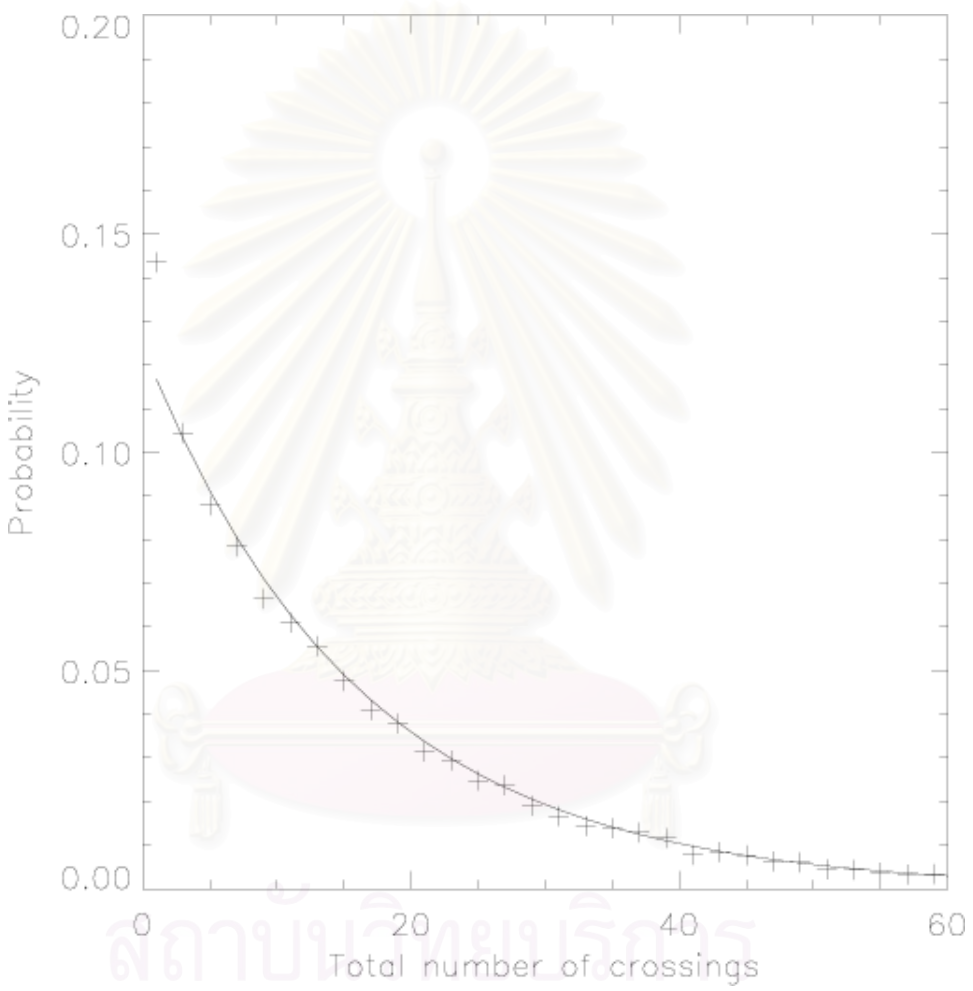

Figure 4.17: The probability distribution vs. the number of shock-field crossings of a nearly perpendicular shock is plotted with the fitted curve at $\delta b/B_0 = 0.5$, $E_{slab} = 0.2$, $l_z = 1$, and $l_\perp = 0.2$.

Now we find a function that can fit the data. We fit the data for the pure slab and the compound case only, because the magnetic field lines in space exhibit diffusive properties. We know that all magnetic field lines must finally cross to the opposite side from the initial side, so the probability of crossing from the initial side to the final side is one. We think that whether the magnetic field crosses the shock again should not depend on the previous crossings because we imagine that the turbulence at one location is completely independent of the turbulence at the other locations, assuming they are seperated by more than l_z or $l_\perp$. Therefore, the probability that the magnetic field line crosses back to the initial side should be a constant and does not depend on the cumulative number of crossings. Let the probability of crossing and re-crossing from upstream to downstream and back to the upstream region be p. Let $P'(n)$ be the probability that the total number of crossings is equal to or greater than n times. The number of crossings cannot be even. (If the number of crossings is even, the magnetic field line is in the upstream region, and there will still be at least one more crossing from the upstream region to the downstream region with unit probability.) We can write $P'(n)$ in terms of p as

$$P'(n) = (1)^{\frac{n+1}{2}} p^{\frac{n-1}{2}}. \tag{4.3}$$

Let $P(n)$ be the probability that the total number of crossings is n. Therefore,

$$\begin{aligned} P(n) &= P'(n) - P'(n+2) = p^{\frac{n-1}{2}} - p^{\frac{n+1}{2}} \\ &= (1-p)p^{\frac{n-1}{2}} \end{aligned} \tag{4.4}$$

The value of p can be found by fitting the simulation results for the number of crossings with (4.4). Table 4.1 shows the probability of the magnetic field line returning to the shock after it crosses from the upstream region to the downstream region. From the table, the probability is changed only when we change $\delta b/B_0$.

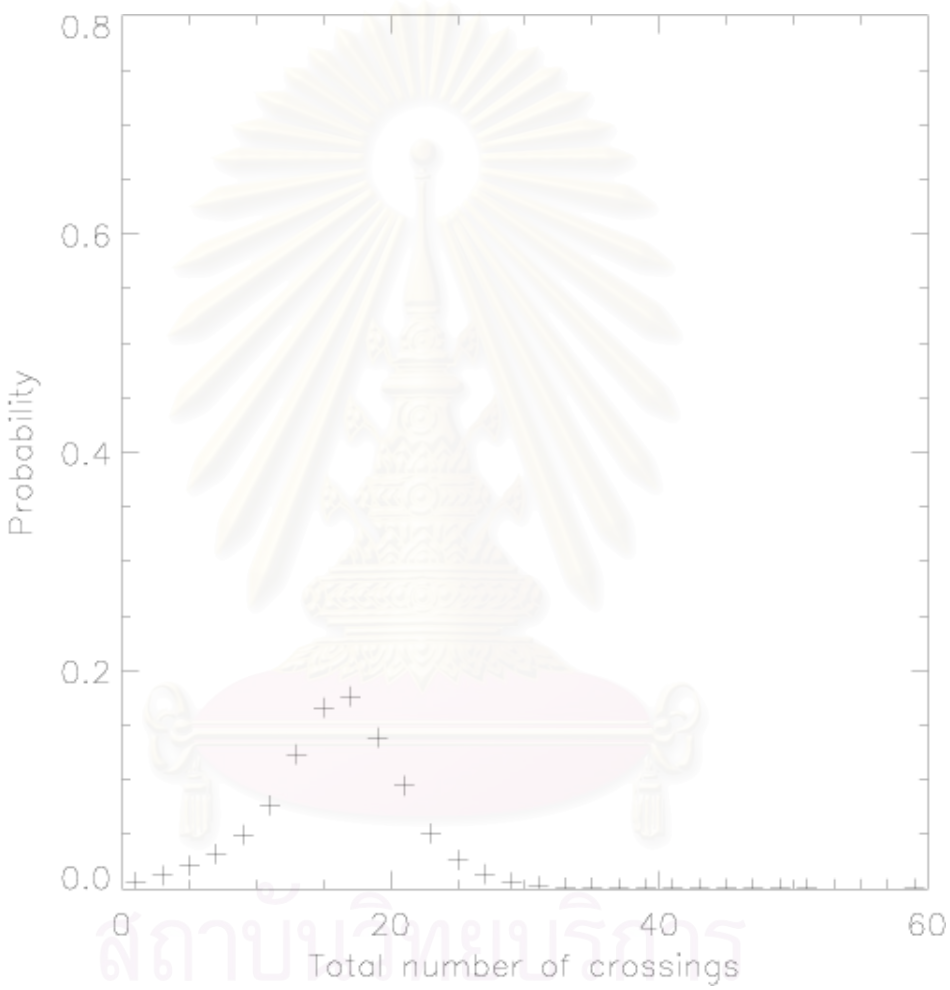

Figure 4.18: The probability distribution vs. the number of shock-field crossings of a nearly perpendicular shock is plotted with the fitted curve at $\delta b/B_0 = 0.5$, $E_{slab} = 0$, $l_\perp = 1.0$.

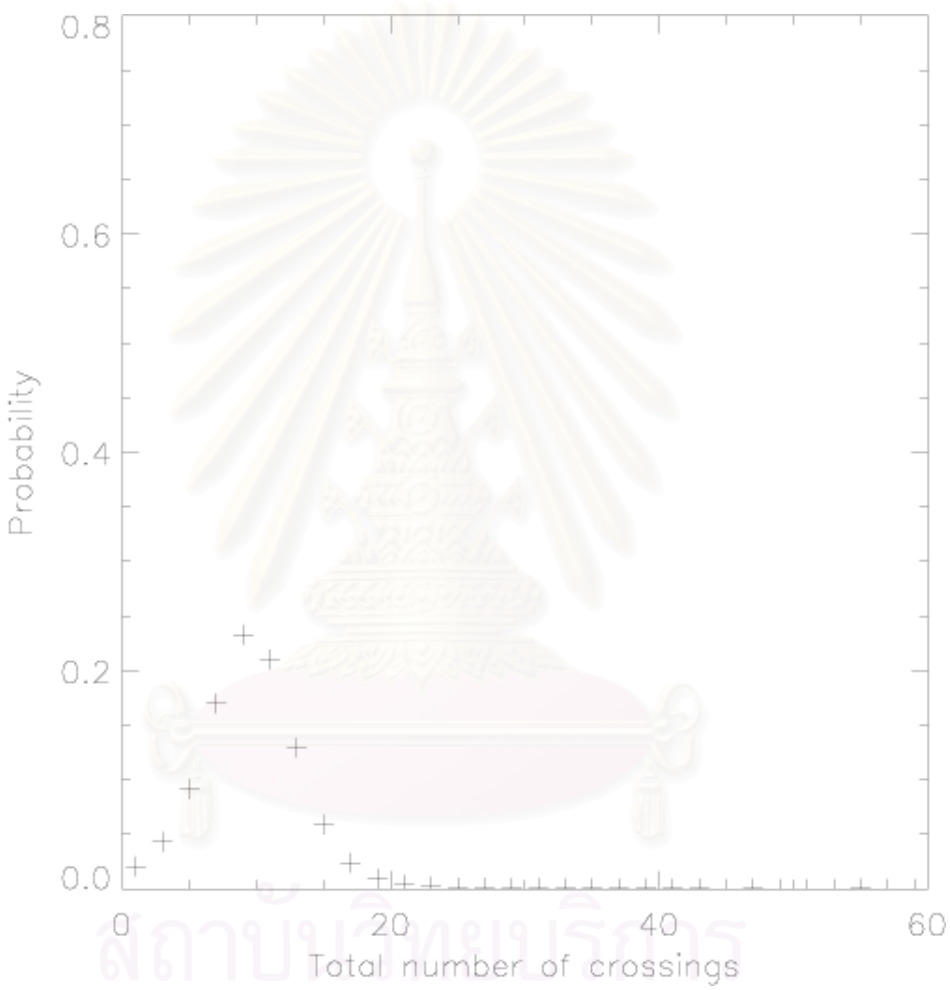

Figure 4.19: The probability distribution vs. the number of shock-field crossings of a nearly perpendicular shock is plotted with the fitted curve at $\delta b/B_0 = 0.3$, $E_{slab} = 0$, $l_\perp = 1.0$.

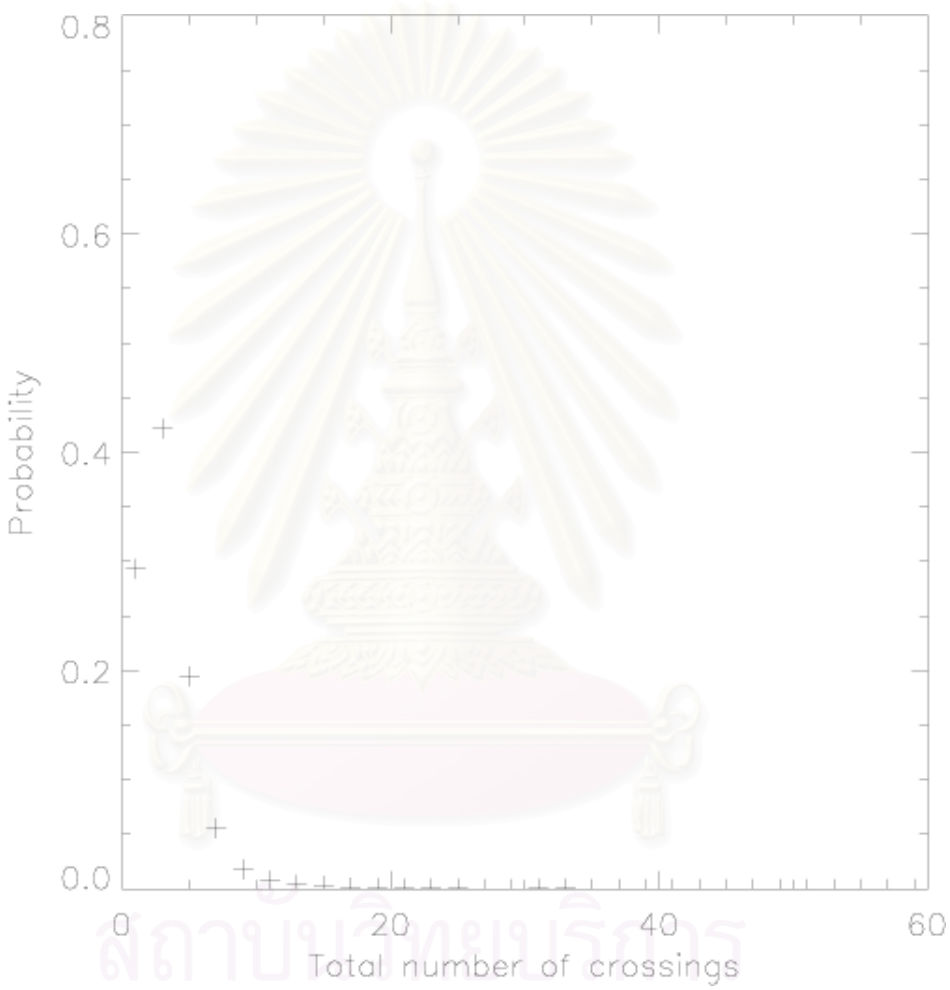

Figure 4.20: The probability distribution vs. the number of shock-field crossings of a nearly perpendicular shock is plotted with the fitted curve at $\delta b/B_0 = 0.1$, $E_{slab} = 0$, $l_\perp = 1.0$.

Table 4.1: The probability of recrossing from downstream to upstream as a function of various parameters.

$\delta b/B_0$	E_{slab}	l_z	$l_\perp$	p
0.5	1.0	1.0	-	0.888
0.5	1.0	0.5	-	0.882
0.5	0.8	1.0	1.0	0.887
0.5	0.5	1.0	1.0	0.888
0.5	0.5	0.5	1.0	0.889
0.5	0.5	1.0	0.2	0.885
0.5	0.2	1.0	1.0	0.886
0.5	0.2	0.5	1.0	0.887
0.5	0.2	1.0	0.2	0.883
0.3	1.0	1.0	-	0.820
0.3	0.8	1.0	1.0	0.826
0.3	0.5	1.0	1.0	0.824
0.3	0.2	1.0	1.0	0.823
0.1	1.0	1.0	-	0.576
0.1	0.8	1.0	1.0	0.629
0.1	0.5	1.0	1.0	0.593
0.1	0.2	1.0	1.0	0.526

4.3 Crossing angle

The crossing angle is defined as the upstream angle between the magnetic field line and the shock normal. From Chapter 2, if the magnetic field is nearly perpendicular to the shock, the energy gained at the shock is large. The magnetic field at the solar wind termination shock is also nearly perpendicular to the shock normal, but the magnetic field is turbulent. Therefore the crossing angle should not be exactly 89°.

Figures 4.21 to 4.23 show the probability density of the crossing angle in the pure slab case with $l_z = 1.0$ au and $\delta b/B_0$ from 0.5 to 0.1. From these Figures, the crossing angle distribution is changed when $\delta b/B_0$ is changed. This effect also occurs in the compound case, with both slab and 2D turbulence. Figures 4.24 to 4.26 show the effect of the $\delta b/B_0$ value on the angle distribution for $E_{slab} = 0.8$, $l_z = 1.0$ au, and $l_\perp = 1.0$ au while Figures 4.27 to 4.29 are for $E_{slab} = 0.5$, and Figures 4.30 to 4.32 are for $E_{slab} = 0.2$. For all of these figures, the value of E_{slab} seems to have no effect on the angle distribution.

The angle distribution also does not depend on l_z and $l_\perp$. Figure 4.33 shows the angle distributions in pure slab turbulence with $l_z = 0.5$ au. For $E_{slab} = 0.5$, the Figure 4.34 differs from 4.35 only in the value of l_z and $l_\perp$, but both of them show the same distribution. For $E_{slab} = 0.2$, the angle distributions from different l_z and $l_\perp$ as shown in Figure 4.36 and 4.37 show the same distribution. The angle distributions also depend on only $\langle \delta b/B_0 \rangle$ even in the pure 2D case as shown in Figures 4.38 to 4.40.

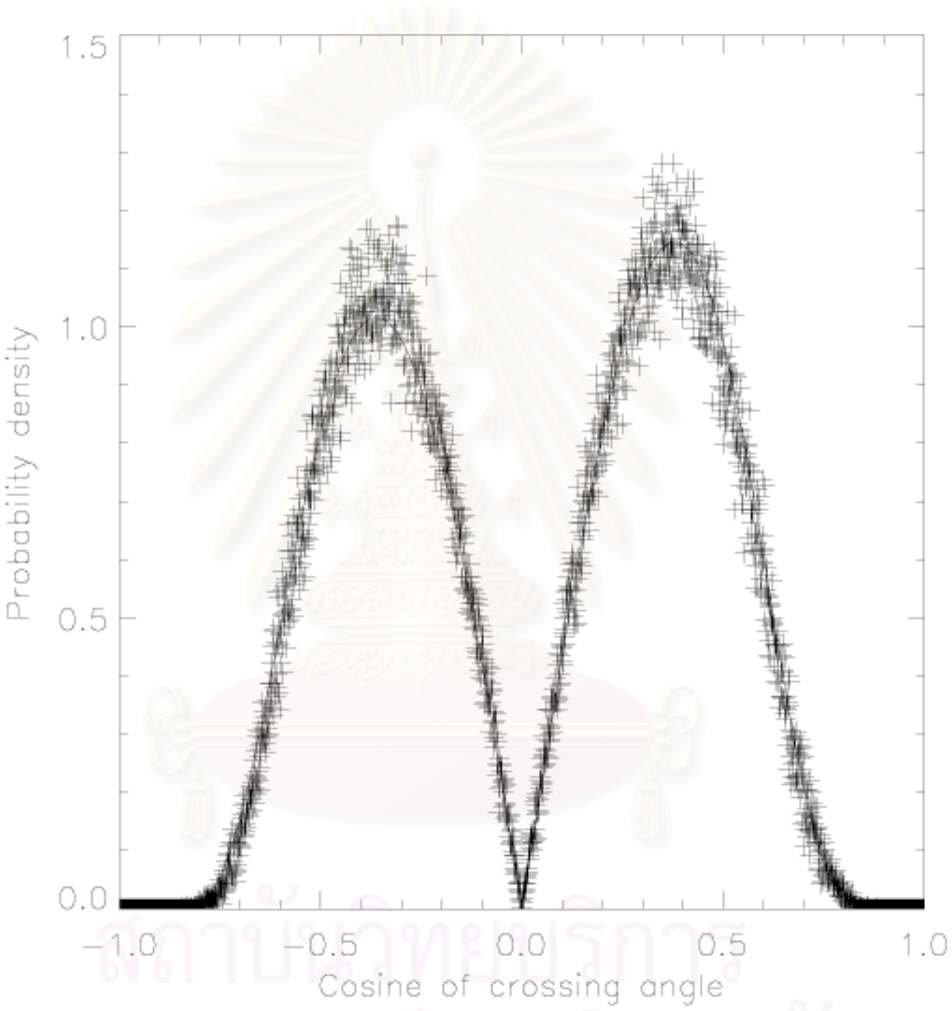

Figure 4.21: The probability density vs. the crossing angle is plotted with the fitted curve at $\delta b/B_0 = 0.5$, $E_{slab} = 1.0$, and $l_z = 1.0$.

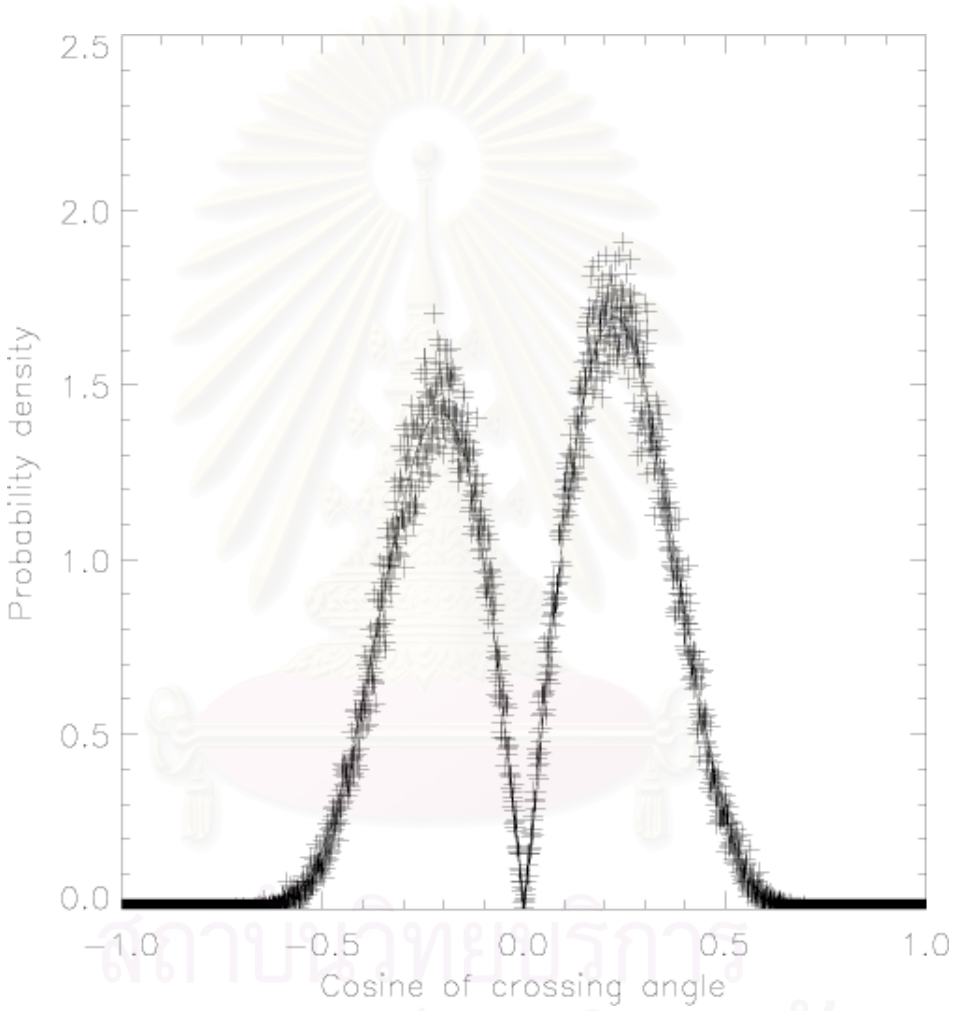

Figure 4.22: The probability density vs. the crossing angle is plotted with the fitted curve at $\delta b/B_0 = 0.3$, $E_{slab} = 1.0$, and $l_z = 1.0$.

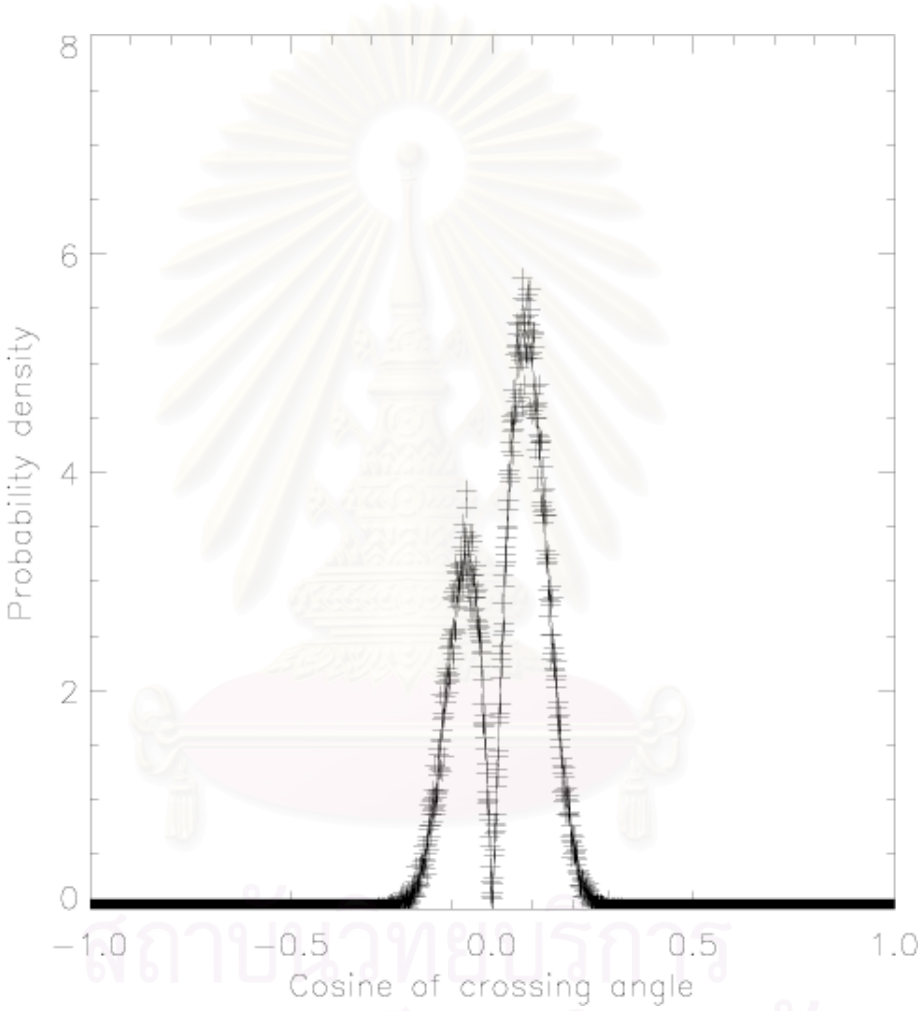

Figure 4.23: The probability density vs. the crossing angle is plotted with the fitted curve at $\delta b/B_0 = 0.1$, $E_{slab} = 1.0$, and $l_z = 1.0$.

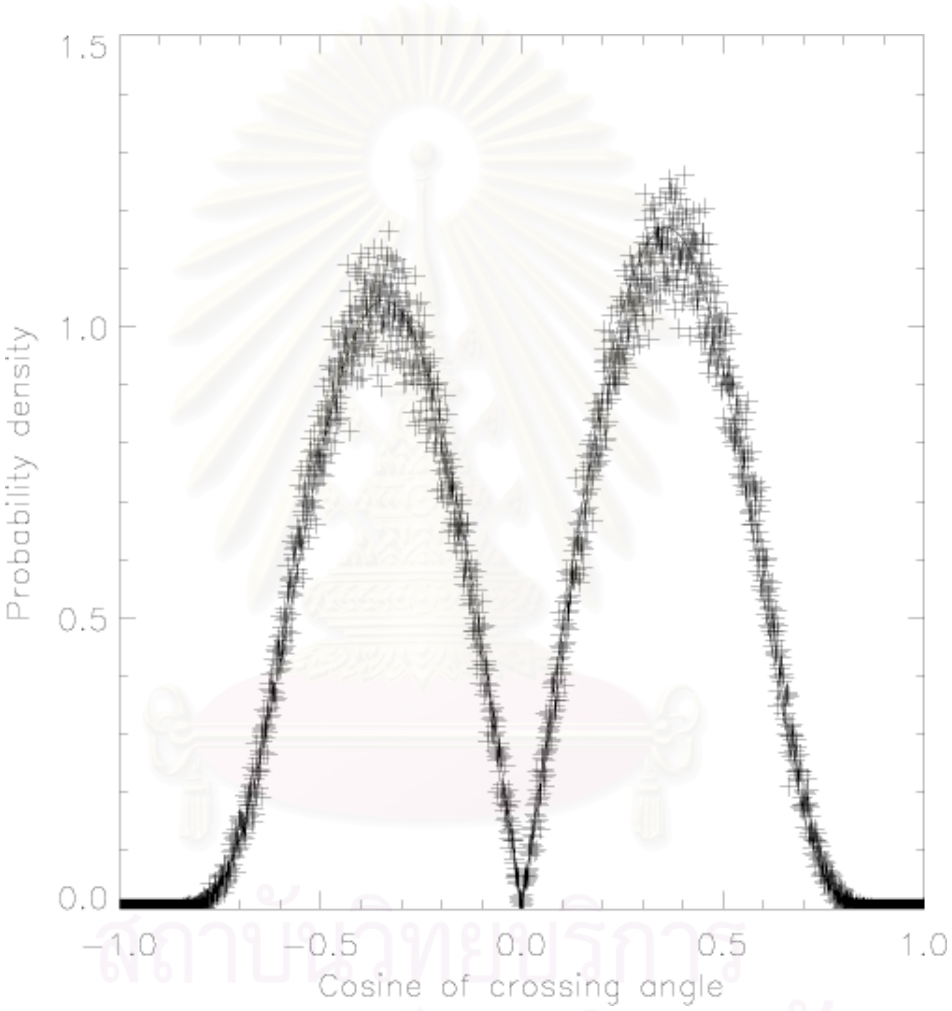

Figure 4.24: The probability density vs. the crossing angle is plotted with the fitted curve at $\delta b/B_0 = 0.5$, $E_{slab} = 0.8$, $l_z = 1.0$, and $l_\perp = 1.0$.

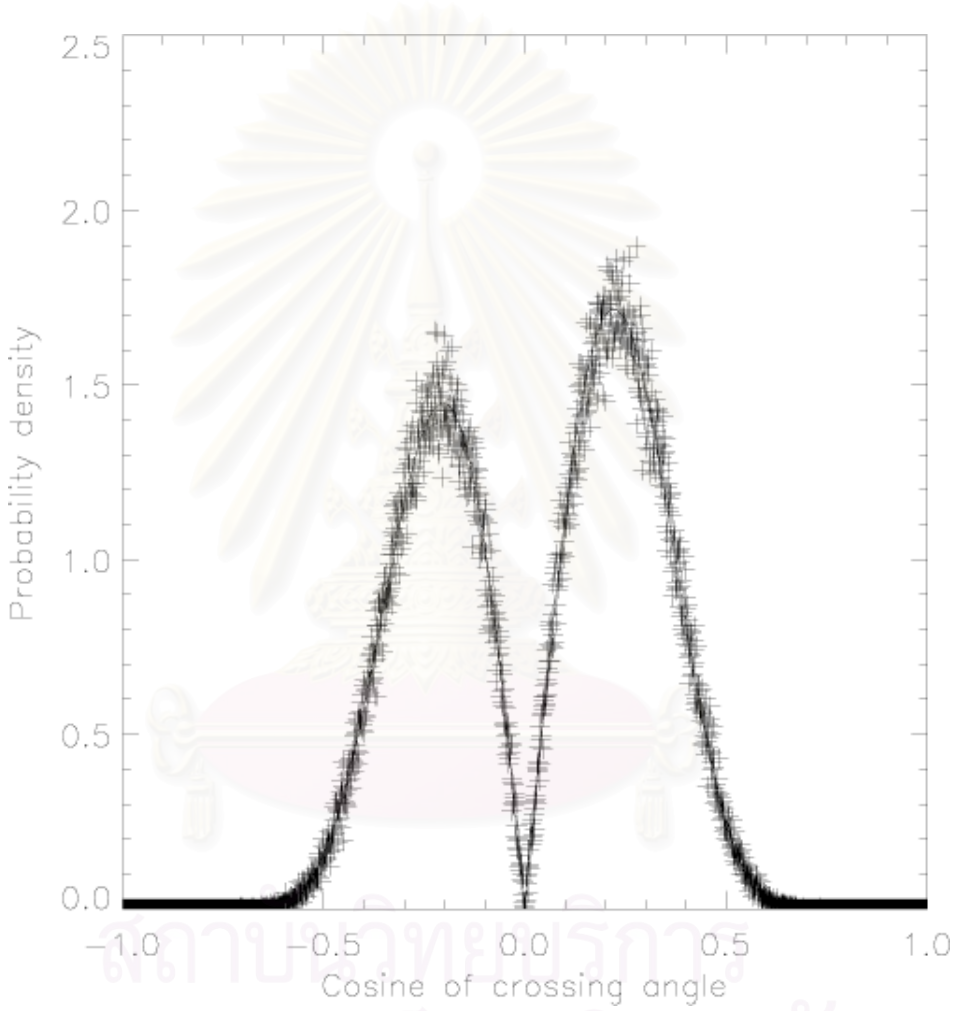

Figure 4.25: The probability density vs. the crossing angle is plotted with the fitted curve at $\delta b/B_0 = 0.3$, $E_{slab} = 0.8$, $l_z = 1.0$, and $l_\perp = 1.0$.

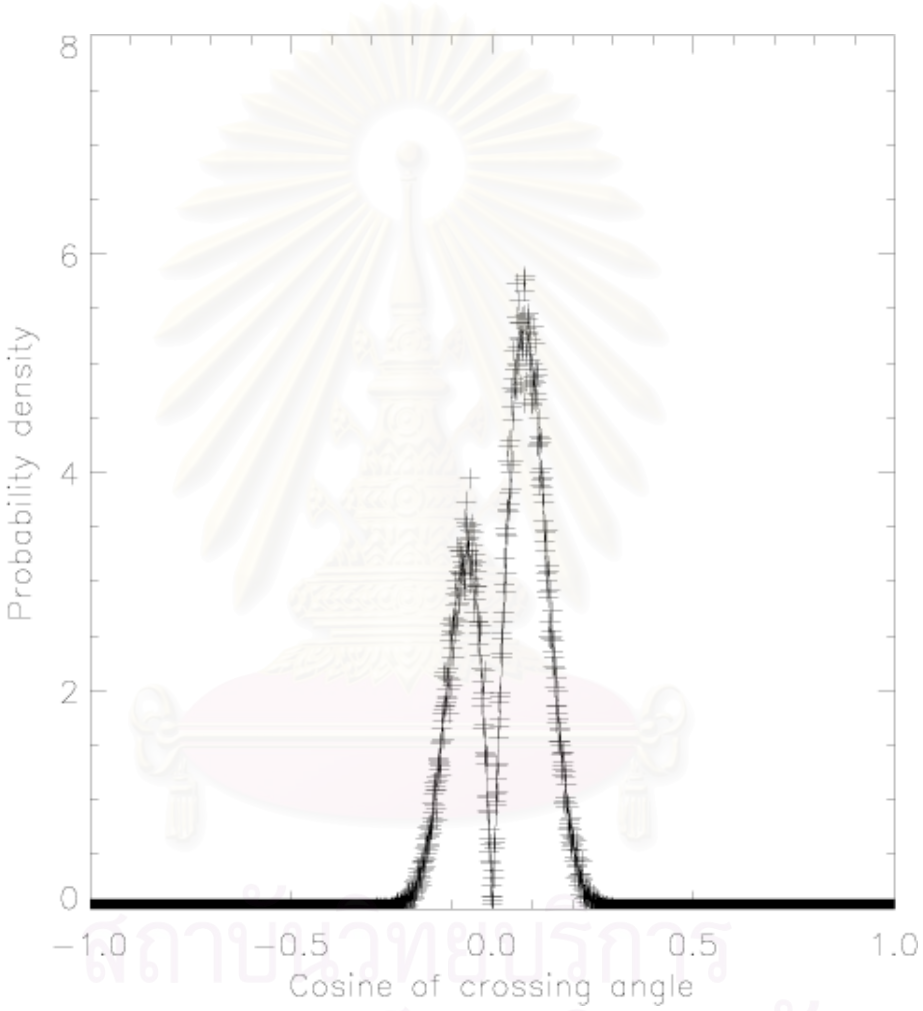

Figure 4.26: The probability density vs. the crossing angle is plotted with the fitted curve at $\delta b/B_0 = 0.1$, $E_{slab} = 0.8$, $l_z = 1.0$, and $l_\perp = 1.0$.

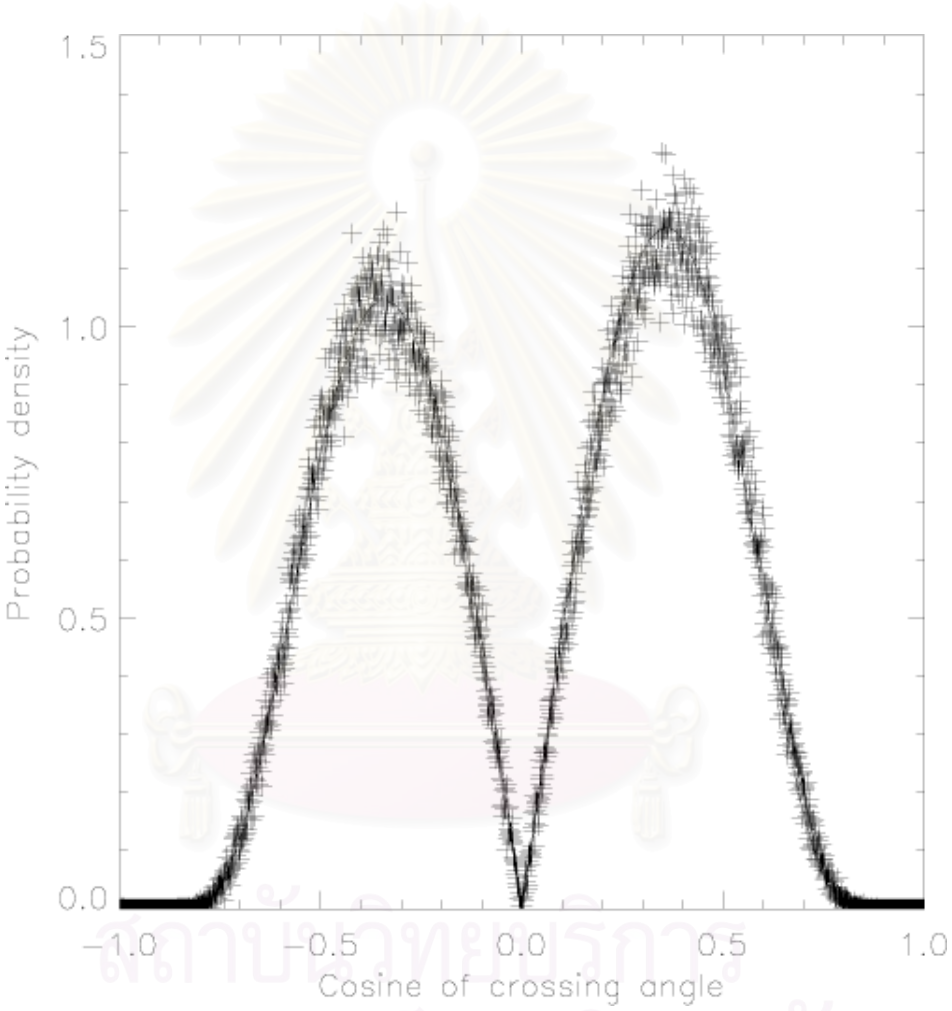

Figure 4.27: The probability density vs. the crossing angle is plotted with the fitted curve at $\delta b/B_0 = 0.5$, $E_{slab} = 0.5$, $l_z = 1.0$, and $l_\perp = 1.0$.

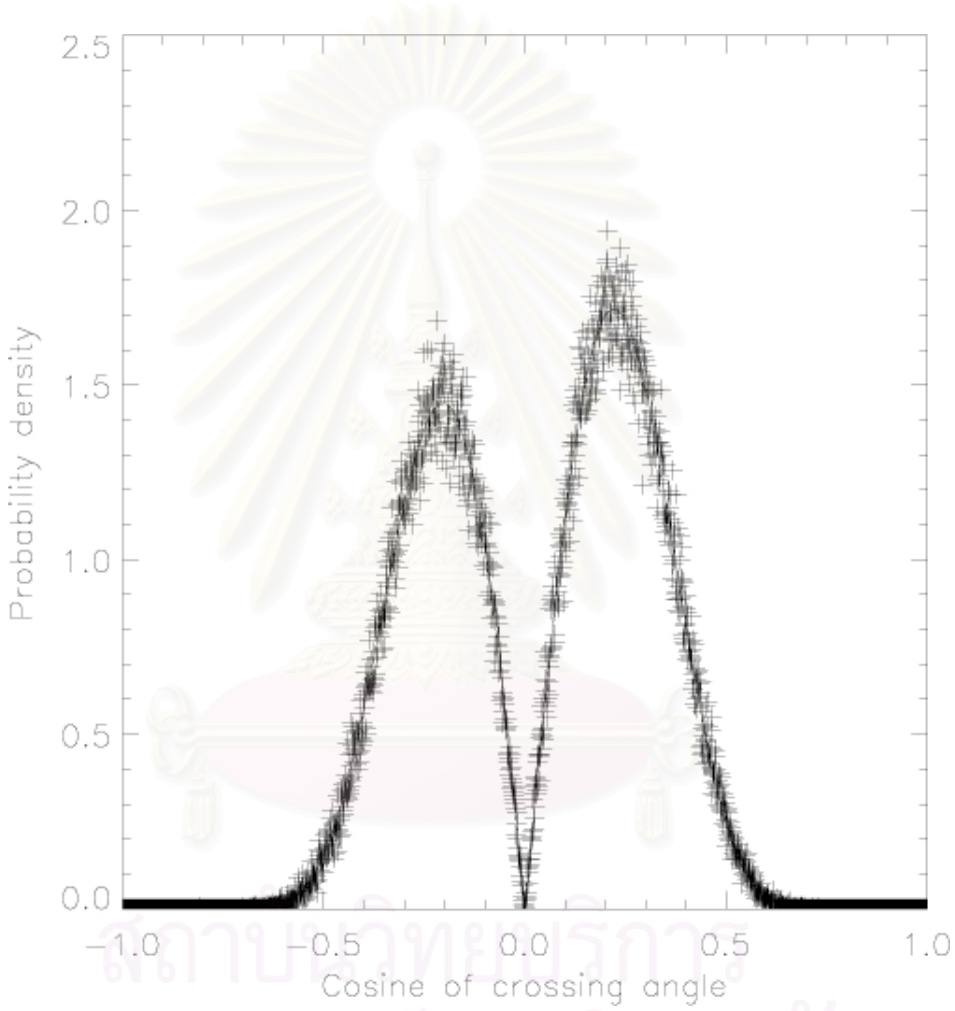

Figure 4.28: The probability density vs. the crossing angle is plotted with the fitted curve at $\delta b/B_0 = 0.3$, $E_{slab} = 0.5$, $l_z = 1.0$, and $l_\perp = 1.0$.

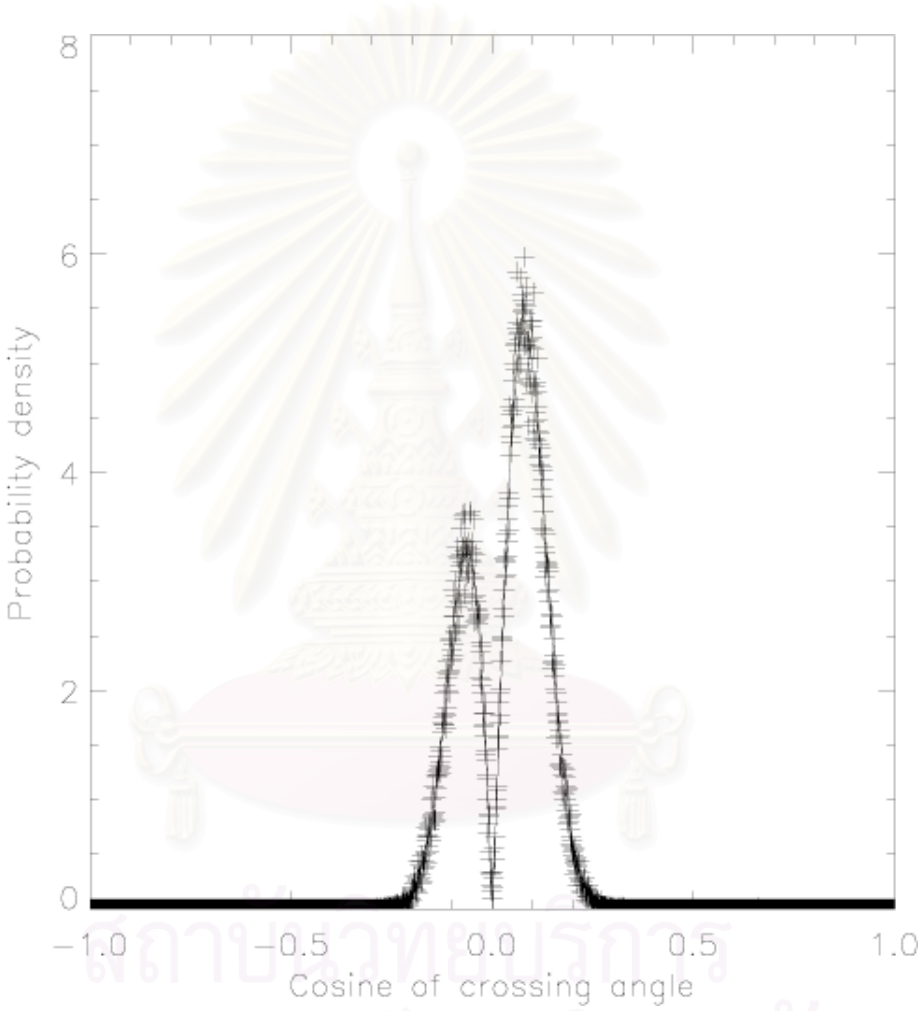

Figure 4.29: The probability density vs. the crossing angle is plotted with the fitted curve at $\delta b/B_0 = 0.1$, $E_{slab} = 0.5$, $l_z = 1.0$, and $l_\perp = 1.0$.

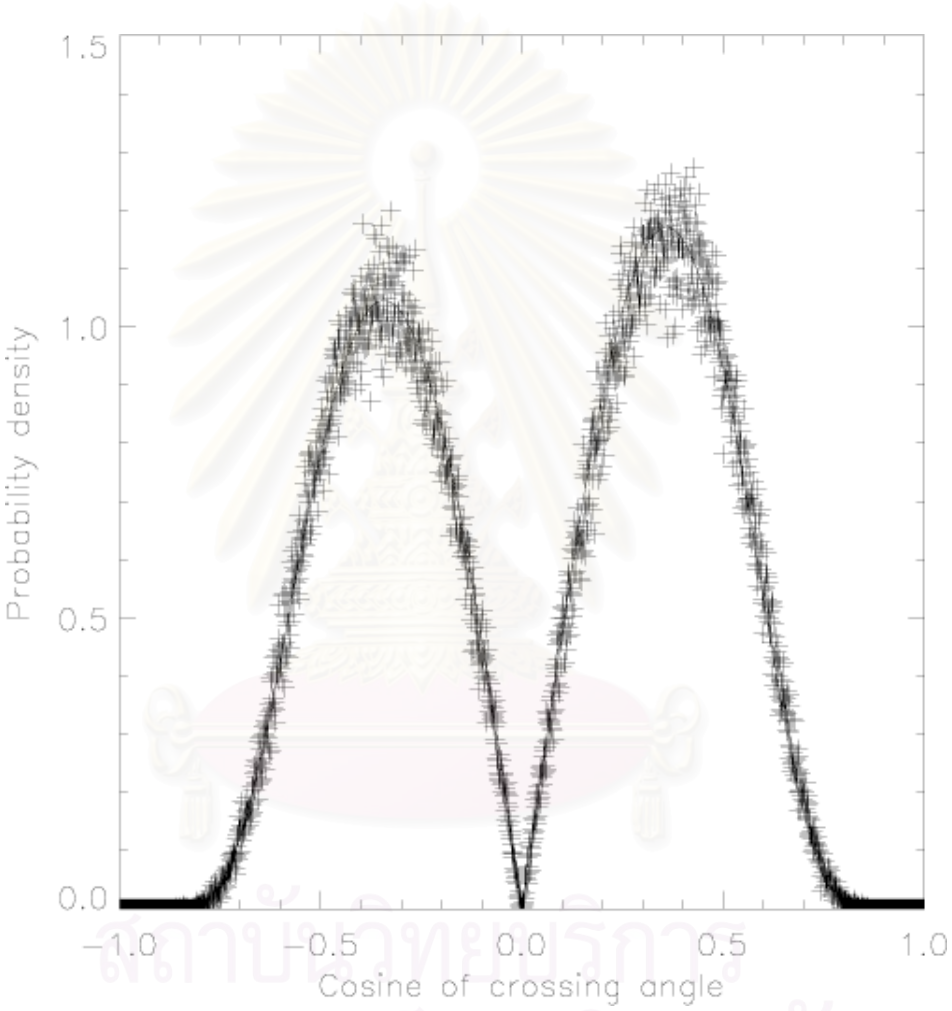

Figure 4.30: The probability density vs. the crossing angle is plotted with the fitted curve at $\delta b/B_0 = 0.5$, $E_{slab} = 0.2$, $l_z = 1.0$, and $l_\perp = 1.0$.

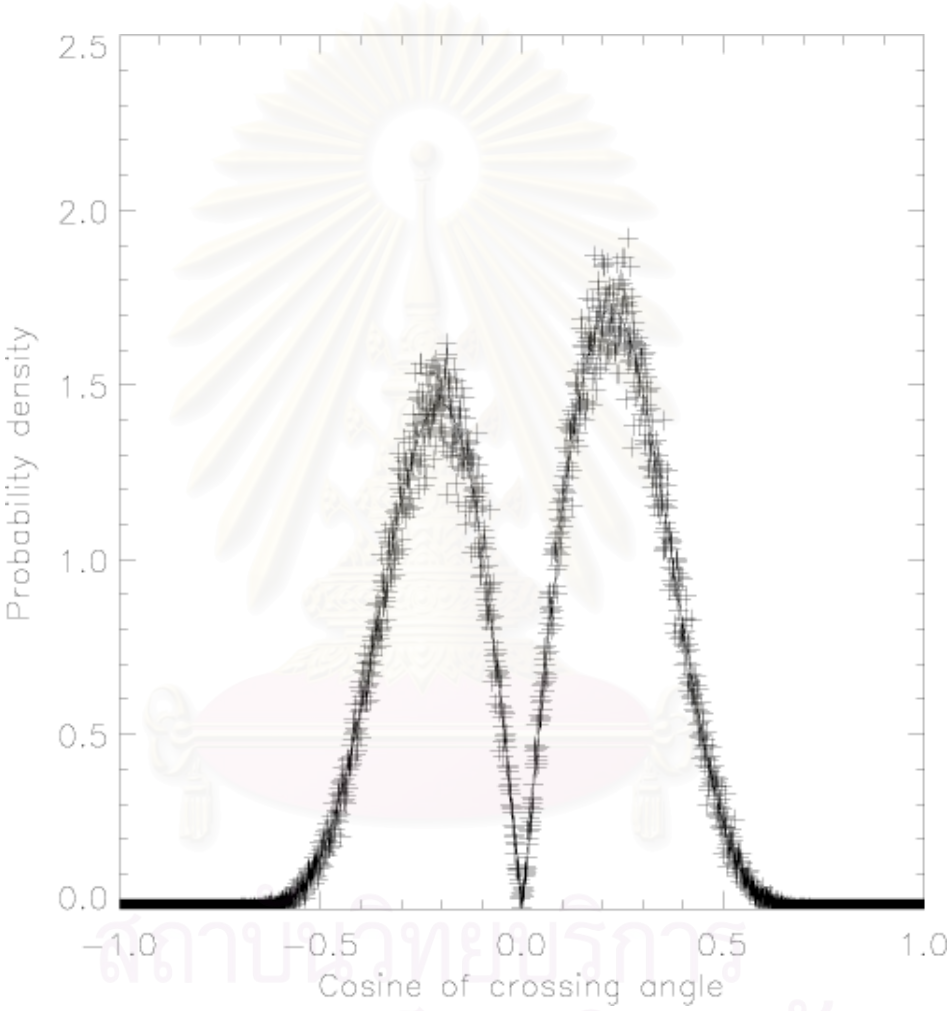

Figure 4.31: The probability density vs. the crossing angle is plotted with the fitted curve at $\delta b/B_0 = 0.3$, $E_{slab} = 0.2$, $l_z = 1.0$, and $l_\perp = 1.0$.

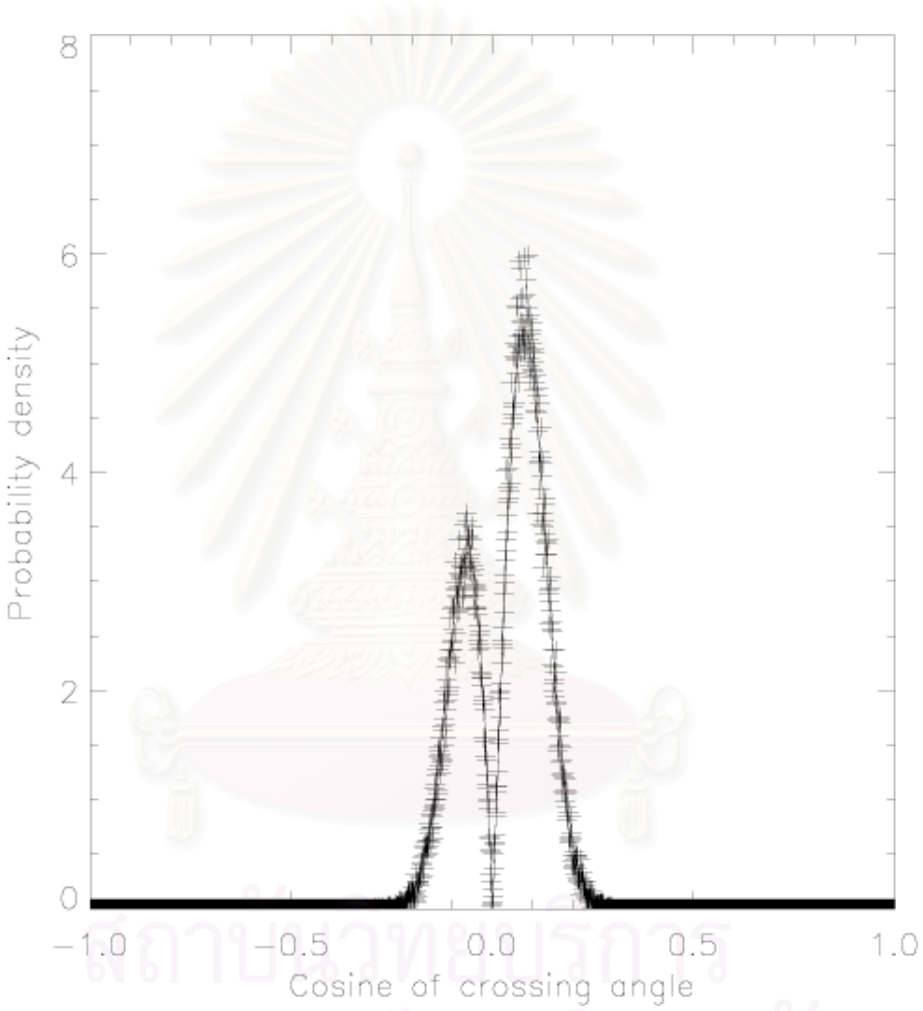

Figure 4.32: The probability density vs. the crossing angle is plotted with the fitted curve at $\delta b/B_0 = 0.1$, $E_{slab} = 0.2$, $l_z = 1.0$, and $l_\perp = 1.0$.

We can find the approximate form of the angle distribution because we know the turbulent magnetic field distribution. The distribution of the turbulent magnetic field is

$$P(b_x)db_x = \frac{1}{\sqrt{2\pi\langle(b_x - b_{0x})^2\rangle}} \exp\left[-\frac{(b_x - b_{0x})^2}{2\langle(b_x - b_{0x})^2\rangle}\right] db_x \tag{4.5}$$

$$P(b_y)db_y = \frac{1}{\sqrt{2\pi\langle b_y^2\rangle}} \exp\left[-\frac{b_y^2}{2\langle b_y^2\rangle}\right] db_y. \tag{4.6}$$

Because the turbulent magnetic field is axisymmetric, $\langle(b_x - b_{0x})^2\rangle = \langle b_y^2\rangle = (1/2)\langle b^2\rangle$. Therefore,

$$P(b_x, b_y)db_x db_y = \frac{1}{\pi\langle b^2\rangle} \exp\left[-\frac{(b_x - b_{0x})^2 x + b_y^2}{\langle b^2\rangle}\right] db_x db_y \tag{4.7}$$

and the average magnetic field is $b_0\hat{z} + b_{0x}\hat{x}$. If we set the shock normal to be $\hat{x}$, the relation between $\cos\theta$ and the turbulent magnetic field is

$$\cos\theta = \frac{b_x}{\sqrt{b_x^2 + b_y^2 + 1}}. \tag{4.8}$$

This cosine of the crossing angle for the average value b_{0x} is

$$\cos\theta_0 = \frac{b_{0x}}{\sqrt{b_{0x}^2 + b_y^2 + 1}}, \tag{4.9}$$

where θ_0 is about 89° in the case of solar wind termination shock. The quantity $\cos\theta$ remains unchanged along the hyperbolic curve defined as

$$\begin{aligned} b_x^2 &= \cos^2\theta\left(b_x^2 + b_y^2 + b_0^2\right) \\ &= \frac{\cos^2\theta\left(b_y^2 + b_0^2\right)}{1 - \cos^2\theta} \end{aligned} \tag{4.10}$$

In our model, we normalize B so that $b_0 = 1$. We will use new coordinates, $\cos\theta$ and b_y, instead of b_x and b_y. Therefore,

$$P(\cos\theta, b_y)d\cos\theta db_y = P(b_x, b_y)db_x db_y. \tag{4.11}$$

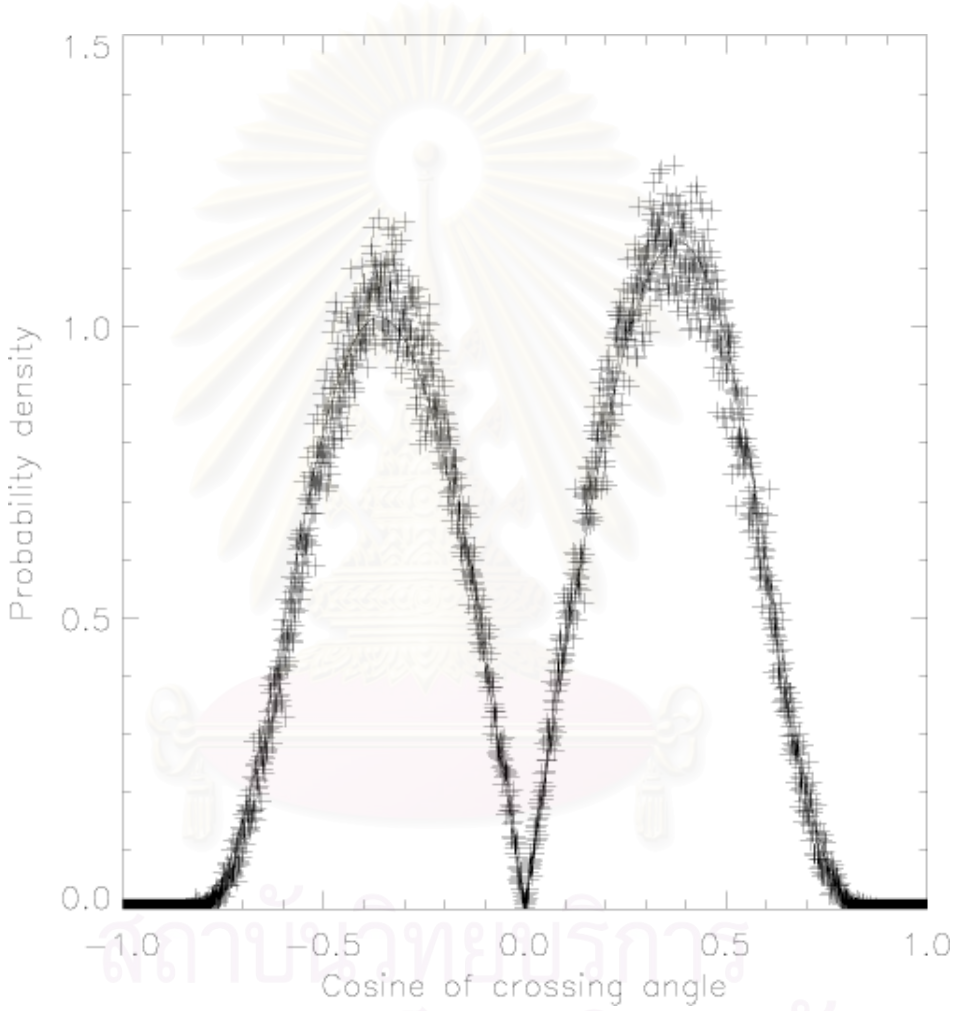

Figure 4.33: The probability density vs. the crossing angles is plotted with the fitted curve at $\delta b/B_0 = 0.5$, $E_{slab} = 1.0$, and $l_z = 0.5$.

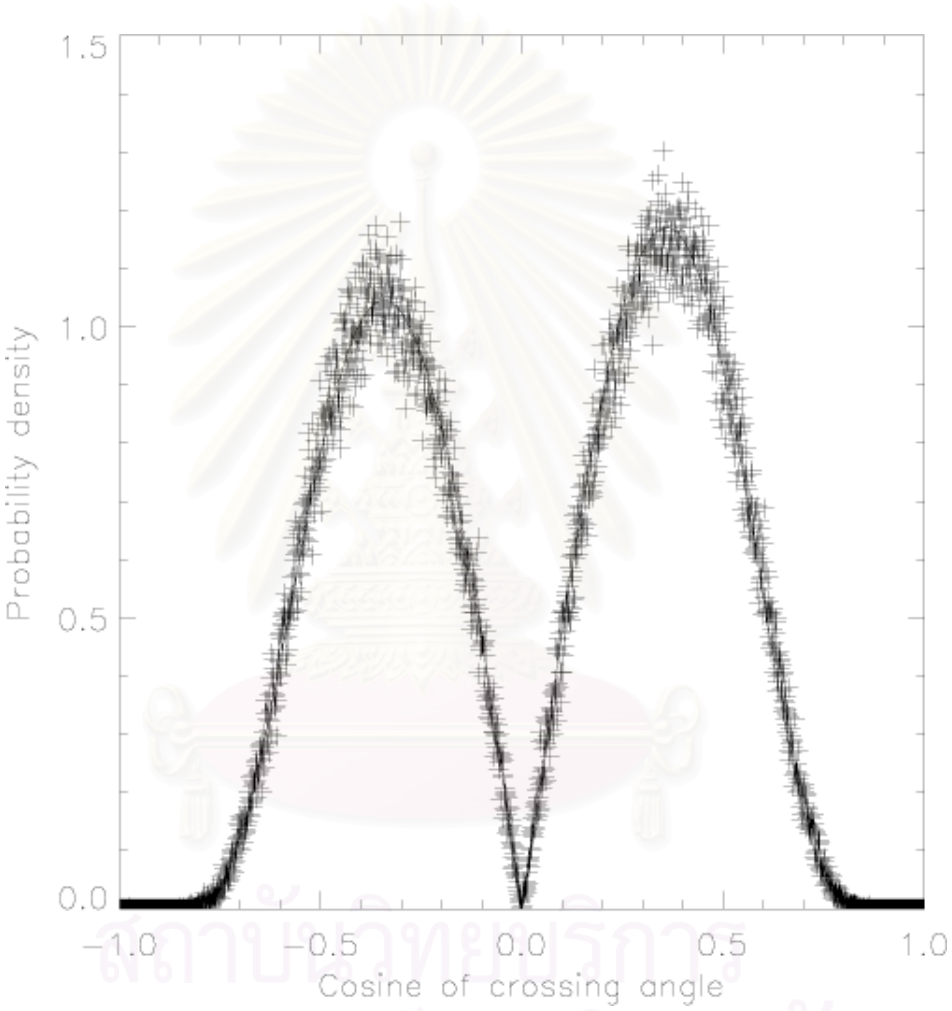

Figure 4.34: The probability density vs. the crossing angles is plotted with the fitted curve at $\delta b/B_0 = 0.5$, $E_{slab} = 0.5$, $l_z = 0.5$, and $l_\perp = 1.0$.

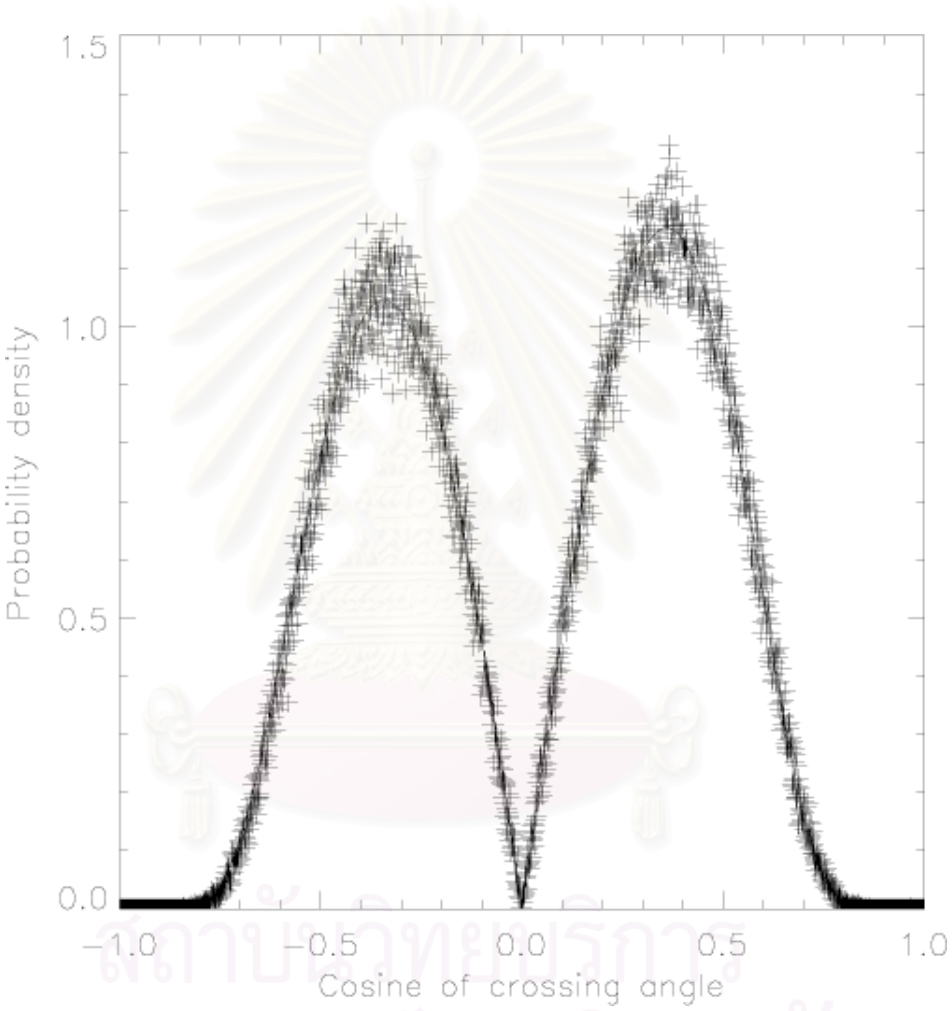

Figure 4.35: The probability density vs. the crossing angles is plotted with the fitted curve at $\delta b/B_0 = 0.5$, $E_{slab} = 0.5$, $l_z = 1.0$, and $l_\perp = 0.2$.

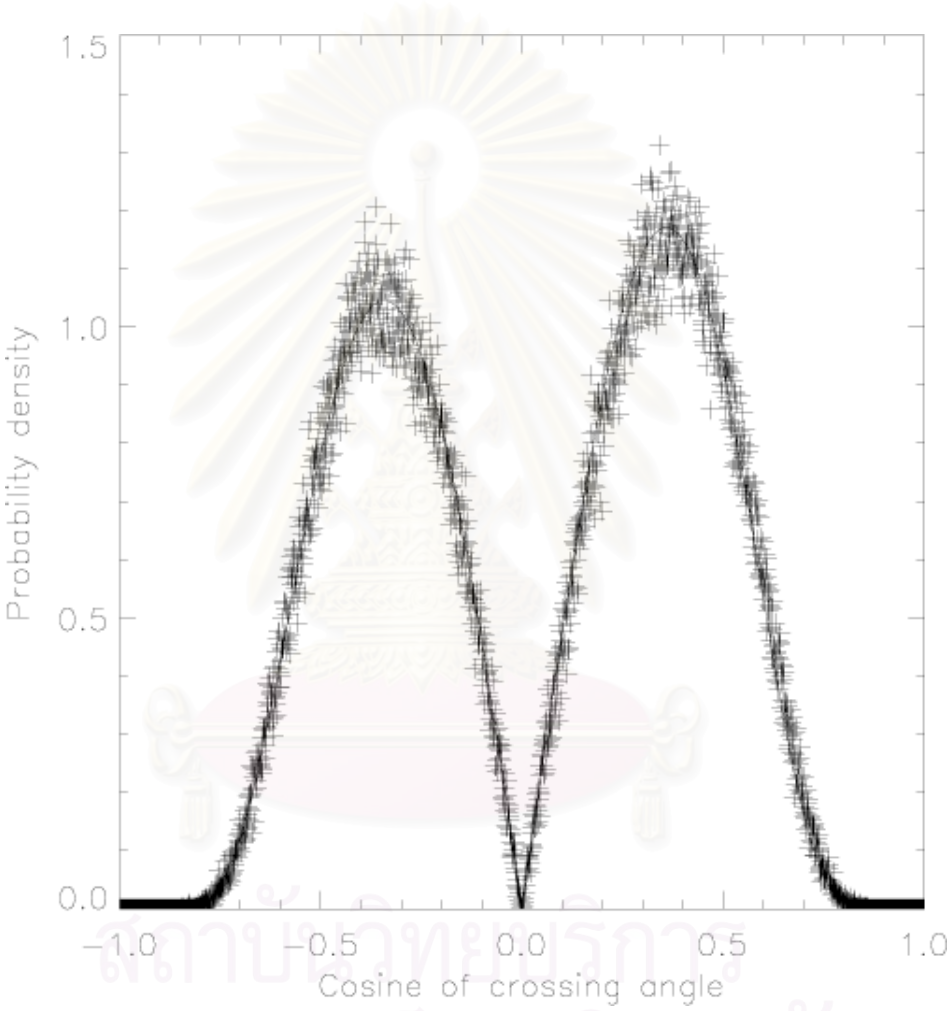

Figure 4.36: The probability density vs. the crossing angles is plotted with the fitted curve at $\delta b/B_0 = 0.5$, $E_{slab} = 0.2$, $l_z = 0.5$, and $l_\perp = 1.0$.

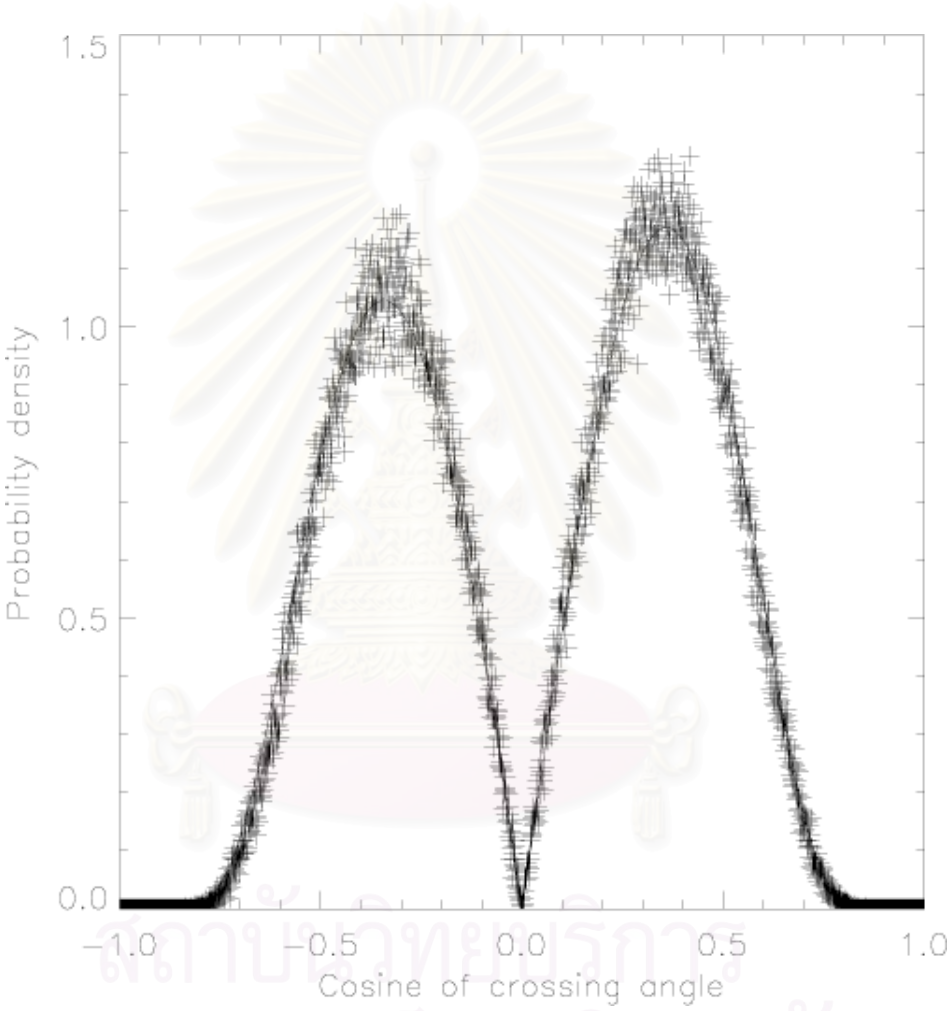

Figure 4.37: The probability density vs. the crossing angles is plotted with the fitted curve at $\delta b/B_0 = 0.5$, $E_{slab} = 0.2$, $l_z = 1$, $l_\perp = 0.2$.

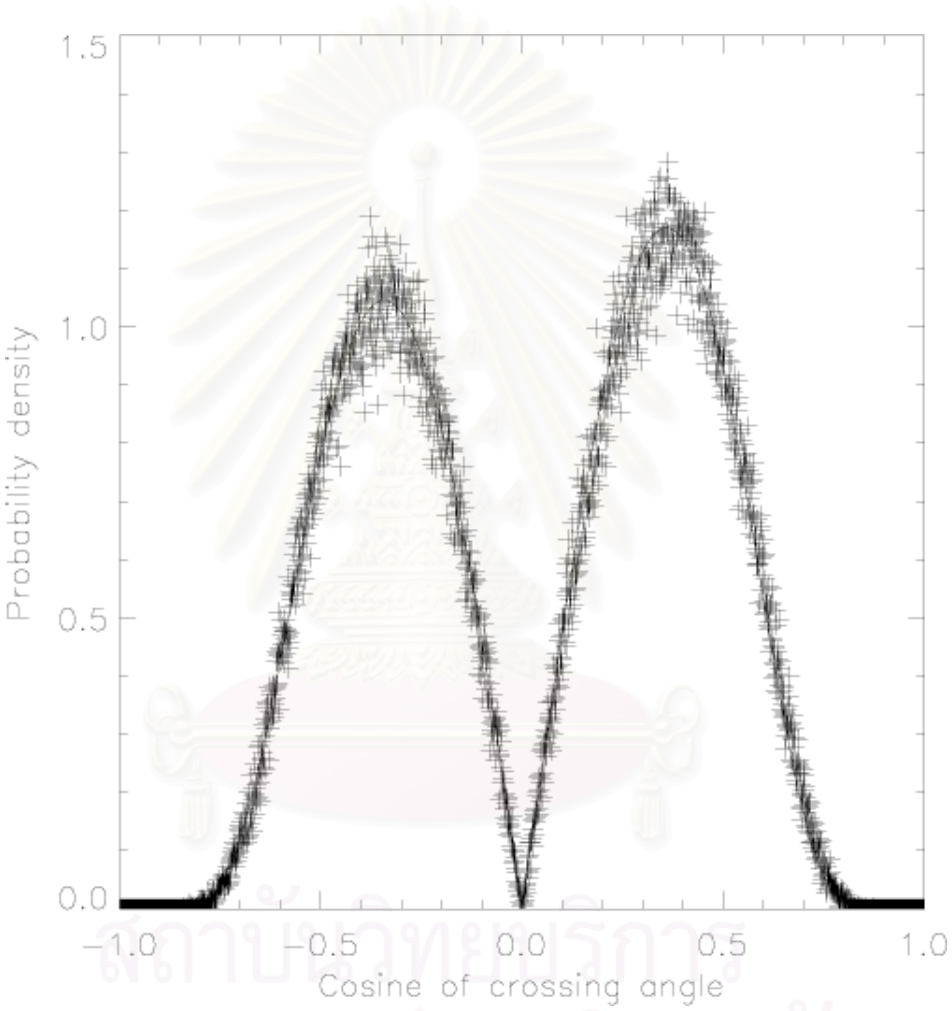

Figure 4.38: The probability density vs. the crossing angles is plotted with the fitted curve at $\delta b/B_0 = 0.5$, $E_{slab} = 0$, and $l_\perp = 1.0$.

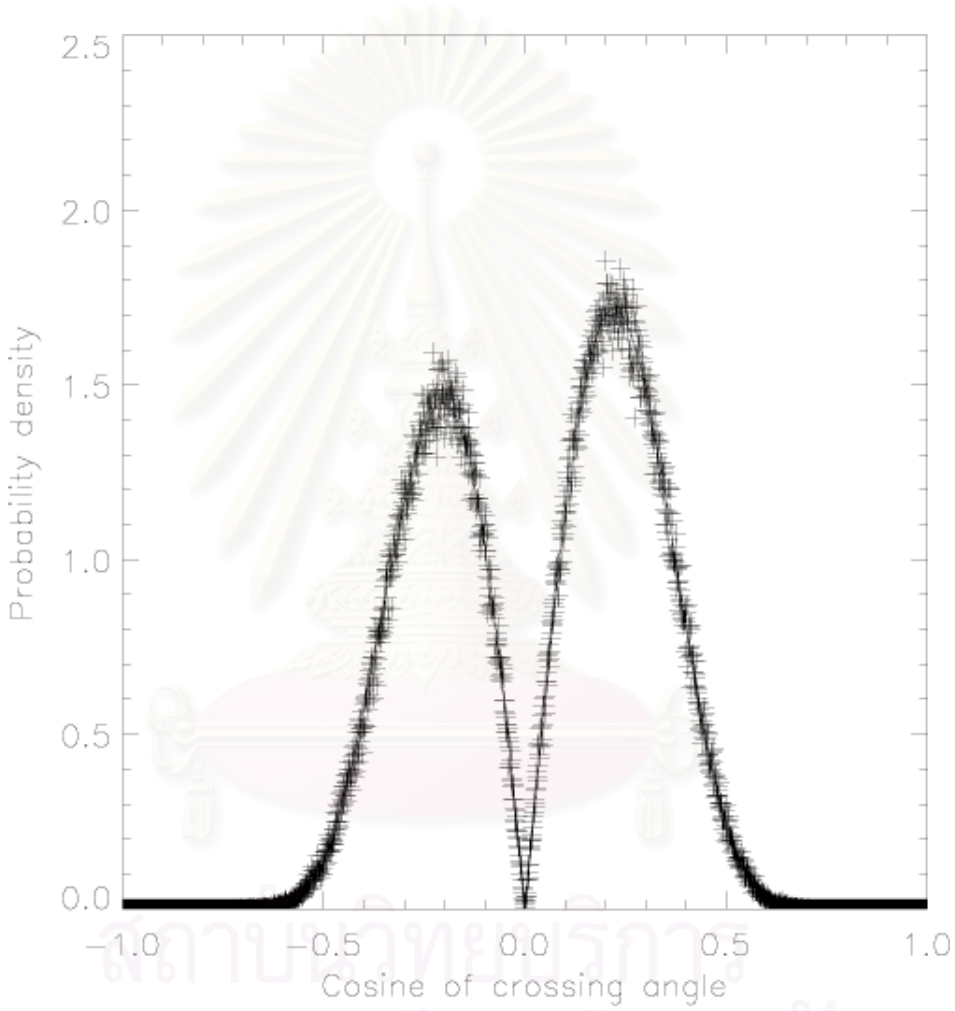

Figure 4.39: The probability density vs. the crossing angles is plotted with the fitted curve at $\delta b/B_0 = 0.3$, $E_{slab} = 0$, and $l_\perp = 1.0$.

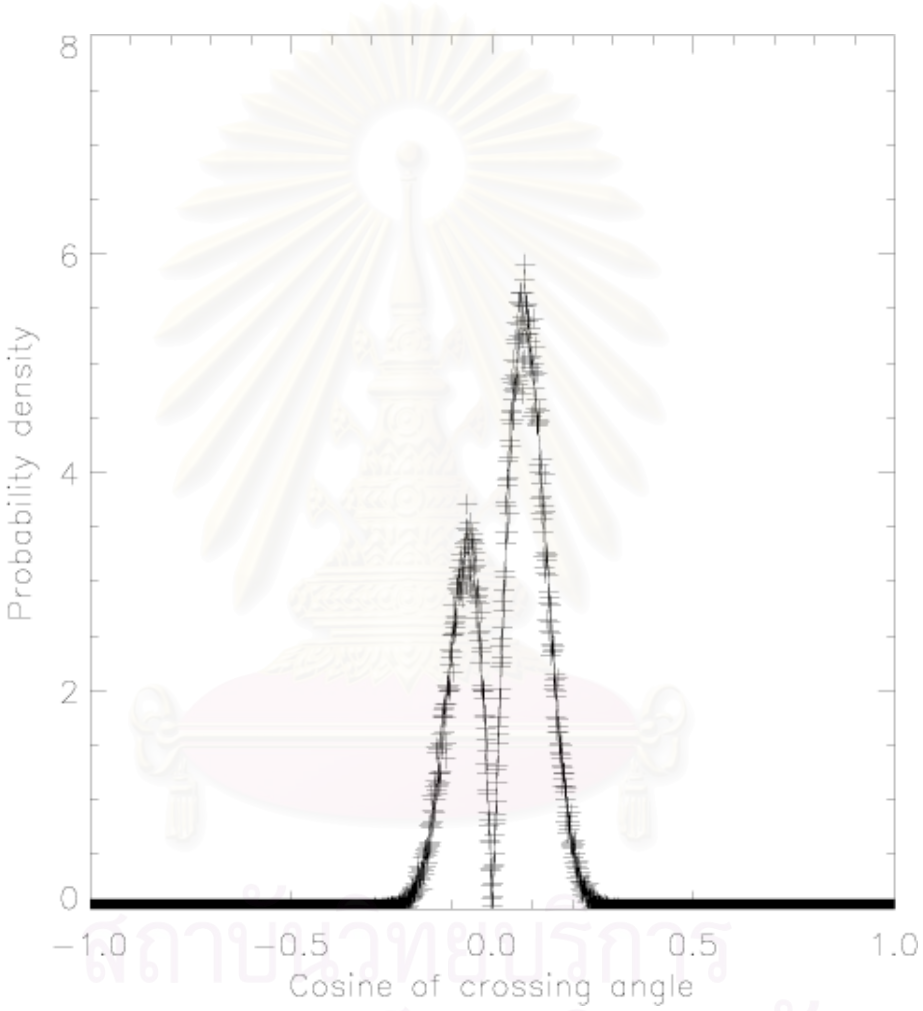

Figure 4.40: The probability density vs. the crossing angles is plotted with the fitted curve at $\delta b/B_0 = 0.1$, $E_{slab} = 0$, and $l_\perp = 1.0$.

Now,

$$P(\cos\theta, b_y) = P(b_x, b_y)\frac{db_x}{d\cos\theta}. \tag{4.12}$$

From (4.10), we can write

$$\begin{aligned} P(b_x, b_y) &= \frac{1}{\pi\langle b^2\rangle}\exp\left[-\frac{1}{\langle b^2\rangle}\left((b_x - b_{0x})^2 + b_y^2\right)\right] \\ &= \frac{1}{\pi\langle b^2\rangle}\exp\left[-\frac{1}{\langle b^2\rangle}\left(\frac{\cos\theta}{\sqrt{1-\cos^2\theta}} - \frac{\cos\theta_0}{\sqrt{1-\cos^2\theta_0}}\right)^2\right] \\ &\quad \times \exp\left\{-\frac{1}{\langle b^2\rangle}b_y^2\left[1 + \left(\frac{\cos\theta}{\sqrt{1-\cos^2\theta}} - \frac{\cos\theta_0}{\sqrt{1-\cos^2\theta_0}}\right)^2\right]\right\} \end{aligned} \tag{4.13}$$

and

$$\left(\frac{\partial b_x}{\partial\cos\theta}\right)_{b_y} = 2\sqrt{b_y^2+1}\left(1-\cos^2\theta\right)^{-\frac{3}{2}}. \tag{4.14}$$

Therefore, (4.12) becomes

$$\begin{aligned} P(\cos\theta, b_y) &= 2\sqrt{b_y^2+1}\left(1-\cos^2\theta\right)^{-\frac{3}{2}}\frac{1}{\pi\langle b^2\rangle} \\ &\quad \times \exp\left[-\frac{1}{\langle b^2\rangle}\left(\frac{\cos\theta}{\sqrt{1-\cos^2\theta}} - \frac{\cos\theta_0}{\sqrt{1-\cos^2\theta_0}}\right)^2\right] \\ &\quad \times \exp\left\{-\frac{1}{\langle b^2\rangle}b_y^2\left[1 + \left(\frac{\cos\theta}{\sqrt{1-\cos^2\theta}} - \frac{\cos\theta_0}{\sqrt{1-\cos^2\theta_0}}\right)^2\right]\right\}. \end{aligned} \tag{4.15}$$

Now, we will integrate over all b_y,

$$\begin{aligned} P(\cos\theta) &= 2\frac{1}{(1-\cos^2\theta)^{\frac{3}{2}}}\exp\left[-\frac{1}{\langle b^2\rangle}\left(\frac{\cos\theta}{\sqrt{1-\cos^2\theta}} - \frac{\cos\theta_0}{\sqrt{1-\cos^2\theta_0}}\right)^2\right] \\ &\quad \times \int_{-\infty}^{\infty}\frac{\sqrt{b_y^2+1}}{\pi\langle b^2\rangle} \\ &\quad \times \exp\left\{-\frac{b_y^2}{\langle b^2\rangle}\left[1 + \left(\frac{\cos\theta}{\sqrt{1-\cos^2\theta}} - \frac{\cos\theta_0}{\sqrt{1-\cos^2\theta_0}}\right)^2\right]\right\}db_y, \end{aligned} \tag{4.16}$$

using

$$\int_{-\infty}^{\infty} \frac{\sqrt{b_y^2+1}}{\pi\langle b^2\rangle} \exp\left\{-\frac{b_y^2}{\langle b^2\rangle}\left[1+\left(\frac{\cos\theta}{\sqrt{1-\cos^2\theta}}-\frac{\cos\theta_0}{\sqrt{1-\cos^2\theta_0}}\right)^2\right]\right\} db_y$$
$$\approx \frac{B}{\sqrt{\left[1+\left(\frac{\cos\theta}{\sqrt{1-\cos^2\theta}}-\frac{\cos\theta_0}{\sqrt{1-\cos^2\theta_0}}\right)^2\right]}}. \quad (4.17)$$

Now (4.16) becomes

$$P(\cos\theta) \approx A\frac{1}{(1-\cos^2\theta)^{\frac{3}{2}}\sqrt{1+\left(\frac{\cos\theta}{\sqrt{1-\cos^2\theta}}-\frac{\cos\theta_0}{\sqrt{1-\cos^2\theta_0}}\right)^2}}$$
$$\times \exp\left[-\frac{1}{\langle b^2\rangle}\left(\frac{\cos\theta}{\sqrt{1-\cos^2\theta}}-\frac{\cos\theta_0}{\sqrt{1-\cos^2\theta_0}}\right)^2\right]. \quad (4.18)$$

From the simulations, we keep the data of a magnetic field line as positions along its trajectory. When the space between each position is small, the vector that points from one position to the next position approximately lies along the magnetic field line. When the magnetic field line crosses a shock, we know the position before crossing, the position after crossing, and the vector as shown in Figure 4.41. The probability that the magnetic field line can cross the shock with angle θ is proportional to $|\cos\theta|$, because if a magnetic field line segment length Δl starts to cross the shock outside a distance $\Delta l\cos\theta$ from the shock, it cannot reach the shock. For $E_{slab} = 1$, the probability that the magnetic field line can cross the shock with angle θ is proportional to $\cot\theta$ because the correlation length is on the z direction. Therefore the distribution of crossing angles for $E_{slab} \neq 1$ is

$$P(\cos\theta) = C_1\frac{|\cos\theta|}{(1-\cos^2\theta)^{3/2}\sqrt{1+\left(\frac{\cos\theta}{\sqrt{1-\cos^2\theta}}-\frac{\cos\theta_0}{\sqrt{1-\cos^2\theta_0}}\right)^2}}$$
$$\times \exp\left[-\frac{1}{\langle b^2\rangle}\left(\frac{\cos\theta}{\sqrt{1-\cos^2\theta}}-\frac{\cos\theta_0}{\sqrt{1-\cos^2\theta_0}}\right)^2\right], \quad (4.19)$$

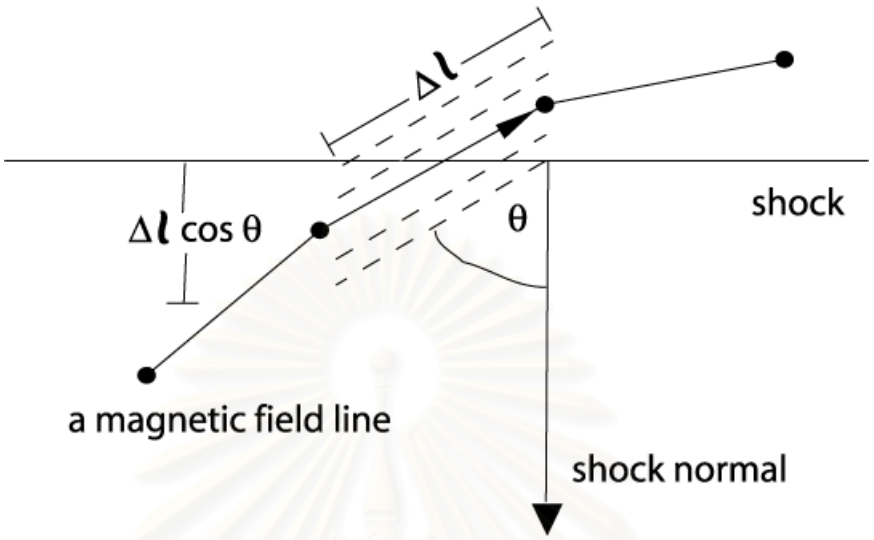

Figure 4.41: The probability that the magnetic field line can cross the shock with angle θ is proportional to $|\cos\theta|$.

Table 4.2: The parameter C_i as a function of $\delta b/B_0$.

$\delta b/B_0$	C_1	C_2
0.5	4.85	4.41
0.3	12.00	11.53
0.1	98.18	97.67

and the distribution of crossing angles for $E_{slab} = 1$ is

$$P(\cos\theta) = C_2 \frac{|\cos\theta|}{(1-\cos^2\theta)^2 \sqrt{1+\left(\frac{\cos\theta}{\sqrt{1-\cos^2\theta}} - \frac{\cos\theta_0}{\sqrt{1-\cos^2\theta_0}}\right)^2}} \times \exp\left[-\frac{1}{\langle b^2\rangle}\left(\frac{\cos\theta}{\sqrt{1-\cos^2\theta}} - \frac{\cos\theta_0}{\sqrt{1-\cos^2\theta_0}}\right)^2\right] \quad (4.20)$$

The values of C_1 and C_2 for each value of $\delta b/B_0$ are shown in Table 4.2.

4.4 Distance between crossings

When charged particles move longer than their mean free path, their pitch angles become random. In our model, the distance between each crossing is used to determine the pitch angle at each crossing. If the distance between two crossings is further than the particle's mean free path, the particle's pitch angle becomes random. If the distance between two crossings is closer than the particle's mean free path, the particle's pitch angle is approximately unchanged. The data on the position of magnetic field lines are collected at intervals of Δz along the z direction, where $\Delta z = 100,000/2^{22} = 0.0238$. Therefore, we are not able to measure the distance between each crossing at intervals shorter than Δz. The data on crossing distances of order Δz are also not accurate.

First, we consider only the pure slab case. Figures 4.42 to 4.44 show the distribution of the distance between each crossing with $l_z = 1$ au from $\delta b/B_0 = 0.5$ to $\delta b/B_0 = 0.1$, respectively. After that, we consider compound turbulence. At $E_{slab} = 0.8$, the distributions of distance are shown in Figures 4.45 to 4.47 for $l_z = 1$ au and $l_\perp = 1$ au from $\delta b/B_0 = 0.5$ to $\delta b/B_0 = 0.1$, respectively. Figures 4.48 to 4.50 show the distribution with $E_{slab} = 0.5$, $l_z = 1$ au, and $l_\perp = 1$ au from from $\delta b/B_0 = 0.5$ to $\delta b/B_0 = 0.1$, respectively, while Figures 4.51 to 4.53 show the distribution with $E_{slab} = 0.2$, $l_z = 1$ au, and $l_\perp = 1$ au from $\delta b/B_0 = 0.5$ to $\delta b/B_0 = 0.1$, respectively.

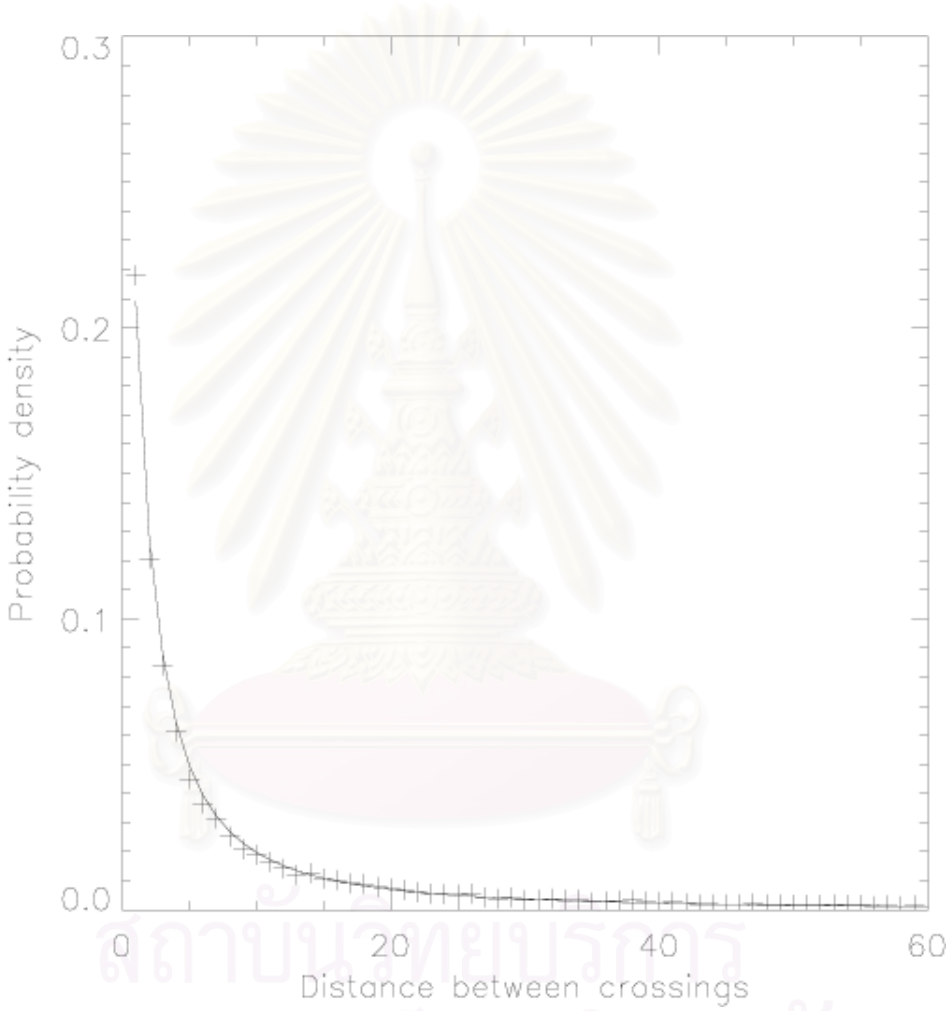

Figure 4.42: Distribution of distance between crossings for $\delta b/B_0 = 0.5$, $E_{slab} = 1.0$, and $l_z = 1.0$.

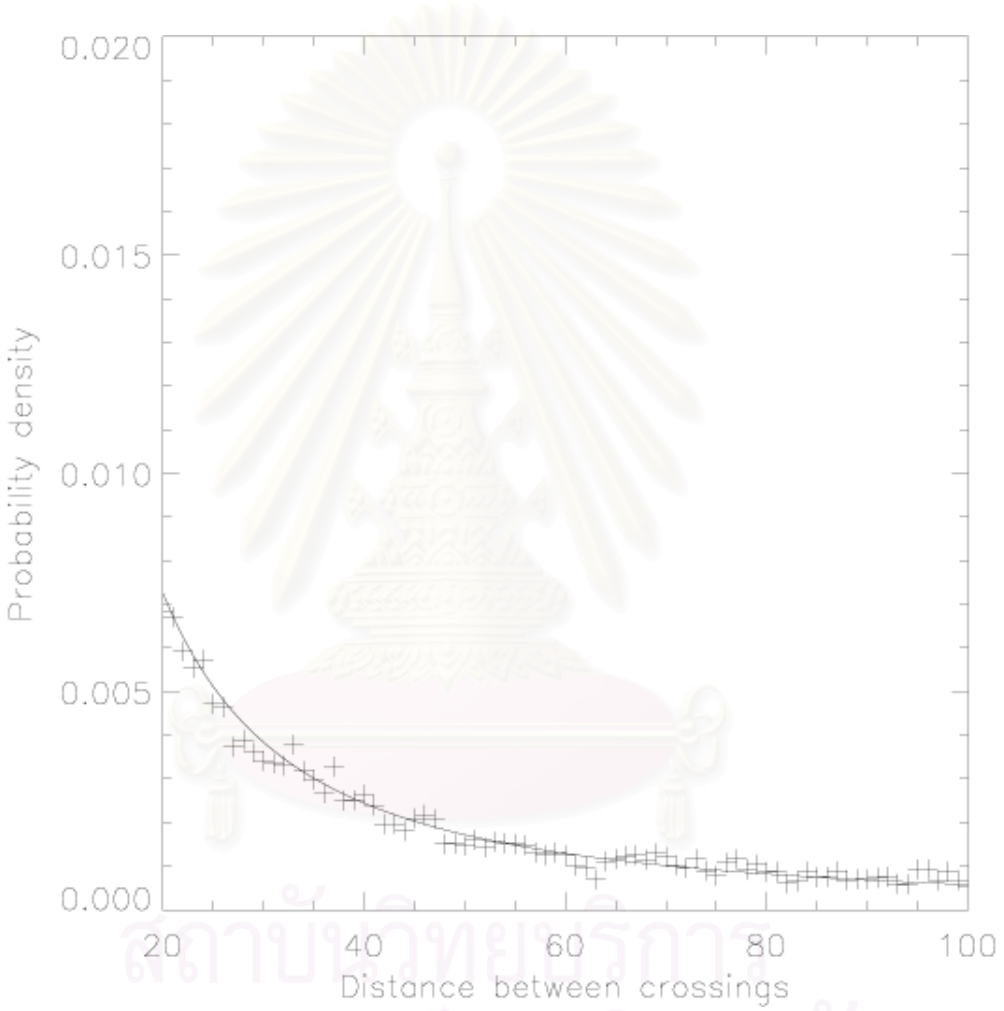

Figure 4.43: Distribution of distance between crossings for $\delta b/B_0 = 0.3$, $E_{slab} = 1.0$, and $l_z = 1.0$.

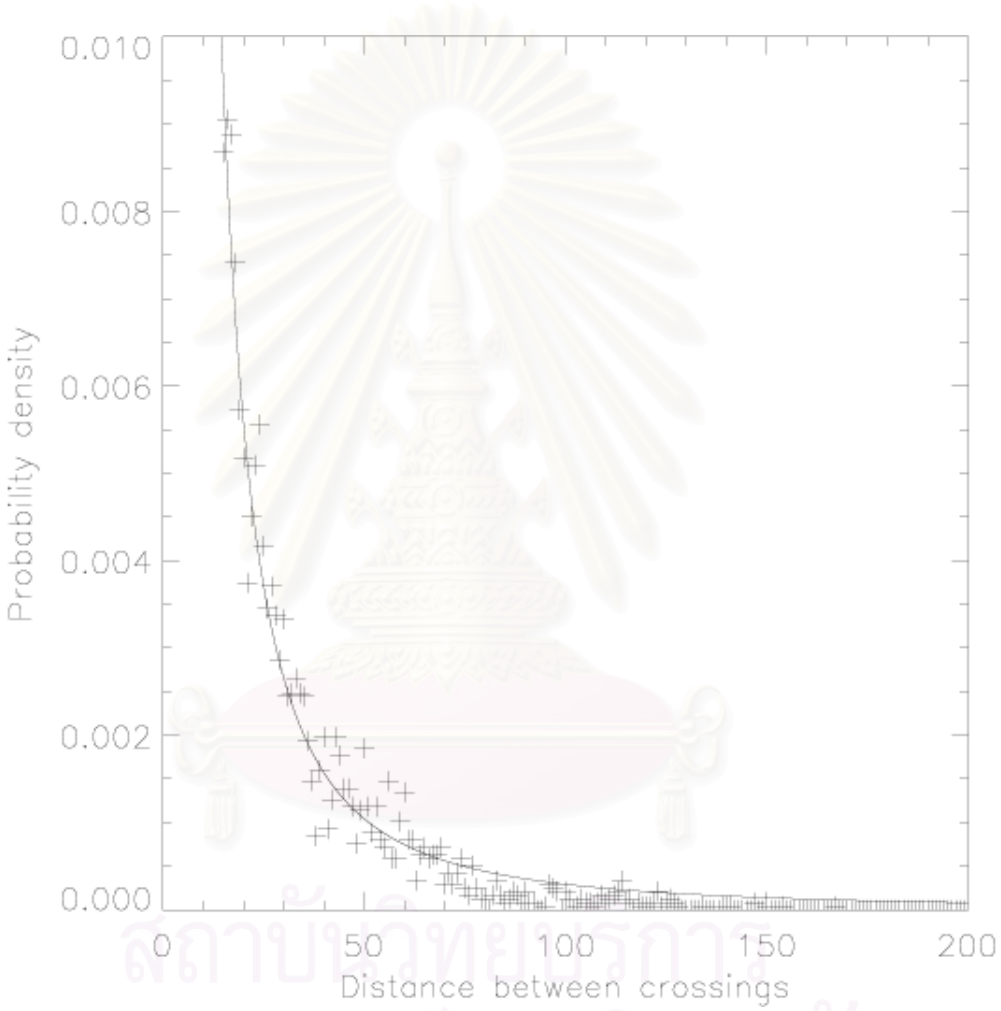

Figure 4.44: Distribution of distance between crossings for $\delta b/B_0 = 0.1$, $E_{slab} = 1.0$, and $l_z = 1.0$.

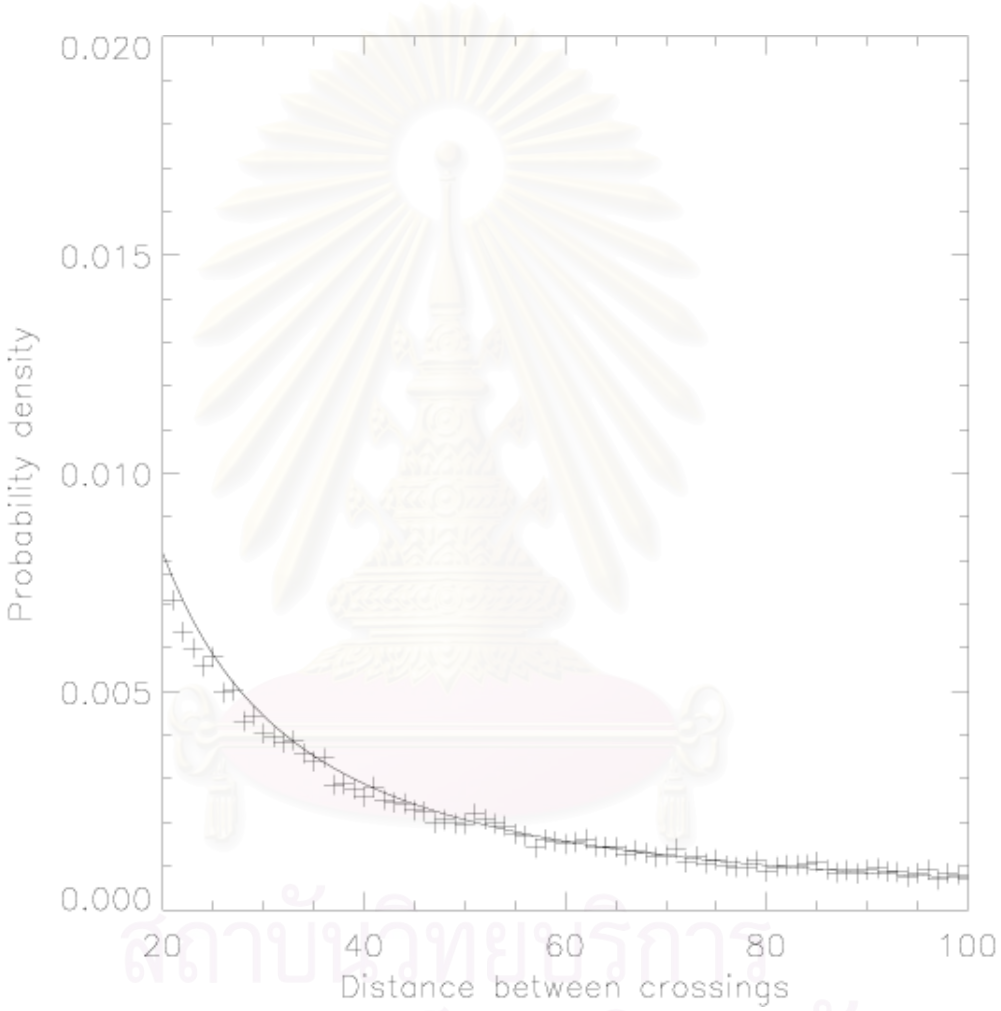

Figure 4.45: Distribution of distance between crossings for $\delta b/B_0 = 0.5$, $E_{slab} = 0.8$, $l_z = 1.0$, and $l_\perp = 1.0$.

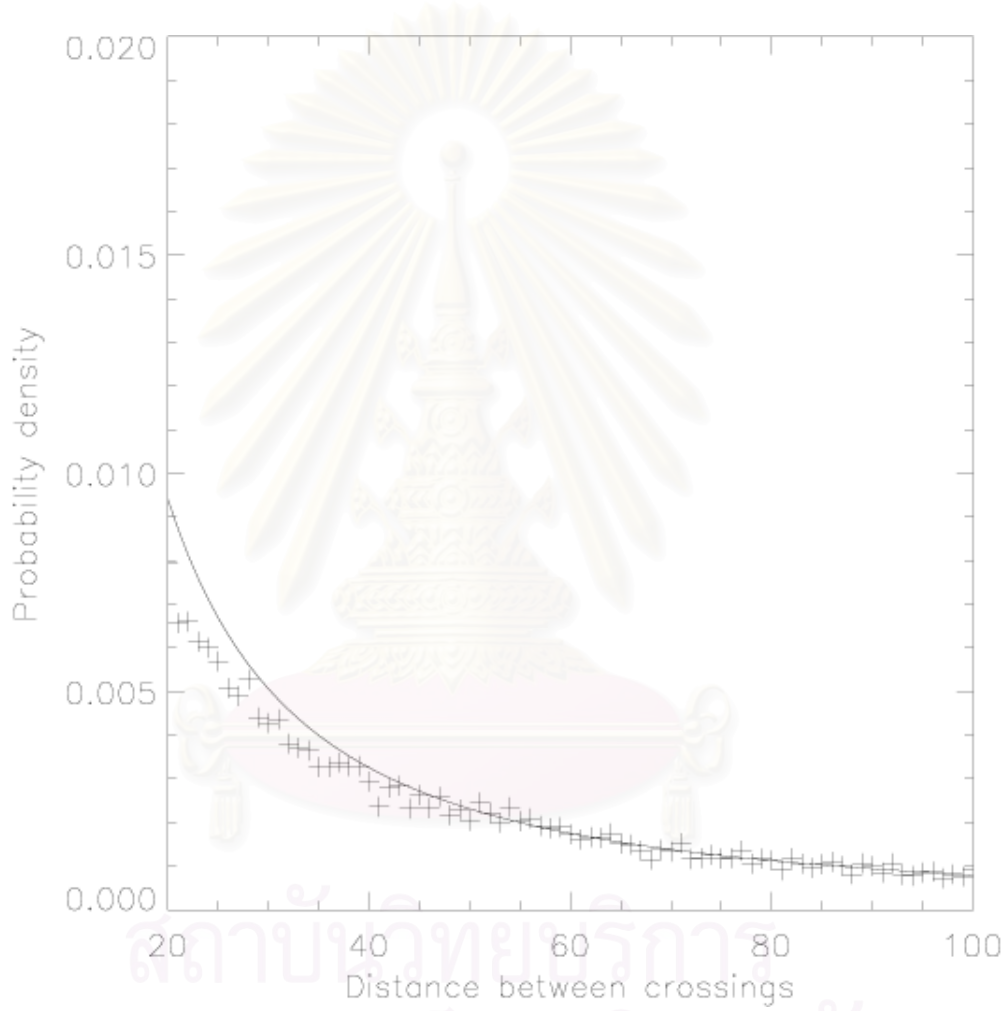

Figure 4.46: Distribution of distance between crossings for $\delta b/B_0 = 0.3$, $E_{slab} = 0.8$, $l_z = 1.0$, and $l_\perp = 1.0$.

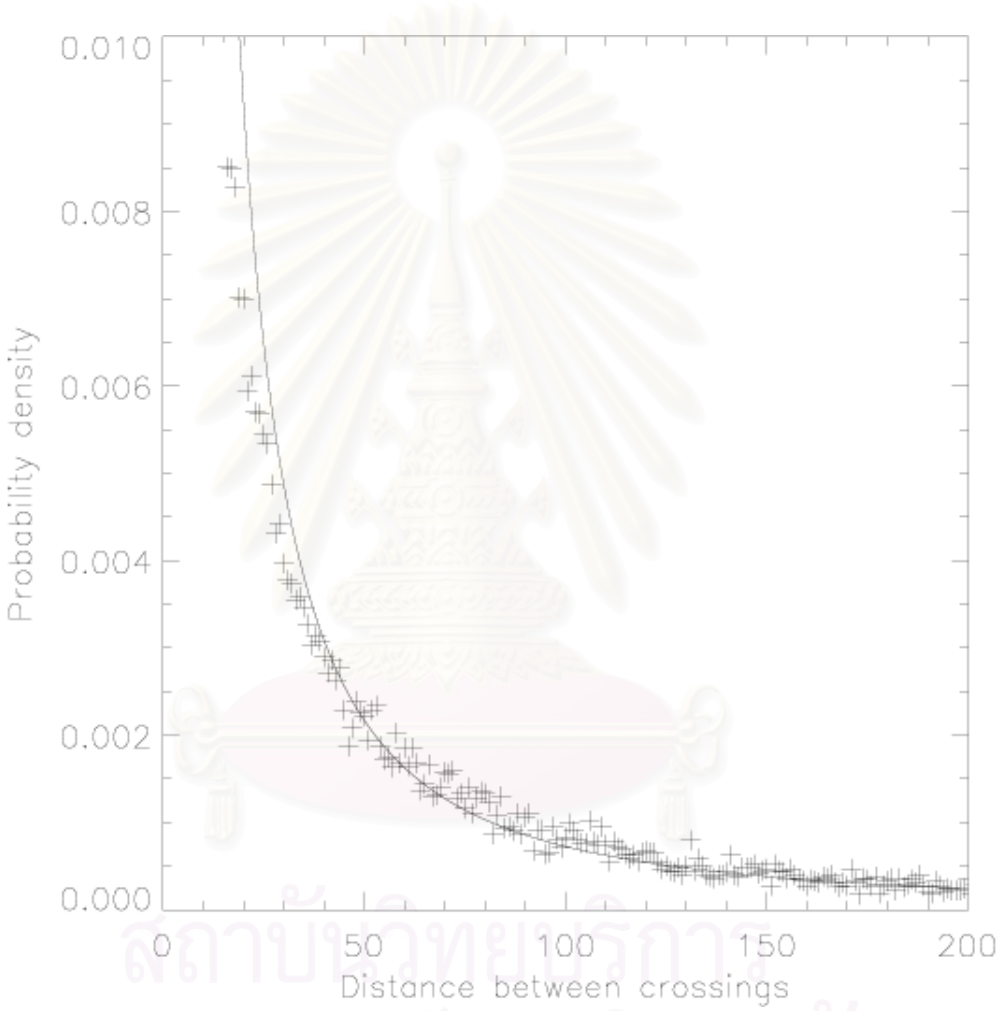

Figure 4.47: Distribution of distance between crossings for $\delta b/B_0 = 0.1$, $E_{slab} = 0.8$, $l_z = 1.0$, and $l_\perp = 1.0$.

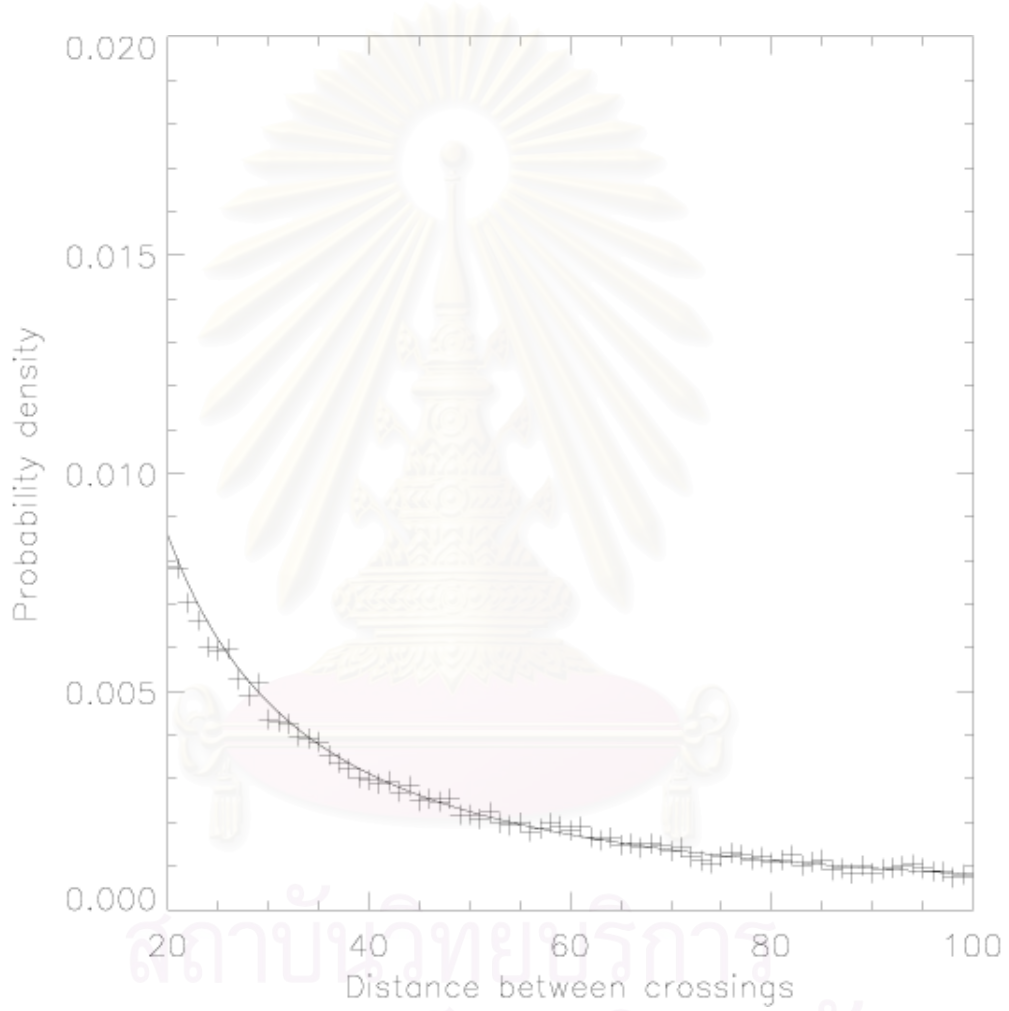

Figure 4.48: Distribution of distance between crossings for $\delta b/B_0 = 0.5$, $E_{slab} = 0.5$, $l_z = 1.0$, and $l_\perp = 1.0$.

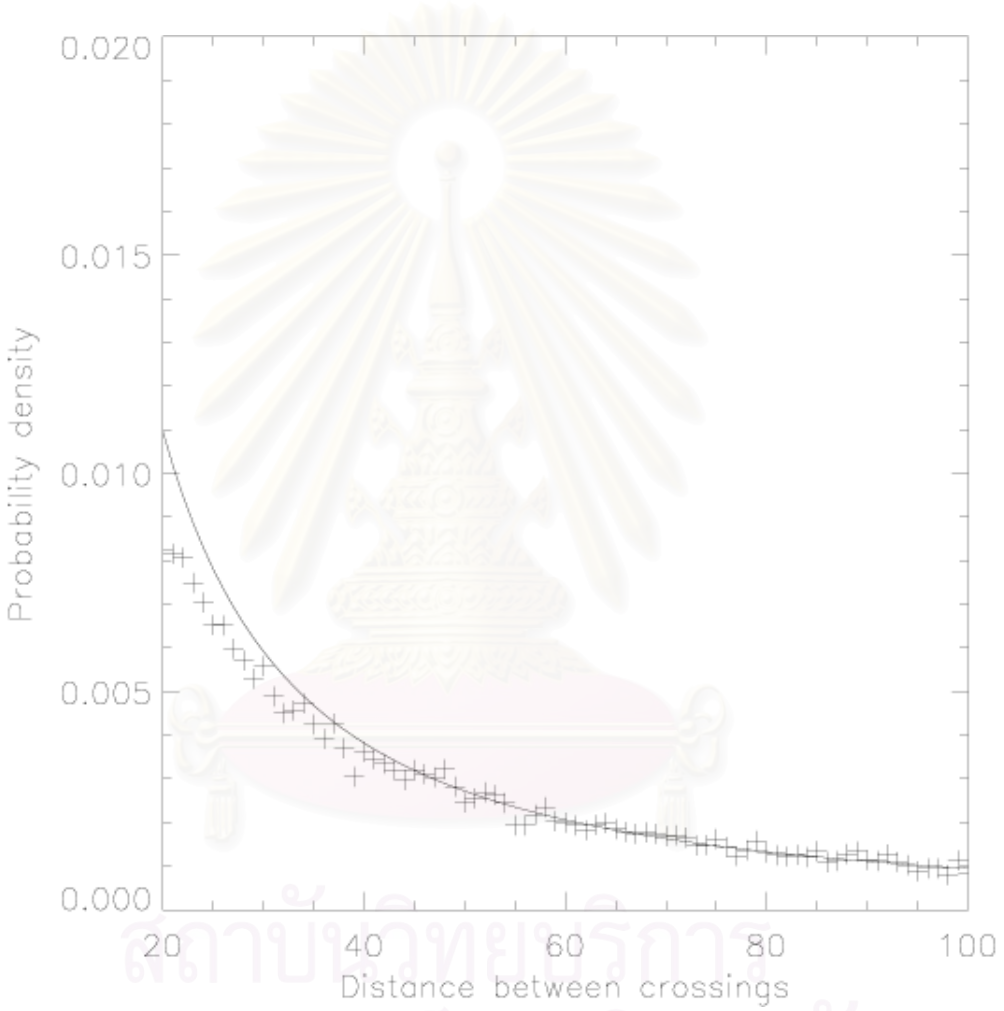

Figure 4.49: Distribution of distance between crossings for $\delta b/B_0 = 0.3$, $E_{slab} = 0.5$, $l_z = 1.0$, and $l_\perp = 1.0$.

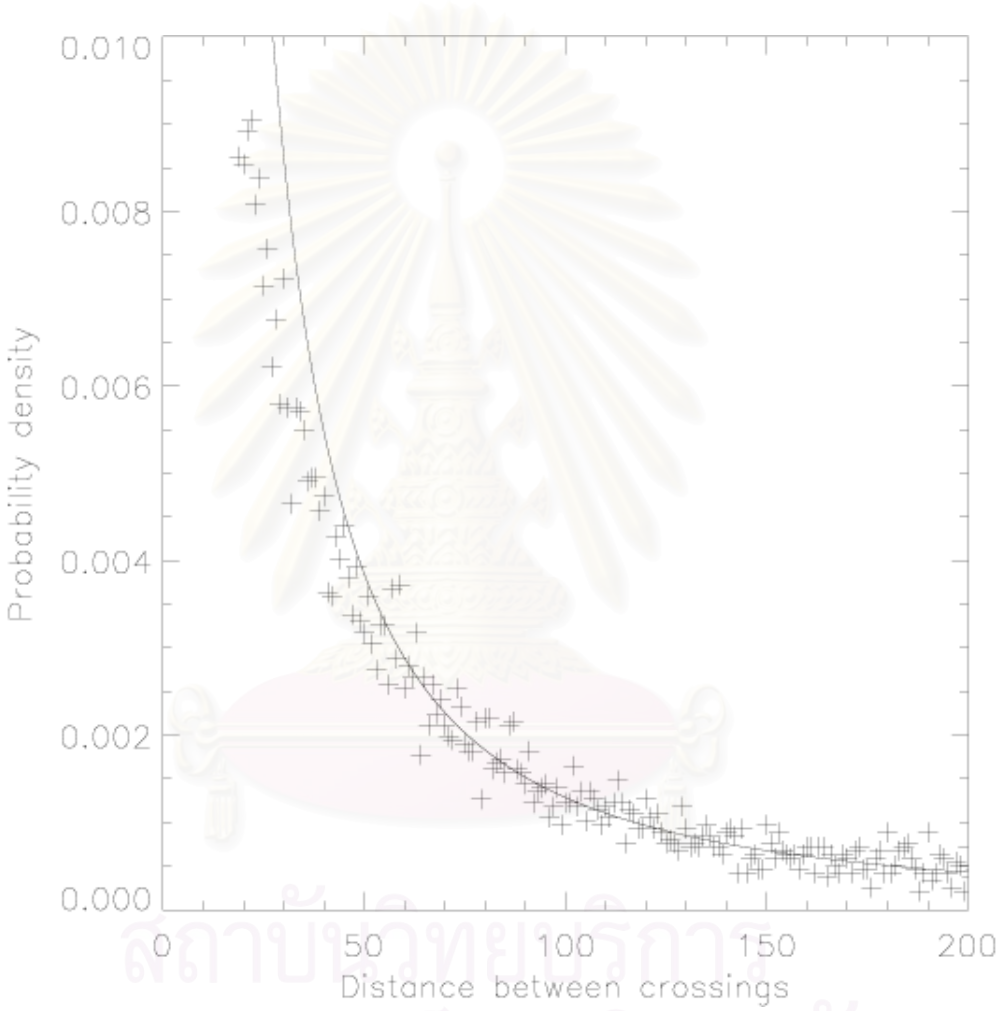

Figure 4.50: Distribution of distance between crossings for $\delta b/B_0 = 0.1$, $E_{slab} = 0.5$, $l_z = 1.0$, and $l_\perp = 1.0$.

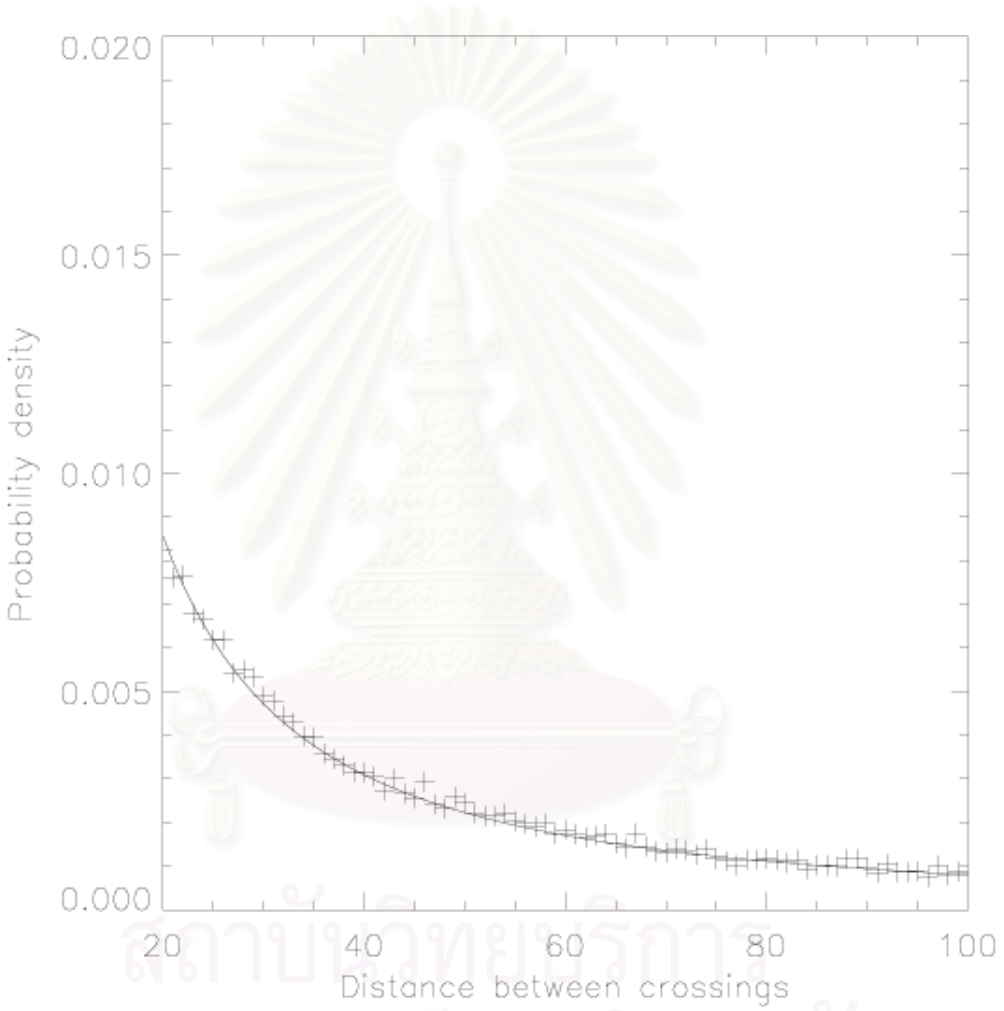

Figure 4.51: Distribution of distance between crossings for $\delta b/B_0 = 0.5$, $E_{slab} = 0.2$, $l_z = 1.0$, and $l_\perp = 1.0$.

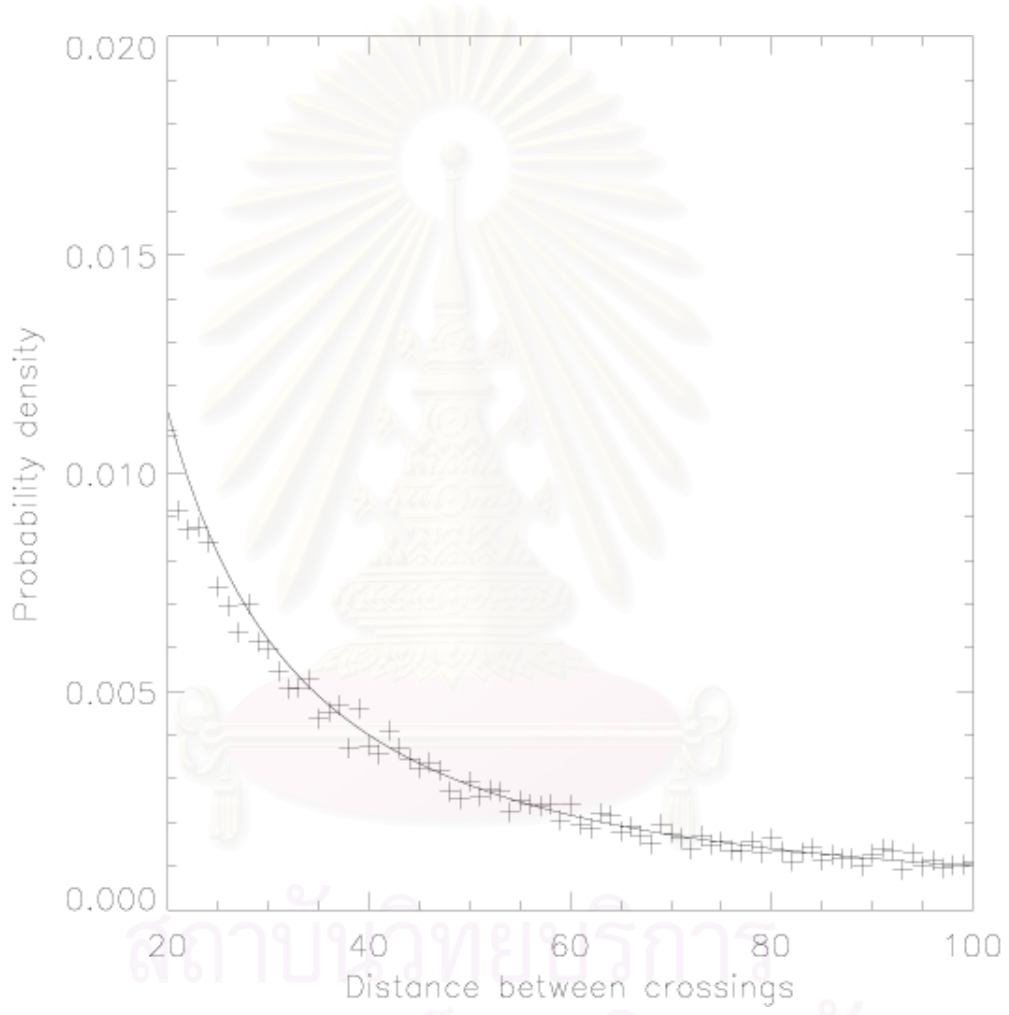

Figure 4.52: Distribution of distance between crossings for $\delta b/B_0 = 0.3$, $E_{slab} = 0.2$, $l_z = 1.0$, and $l_\perp = 1.0$.

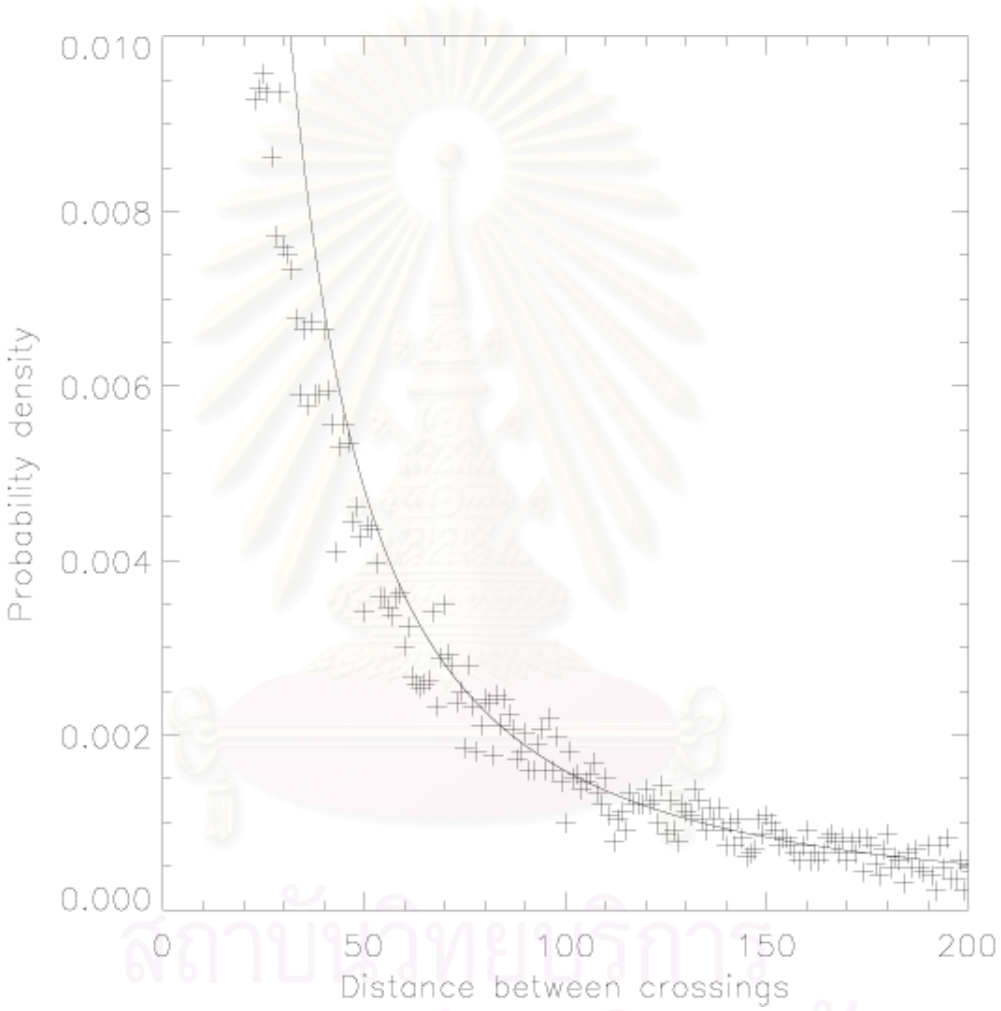

Figure 4.53: Distribution of distance between crossings for $\delta b/B_0 = 0.1$, $E_{slab} = 0.2$, $l_z = 1.0$, and $l_\perp = 1.0$.

For the pure 2D case, Figures 4.54 to 4.56 show the distribution of the distance between crossings with $l_\perp = 1$ au from $\delta b/B_0 = 0.5$ to $\delta b/B_0 = 0.1$, respectively.

Next we vary the values of l_z and $l_\perp$. Figure 4.57 shows the distribution of crossing distance in the pure slab case with $l_z = 0.5$ au, and $\delta b/B_0 = 0.5$. At $E_{slab} = 0.5$ and $\delta b/B_0 = 0.5$, Figure 4.58 shows the distribution of crossing distance with $l_z = 0.5$ au and $l_\perp = 1$ au, and Figure 4.59 shows the distribution of crossing distance with $l_z = 1$ au and $l_\perp = 0.2$ au. At $E_{slab} = 0.2$ and $\delta b/B_0 = 0.5$, Figure 4.60 shows the distribution of crossing distance with $l_z = 0.5$ au and $l_\perp = 1$ au, and Figure 4.61 shows the distribution of crossing distance with $l_z = 1$ au and $l_\perp = 0.2$ au.

The distribution of crossing distance for the cases of pure slab and compound turbulence can be fitted with $P(l) = al^b$ since the magnetic field line random walk is fractal and scale invariant, but the 2D case cannot be fitted with this form because the islands have a fixed scale size. Because we collect the discrete data, the data for small distances are not accurate. Therefore we fit only the data with the distance higher than the average distance. Table 4.3 shows the parameters a, b, and the average crossing distances $\bar{d}$ after we fit the data in each case.

The average distance increases as $\delta b/B_0$ increases for the pure slab and compound case, but decreases as $\delta b/B_0$ increases for the pure 2D case. In the pure 2D case, magnetic field lines have periodic helix-like trajectory. The number of loops per unit length in the z direction is constant. If we imagine z as time, the turbulent magnetic field is the velocity of a particle. The magnetic field line in the x-y plane is the trajectory of the particle. If the magnitude of the velocity

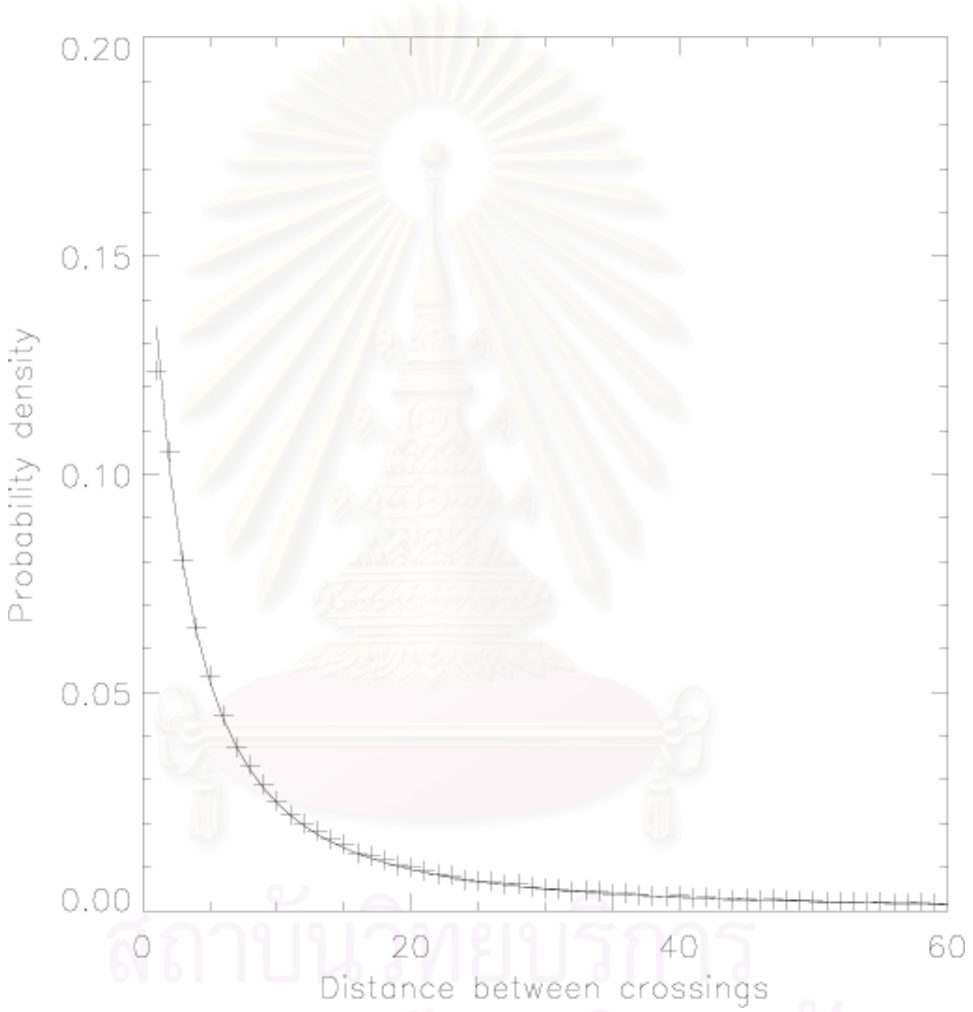

Figure 4.54: Distribution of distance between crossings for $\delta b/B_0 = 0.5$, $E_{slab} = 0$, and $l_\perp = 1.0$.

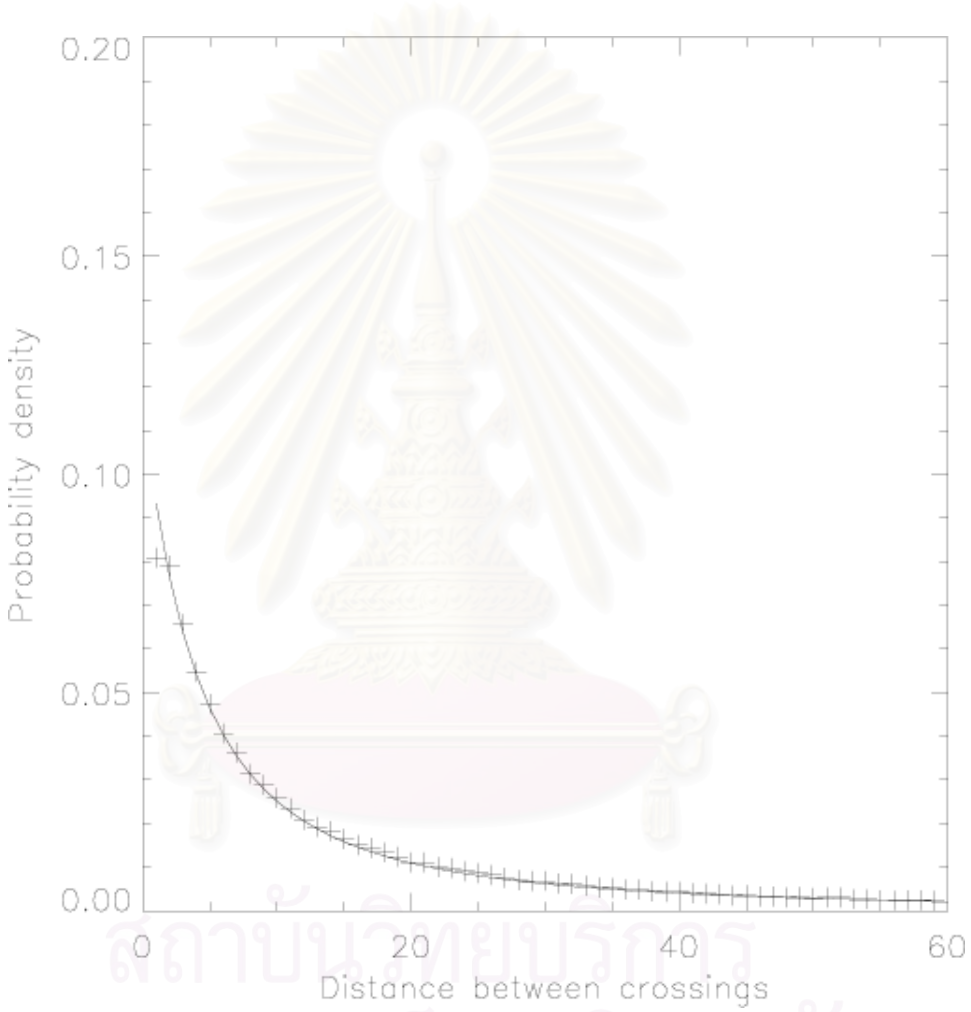

Figure 4.55: Distribution of distance between crossings for $\delta b/B_0 = 0.3$, $E_{slab} = 0$, and $l_\perp = 1.0$.

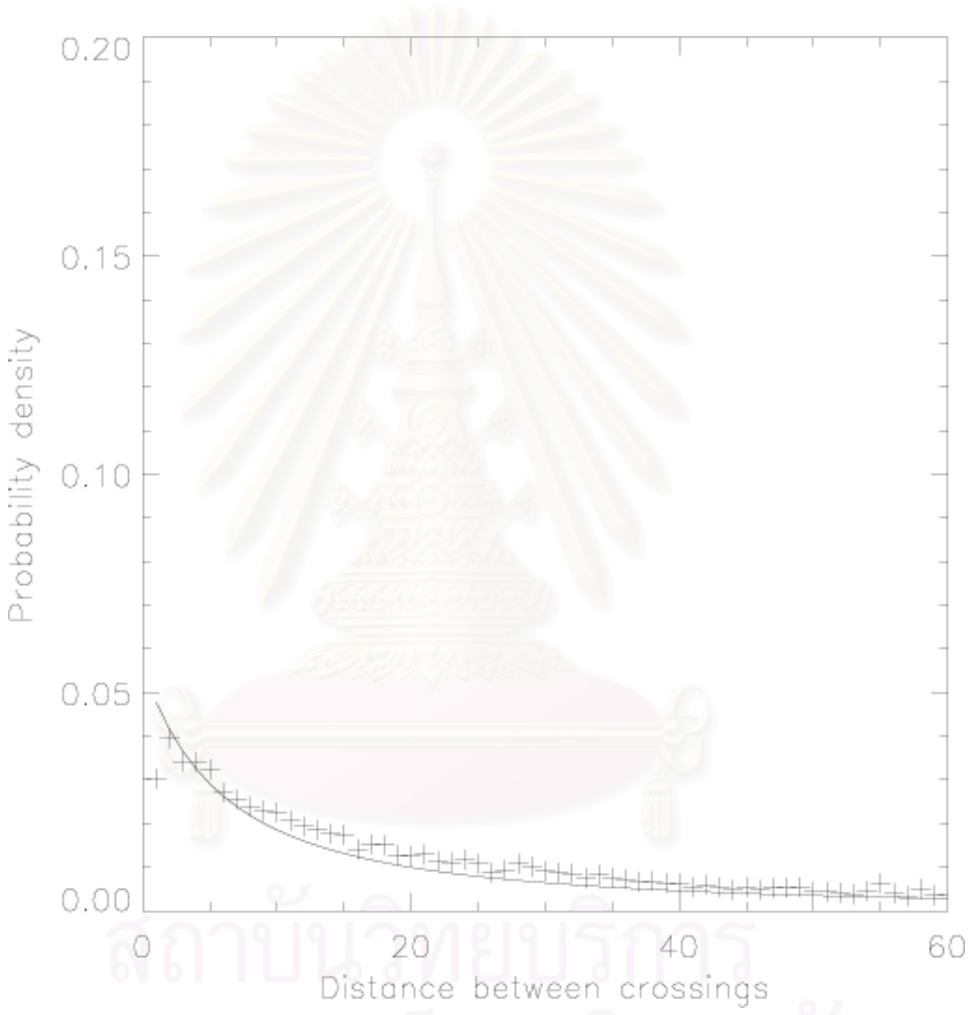

Figure 4.56: Distribution of distance between crossings for $\delta b/B_0 = 0.1$, $E_{slab} = 0$, and $l_\perp = 1.0$.

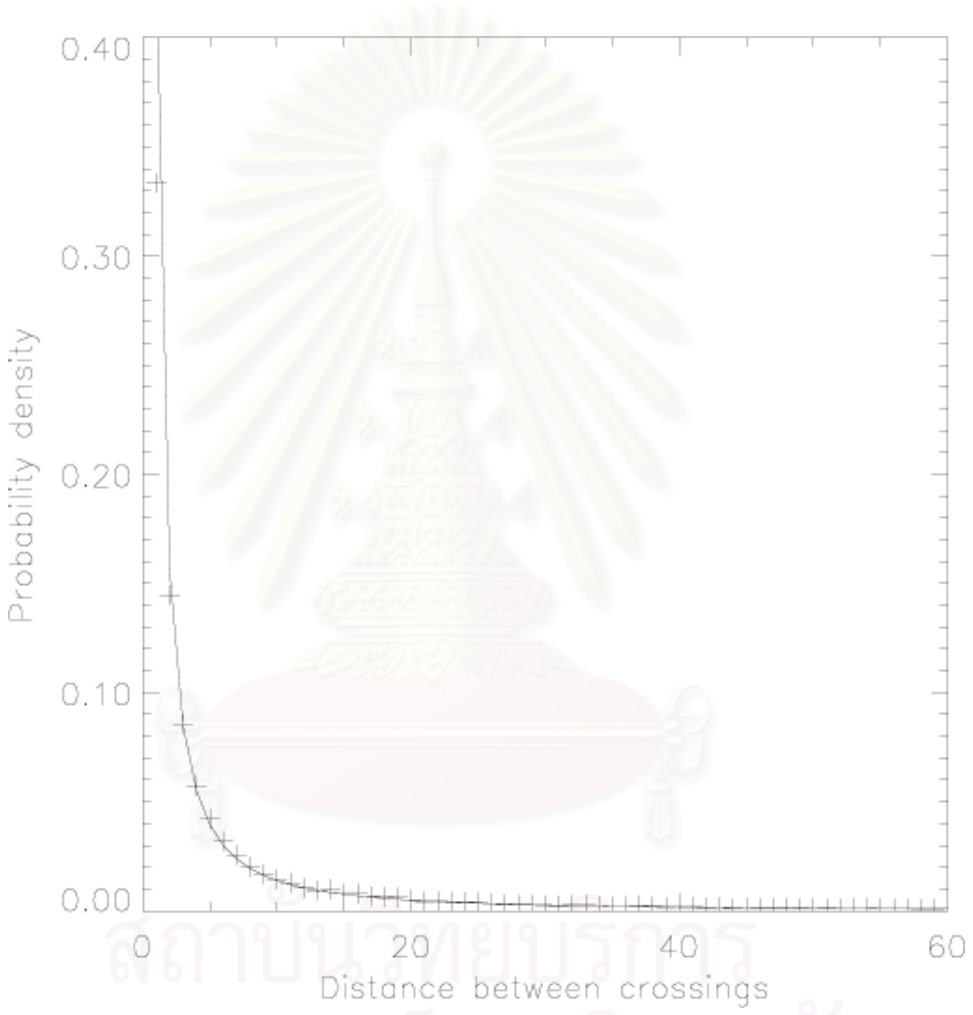

Figure 4.57: Distribution of distance between crossings for $\delta b/B_0 = 0.5$, $E_{slab} = 1$, and $l_z = 0.5$.

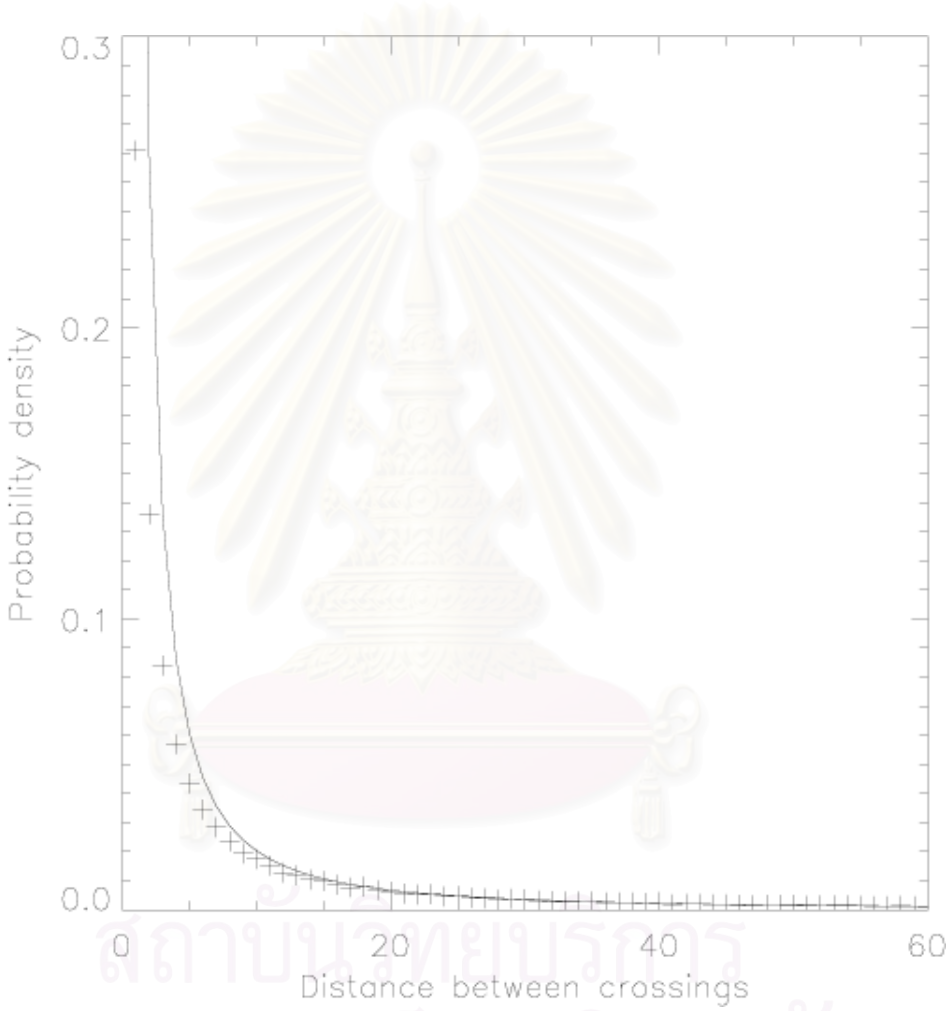

Figure 4.58: Distribution of distance between crossings for $\delta b/B_0 = 0.5$, $E_{slab} = 0.5$, $l_z = 0.5$, and $l_\perp = 1.0$.

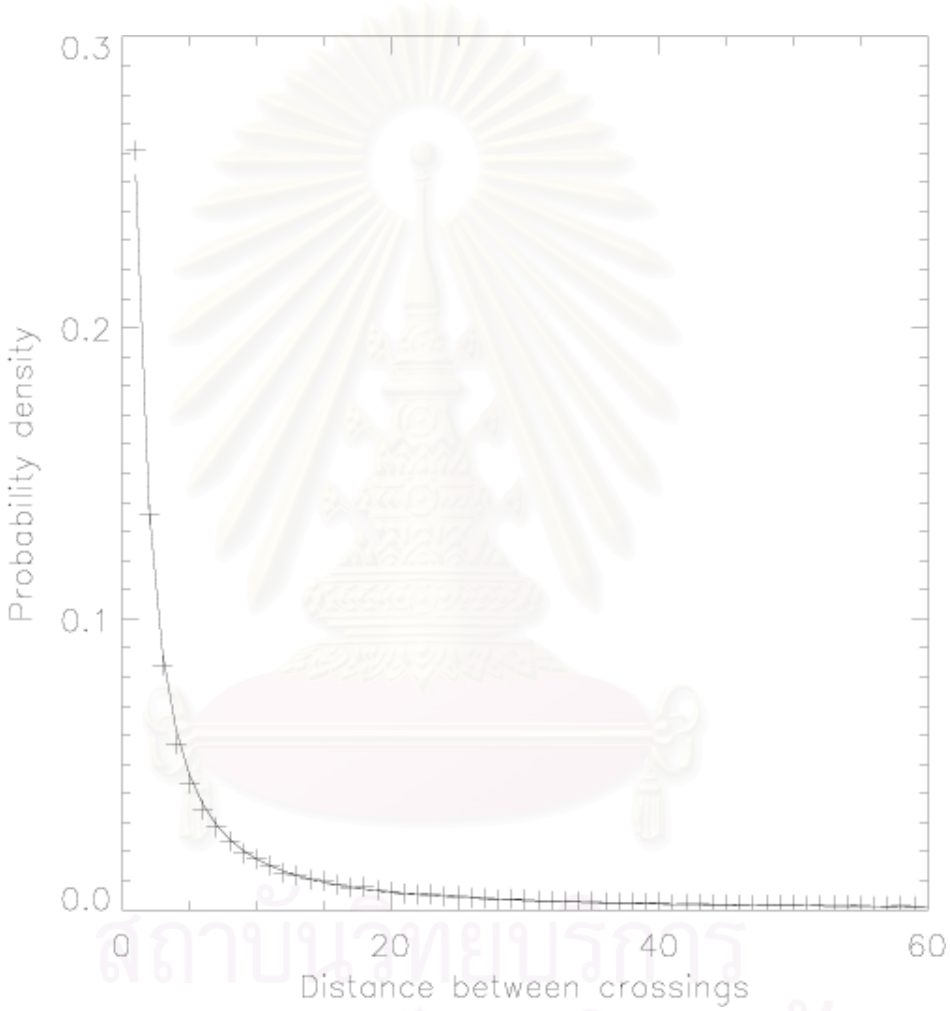

Figure 4.59: Distribution of distance between crossings for $\delta b/B_0 = 0.5$, $E_{slab} = 0.5$, $l_z = 1.0$, and $l_\perp = 0.2$.

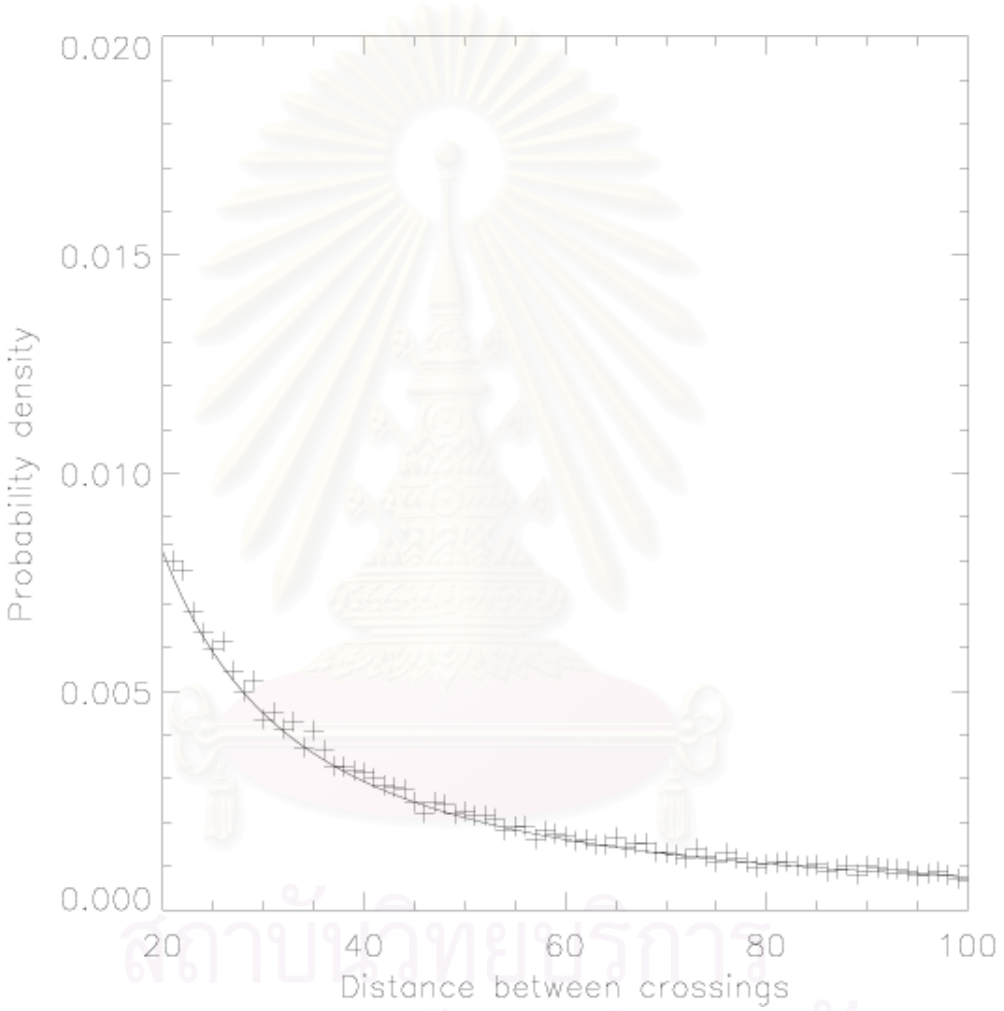

Figure 4.60: Distribution of distance between crossings for $\delta b/B_0 = 0.5$, $E_{slab} = 0.2$, $l_z = 0.5$, and $l_\perp = 1.0$.

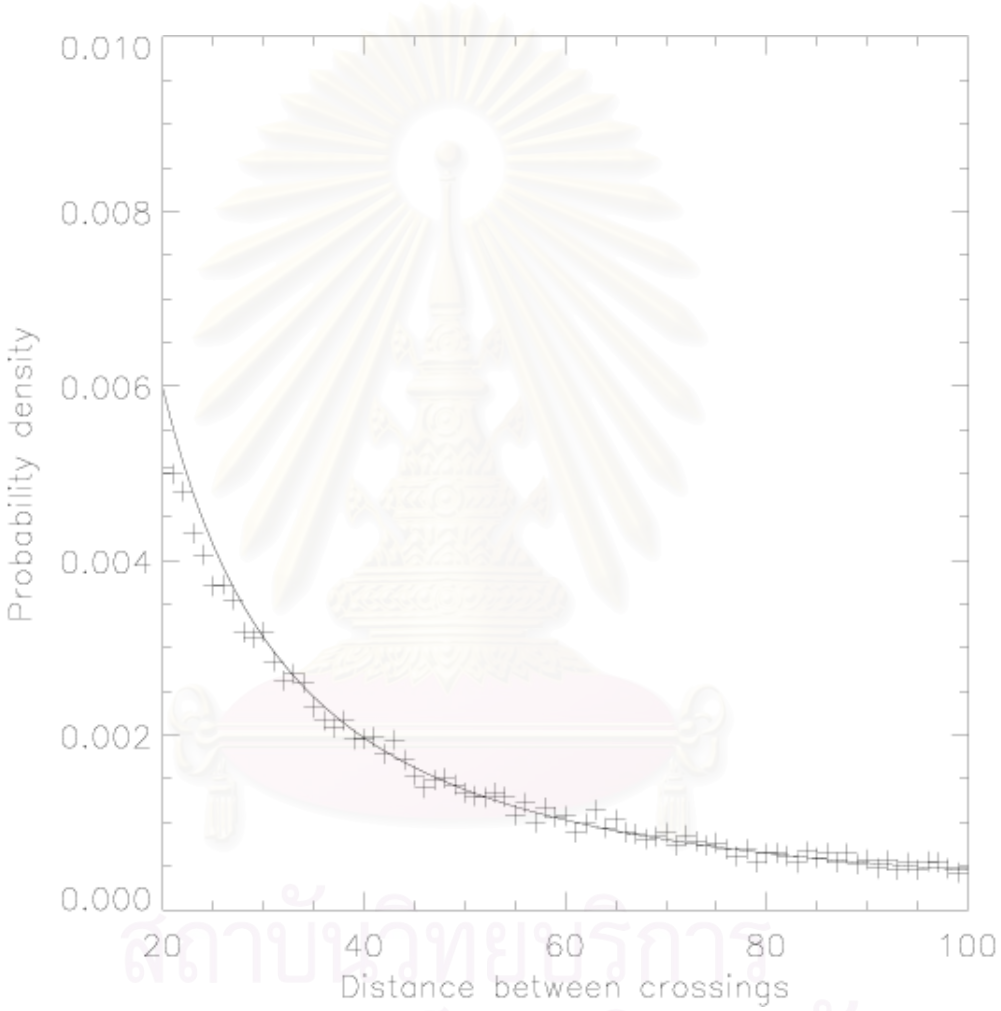

Figure 4.61: Distribution of distance between crossings for $\delta b/B_0 = 0.2$, $E_{slab} = 0.2$, $l_z = 1.0$, and $l_\perp = 0.2$.

Table 4.3: The average crossing distance, a, and b for various values of $\delta b/B_0$, E_{slab}, l_z, and $l_\perp$.

$\delta b/B_0$	E_{slab}	l_z	$l_\perp$	$\bar{d}$	a	b
0.5	1.0	1.0	-	37.48	0.48	-1.43
0.5	1.0	0.5	-	19.09	0.44	-1.50
0.5	0.8	1.0	1.0	58.85	0.73	-1.50
0.5	0.5	1.0	1.0	74.44	0.68	-1.46
0.5	0.5	0.5	1.0	64.99	0.69	-1.48
0.5	0.5	1.0	0.2	30.82	0.77	-1.58
0.5	0.2	1.0	1.0	73.18	0.70	-1.47
0.5	0.2	0.5	1.0	66.74	0.69	-1.48
0.5	0.2	1.0	0.2	24.21	0.72	-1.60
0.3	1.0	1.0	-	22.21	0.80	-1.57
0.3	0.8	1.0	1.0	48.80	0.92	-1.53
0.3	0.5	1.0	1.0	64.08	1.04	-1.52
0.3	0.2	1.0	1.0	68.19	1.05	-1.51
0.1	1.0	1.0	-	8.12	1.34	-1.83
0.1	0.8	1.0	1.0	28.64	1.05	-1.58
0.1	0.5	1.0	1.0	49.87	1.86	-1.58
0.1	0.2	1.0	1.0	62.84	2.52	-1.60
0.5	0	-	1.0	31.55	-	-
0.3	0	-	1.0	44.72	-	-
0.1	0	-	1.0	70.26	-	-

increases, the angular frequency increases. Returning to the case of the turbulent magnetic field, the increasing angular frequency corresponds to a greater number of loops per unit length. Therefore, if we increase $\delta b/B_0$, there are more loops. Then the distance between crossings decreases as $\delta b/B_0$ increases for the pure 2D case.

If the magnetic field lines can diffuse, including the slab part, the magnetic field lines seem to cross with the larger distance when $\delta b/B_0$ is greater. Even if E_{slab} is as small as 0.2, the average distance between crossings still increases as $\delta b/B_0$ increases.

If b/B_0 is fixed the scale in the x or y direction is proportional to the scale in the z direction. In the pure slab case, the scale in the z direction of the magnetic field lines is defined by l_z. If we multiply l_z by n, the field line is expanded by n. After that, the distance between crossings is multiplied by n.

4.5 Summary

The distribution of the number of crossings depends on only $\delta b/B_0$ in all cases, and can be fit to $(1-p)p^{\frac{n-1}{2}}$, where p is the probability of a field line crossing shock from downstream to upstream, and n is the number of crossings. This quantity does not depend on the scale of the magnetic field line, so if we change the scale lengths l_z and $l_\perp$, these quatities remain unchanged. In the pure 2D case, not all distributions of the number of crossings are exponential curves because the field lines do not diffuse.

The distribution of the crossing angle also depends on only $\delta b/B_0$ and

E_{slab}. It can be fitted to

$$P(\cos\theta) = C_1 \frac{|\cos\theta|}{(1-\cos^2\theta)^{3/2}\sqrt{1+\left(\frac{\cos\theta}{\sqrt{1-\cos^2\theta}}-\frac{\cos\theta_0}{\sqrt{1-\cos^2\theta_0}}\right)^2}} \times \exp\left[-\frac{1}{\langle b^2\rangle}\left(\frac{\cos\theta}{\sqrt{1-\cos^2\theta}}-\frac{\cos\theta_0}{\sqrt{1-\cos^2\theta_0}}\right)^2\right], \quad (4.21)$$

for $E_{slab} \neq 1$, and for $E_{slab} = 1$,

$$P(\cos\theta) = C_2 \frac{|\cos\theta|}{(1-\cos^2\theta)^{2}\sqrt{1+\left(\frac{\cos\theta}{\sqrt{1-\cos^2\theta}}-\frac{\cos\theta_0}{\sqrt{1-\cos^2\theta_0}}\right)^2}} \times \exp\left[-\frac{1}{\langle b^2\rangle}\left(\frac{\cos\theta}{\sqrt{1-\cos^2\theta}}-\frac{\cos\theta_0}{\sqrt{1-\cos^2\theta_0}}\right)^2\right], \quad (4.22)$$

where C_1 and C_2 are normalization factors. If $\delta b/B_0$ is greater, the average crossing angle is smaller because the magnetic field lines diffuse faster and further.

The distribution of the distance between crossings depends on l_z, $l_\perp$ and $\delta b/B_0$, and can be fit to al^b, where l is the distance between crossings. The parameters l_z and $l_\perp$ are the scale lengths of the magnetic field line, and the distance between crossings increases as l_z and $l_\perp$ increase. In the pure slab case, if $\delta b/B_0$ is greater, the diffusion rate increases. Therefore, the magnetic field line can have a longer distance between crossings as its trajectory spreads further in space. In the pure 2D case, if $\delta b/B_0$ is greater, the number of field line loops per unit length increases and the distance between crossings is smaller. In the compound 2D + slab turbulence, if $\delta b/B_0$ is greater, the number of crossings is greater, and the distance between crossings is longer even when the value of E_{slab} is small as 0.2.

Chapter 5

Model of particle acceleration at nearly perpendicular shocks

This chapter will introduce the sawtooth mechanism of the particle acceleration at shocks in random magnetic field. If the turbulent magnetic field lines cross the shock like a sawtooth, a particle that follows the magnetic field lines can diffuse along the shock, and cross the shock many times. First, we consider the case of a non-turbulent magnetic field, and then a turbulent magnetic field with all crossings taking place within the particle scattering mean free path. Finally, we consider turbulent magnetic fields with multiple field-shock crossings beyond the particle scattering mean free path.

5.1 The momentum change after one magnetic field-shock crossing

In Chapter 2, we considered only one magnetic field-shock crossing in the acceleration model as shown in Figure 5.1. The average momemtum change for each cycle, upstream to upstream again, is calculated from the momentum change and the flux of reflected particles and transmitted particles. The average momentum change and the flux of the reflected particles and those of the transmitted particles are different, which was not considered in the previous work reviewed in Chapter 2. Now we consider the momentum change for both reflected and transmitted particles, and also the flux of each type of particles.

Let v_p be the initial speed of the particle at the plasma frame. Let U_1 be the average speed of the upstream plasma in the normal incidence frame, and

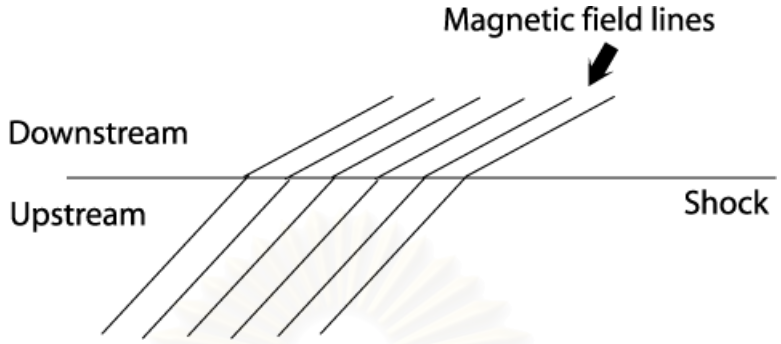

Figure 5.1: Much previous work on shock acceleration theory only considered one magnetic field-shock crossing.

let θ_1 be the angle between the shock normal and the upstream magnetic field at the crossing position. If the particle starts at the upstream frame with the pitch angle μ_1, the velocity v in the de Hoffman-Teller frame becomes

$$\begin{aligned} v &= \sqrt{(\mu_1 v_p + U_1 \sec\theta_1)^2 + (1-\mu_1^2)v_p^2} \\ &= v_p\left(1 + \frac{\mu_1 U_1 \sec\theta_1}{v_p}\right), \end{aligned} \tag{5.1}$$

when we work to first order in U/v. If the particle is reflected back to the upstream region as shown in Figure 5.2, the speed of the particle in the upstream frame is

$$\begin{aligned} v_p' &= \sqrt{(\mu_3 v - U_1 \sec\theta_1)^2 + (1-\mu_3^2)v^2} \\ &= v\left(1 - \frac{\mu_3 U_1 \sec\theta_1}{v}\right), \end{aligned} \tag{5.2}$$

where μ_3 is the pitch angle after the reflection. The speed change is

$$\begin{aligned} v_p' - v_p &= v\left(1 - \frac{\mu_3 U_1 \sec\theta_1}{v}\right) - v_p \\ &= \mu_1 U_1 \sec\theta_1 - \mu_3 U_1 \sec\theta_1, \end{aligned} \tag{5.3}$$

when we work to first order in U/v.

Let U_2 be the average speed of downstream plasma in the normal incidence frame, and θ_2 be the angle between the shock normal and the downstream magnetic field at the crossing position. If the particle is transmitted into the downstream region and has the pitch angle μ_2, the speed of the particle in the downstream frame is

$$\begin{aligned} v'_p &= \sqrt{(\mu_2 v - U_2 \sec\theta_2)^2 + (1-\mu_2^2)v^2} \\ &= v\left(1 - \frac{\mu_2 U_2 \sec\theta_2}{v}\right), \end{aligned} \tag{5.4}$$

The speed change is

$$\begin{aligned} v'_p - v_p &= v\left(1 - \frac{\mu_2 U_2 \sec\theta_2}{v}\right) - v_p \\ &= \mu_1 U_1 \sec\theta_1 - \mu_2 U_2 \sec\theta_2, \end{aligned} \tag{5.5}$$

when we work to first order in U/v.

If the particle comes from the downstream region with the speed v_p, after it is transmitted into the upstream region, the particle speed v in the de Hoffman-Teller frame is

$$\begin{aligned} v &= \sqrt{(\mu_4 v_p + U_2 \sec\theta_2)^2 + (1-\mu_4^2)v_p} \\ &= v_p\left(1 + \frac{\mu_4 U_2 \sec\theta_2}{v_p}\right), \end{aligned} \tag{5.6}$$

where μ_4 is the pitch angle of the transmitted particle before the transmission into the downstream frame. When the particle is transmitted into the upstream region, the speed of the particle in the upstream frame is

$$\begin{aligned} v'_p &= \sqrt{(\mu_5 v - U_1 \sec\theta_1)^2 + (1-\mu_5^2)v} \\ &= v\left(1 - \frac{\mu_5 U_1 \sec\theta_1}{v}\right), \end{aligned} \tag{5.7}$$

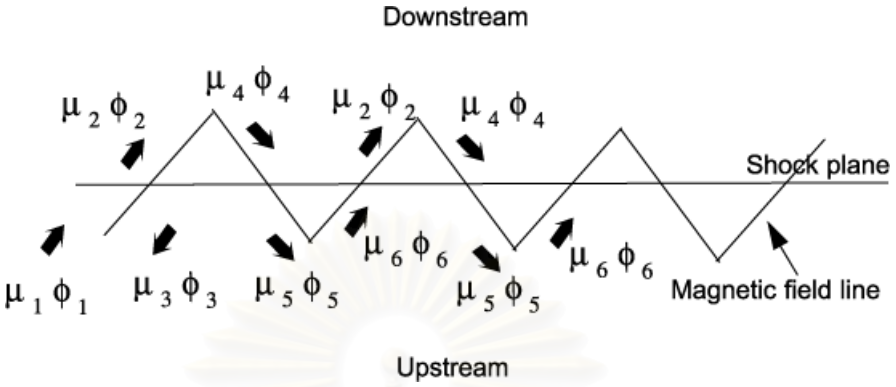

Figure 5.2: The sets of pitch angle and gyrophase values.

where μ_5 is the pitch angle of the transmitted particle after the transmission into the upstream frame. The speed change is

$$\begin{aligned} v_p' - v_p &= v\left(1 - \frac{\mu_5 U_1 \sec\theta_1}{v}\right) - v_p \\ &= \mu_4 U_1 \sec\theta_4 - \mu_5 U_1 \sec\theta_1, \end{aligned} \tag{5.8}$$

Now we will find the average momentum change for the reflected and transmitted particles. Let Δp_1 be the average momentum change when the particle is reflected at the shock. We integrate equation (5.3) from $\mu = 0$ to μ_m, the maximum value of the pitch angle cosine for a reflected particle, and for ϕ from 0 to 2π, and then divide it by $\int_0^{\mu_m}\int_0^{2\pi} \mu_1 d\mu_1 d\phi_1 = \pi\mu_m^2$ to average the speed change. The momentum change is

$$\begin{aligned} \Delta p_1 &= \frac{1}{\pi\mu_m^2}\int_0^{\mu_m}\int_0^{2\pi} m(v_p' - v_p)\mu_1 d\mu_1 d\phi_1 \\ &= \frac{m}{\pi\mu_m^2}\int_0^{\mu_m}\int_0^{2\pi} \left(\mu_1 U_1 \sec\theta_1 - \mu_3 U_1 \sec\theta_1\right)\mu_1 d\mu_1 d\phi_1 \\ &= 4\frac{m}{\mu_m^2} U_1 \sec\theta_1 \int_0^{\mu_m} \mu^2 d\mu \\ &= \frac{4}{3} m U_1 \sec\theta_1 \mu_m, \end{aligned} \tag{5.9}$$

where m is the mass of particles, $\mu_3 = -\mu_1$, and $\mu_m = \sqrt{1 - B_1/B_2} = \sqrt{1 - \sec\theta_1/\sec\theta_2}$. Then we can write

$$\frac{\Delta p_1}{p} = \frac{4}{3}\frac{U_1 \sec\theta_1 \mu_m}{v} \tag{5.10}$$

For transmitted particles, we integrate equation (5.3) from $\mu = \mu_m$ to 1 and for ϕ from 0 to 2π and divide it by $\int_{\mu_m}^{1}\int_0^{2\pi} \mu_1 d\mu_1 d\phi_1 = \pi(1-\mu_m^2)$ to average the speed change. We use Liouville's theorem,

$$\frac{1}{B_1}\mu_1 d\mu_1 d\phi_1 = \frac{1}{B_2}\mu_2 d\mu_2 d\phi_2, \tag{5.11}$$

where B_1 and B_2 are the magnitudes of the magnetic field in the upstream region and the downstream region near the crossing position to find the average momentum change Δp_2. Therefore,

$$\begin{aligned}
\Delta p_2 &= \frac{1}{\pi(1-\mu_m^2)}\int_{\mu_m}^{1}\int_0^{2\pi} m(v_p' - v_p)\mu_1 d\mu_1 d\phi_1 \\
&= \frac{m}{\pi(1-\mu_m^2)}\int_{\mu_m}^{1}\int_0^{2\pi} \left(\mu_1 U_1 \sec\theta_1 - \mu_2 U_2 \sec\theta_2\right)\mu_1 d\mu_1 d\phi_1 \\
&= \frac{2m}{1-\mu_m^2}\left[U_1 \sec\theta_1 \int_{\mu_m}^{1}\mu^2 d\mu - U_2 \sec\theta_2 \frac{B_1}{B_2}\int_0^{1}\mu^2 d\mu\right] \\
&= \frac{2m}{3(1-\mu_m^2)}\left[U_1 \sec\theta_1 (1-\mu_m^3) - U_2 \sec\theta_1\right],
\end{aligned} \tag{5.12}$$

and can be written as

$$\begin{aligned}
\frac{\Delta p_2}{p} &= \frac{2}{3(1-\mu_m^2)}\frac{U_1 \sec\theta_1(1-\mu_m^3) - U_2\sec\theta_1}{v} \\
&= \frac{2}{3}\left[\frac{U_1 \sec\theta_2(1-\mu_m^3) - U_2\sec\theta_2}{v}\right],
\end{aligned} \tag{5.13}$$

using $1 - \mu_m^2 = \sec\theta_1/\sec\theta_2$.

If the particles are transmitted from the downstream region into the upstream region, the momentum change is

$$\Delta p_3 = \frac{1}{\pi}\int_0^{-1}\int_0^{2\pi} m(v_p' - v_p)\mu_4 d\mu_4 d\phi_4$$

$$
\begin{aligned}
&= \frac{1}{\pi}\int_0^{-1}\int_0^{2\pi}\left(\mu_4 U_2 \sec\theta_2 - \mu_5 U_1 \sec\theta_1\right)\mu_4 d\mu_4 d\phi_2 \\
&= 2m\left[U_2 \sec\theta_2 \int_0^{-1}\mu^2 d\mu - U_1 \sec\theta_1 \frac{B_2}{B_1}\int_{-\mu_m}^{-1}\mu^2 d\mu\right] \\
&= \frac{2m}{3}\left[U_1 \sec\theta_2(1-\mu_m^3) - U_2 \sec\theta_2\right], \qquad (5.14)
\end{aligned}
$$

and can be written as

$$
\frac{\Delta p_3}{p} = \frac{2}{3}\left[\frac{U_1 \sec\theta_2(1-\mu_m^3) - U_2 \sec\theta_2}{v}\right]. \qquad (5.15)
$$

If we set the flux of particles to the shock from the upstream region to be one, the flux of the reflecting particles is μ_m^2, and the flux of the transmitted particles will be $1-\mu_m^2$. The flux-averaged momentum change is then

$$
\begin{aligned}
\frac{\Delta p}{p} &= \mu_m^2 \frac{\Delta p_1}{p} + (1-\mu_m^2)\left(\frac{\Delta p_2 + \Delta p_3}{p}\right) \\
&= \frac{4}{3}\frac{U_1 \sec\theta_1 \mu_m^3}{v} + \frac{4}{3}\frac{U_1 \sec\theta_1(1-\mu_m^3) - \frac{B_1}{B_2}U_2 \sec\theta_2}{v} \\
&= \frac{4}{3}\frac{1}{v}\left[U_1 \sec\theta_1 - \frac{B_1}{B_2}U_2 \sec\theta_2\right], \qquad (5.16)
\end{aligned}
$$

This is the average momentum change when a particle starts at the upstream region, then goes to the shock, and finally comes back into the upstream region again.

In our case, the magnetic field line can cross the shock more than one time. When we can calculate the momentum change for the case of many magnetic field-shock crossings, we sometimes need to start the particle at the downstream region and find the average momentum change when it gets back to the downstream region again. Now we will show that this calculation gives the same power law index of the cosmic ray spectrum. Let the flux of particles going to the shock from the downstream region be one. The particle must be transmitted through

the shock twice, at the first and the final particle-shock crossings. It can be reflected at the shock many times if it has a large pitch angle when it reaches the shock from the upstream region. Let n be the average number of particle reflections. The value of n can be found from

$$\begin{aligned} n &= \sum_{m=0}^{\infty} m \left(1 - \frac{B_1}{B_2}\right)^m \frac{B_1}{B_2} \\ n - \left(1 - \frac{B_1}{B_2}\right) n &= \frac{B_1}{B_2} \sum_{m=1}^{\infty} \left(1 - \frac{B_1}{B_2}\right)^m \\ n &= \frac{B_1}{B_2} \left[\frac{1}{1 - \left(1 - \frac{B_1}{B_2}\right)} \sum_{m=1}^{\infty} \left(1 - \frac{B_1}{B_2}\right)^m \right] \\ &= \frac{1 - \frac{B_1}{B_2}}{\frac{B_1}{B_2}} \\ &= \frac{B_2}{B_1} - 1 \\ &= \frac{\mu_m^2}{1 - \mu_m^2} \end{aligned} \tag{5.17}$$

Therefore the average momentum change is

$$\begin{aligned} \frac{\Delta p'}{p} &= \frac{\mu_m^2}{1 - \mu_m^2} \frac{\Delta p_1}{p} + \frac{\Delta p_2}{p} + \frac{\Delta p_3}{p} \\ &= \frac{4}{3} \frac{B_2}{B_1} \frac{1}{v} \left[U_1 \sec\theta_1 - \frac{B_1}{B_2} U_2 \sec\theta_2 \right], \end{aligned} \tag{5.18}$$

Recall that the power law index of the integral spectrum is the ratio of the escape probability to the mean momentum gain (see §2.8). The value of $\Delta p'$ is $(B_2/B_1)\Delta p$, but the escape probability corresponding to Δp is $4U_2 \cos\theta_2/(v \cos\theta_1)$, while the escape probability corresponding to $\Delta p'$ is $4U_2 \cos\theta_2/(v \cos\theta_2) = 4U_2/v$. Thus we can get the same power law index wherever the start of the cycle is.

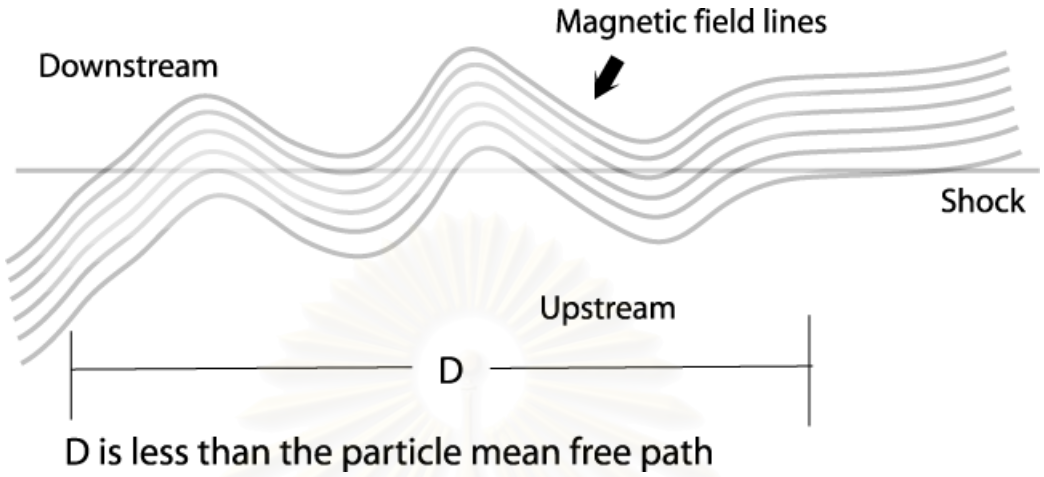

Figure 5.3: Multiple magnetic field-shock crossings within the particle mean free path

5.2 The momentum change after multiple magnetic field-shock crossings

5.2.1 The momentum change after multiple magnetic field-shock crossings within the particle mean free path λ

Now we consider the case of many shock-field crossings as shown in Figure 5.3. We assume that the pitch angle change conserves the adiabatic invariant over distances less than the particle scattering mean free path, and it changes randomly over longer distances.

We have simulated the pitch angle change that conserves the adiabatic invariant along the turbulent magnetic field line within the length of λ. We set the particle mean free path to be much greater than the correlation length of the magnetic fluctuations. Figure 5.4 shows the average number of crossings for each value of the pitch angle cosine (plus signs) from the simulation of the magnetic field lines for $\delta b/B_0 = 0.5$, $E_{slab} = 0.2$, $l_z = 1$, and $l_\perp = 1$. We assume that the

particles will follow the magnetic field line and conserve the adiabatic invariant over $\lambda = 1,000$ au. In our model, we approximate this distribution by a step function (solid line), where μ_m is defined as $\sqrt{1 - \langle B_1 \rangle / \langle B_2 \rangle}$, and $\langle B_1 \rangle$ and $\langle B_2 \rangle$ are the average magnetic field in the upstream region and the downstream region, respectively. Therefore when the particle goes to the shock from the upstream region, we can approximate that if the pitch angle cosine of the particle is greater than μ_m, the particle can be transmitted along the distance D of the group of shock-field crossings as shown in Figure 5.3, and if the pitch angle cosine of the particle is smaller than μ_m, the particle is reflected at the first shock-field crossing. When the particle goes to the shock from the downstream region, most particles can be transmitted along the distance D. The probability of the transmission depends on the scale of λ.

Now we have two sets of particles, the reflected particles and the transmitted particles. The average momentum change of the reflected particles is Δp_1, and the average momentum change of the transmitted particles is $n_c \Delta p_2$, where n_c is the average number of shock-field crossings within a scattering mean free path. The de Hoffman-Teller frame is varied for each particle-shock crossing, since the shock-field crossing angle is changed for each particle-shock crossing. For each time particle crosses the shock, the momentum change increases in the plasma frame, and this increasing momentum can be easily shown in the normal incident frame to be the result of shock drift acceleration, which always increase the particle's momentum. Thus we can add up the momentum changes to be $n_c \Delta p_2$.

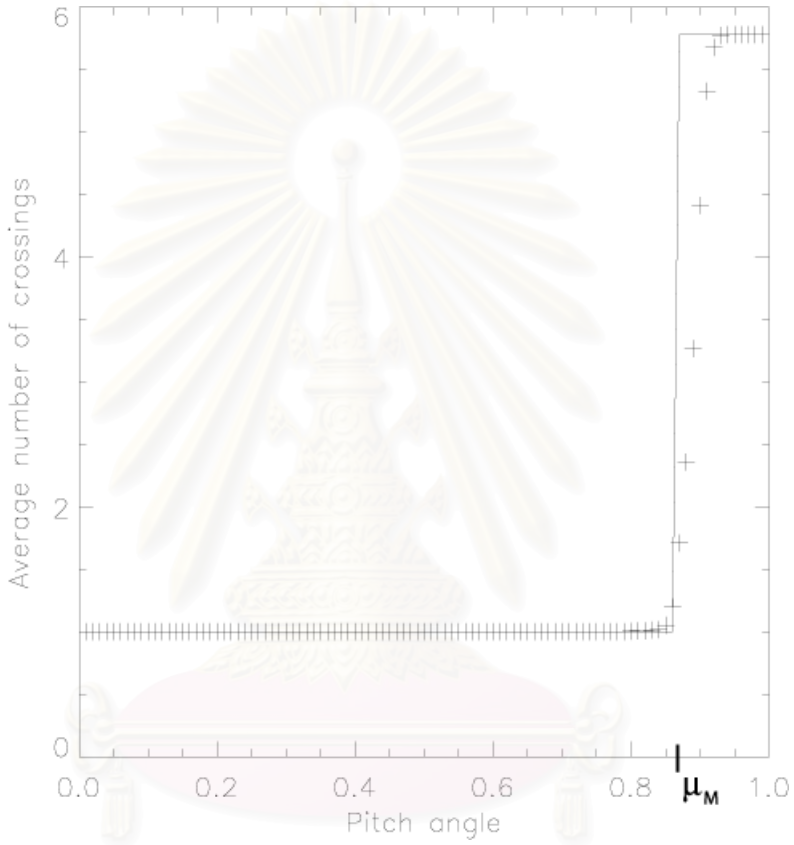

Figure 5.4: Plus signs show the average number of particle transmissions through the shock at each value of the pitch angle for $\delta b/B_0 = 0.5$, $E_{slab} = 0.2$, $l_z = 1$, and $l_\perp = 1$. In our model, we approximate this distribution by a step function (solid line), where μ_m is defined as $\sqrt{1 - \langle B_1 \rangle / \langle B_2 \rangle}$. In our approximation, particles with a pitch angle cosine greater than μ_m can be transmitted through all field-shock crossings within a mean free path, while particles with $\mu < \mu_m$ are reflected at the first crossing.

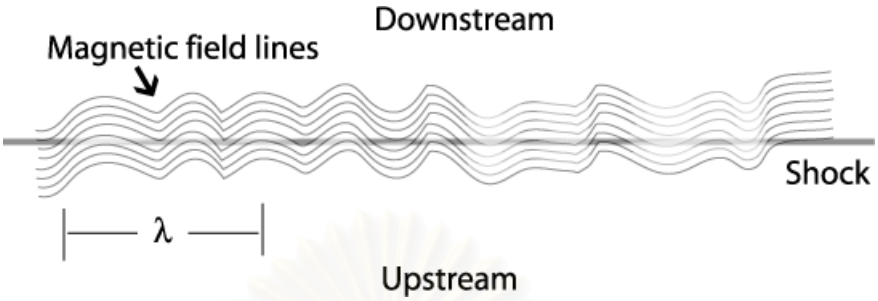

Figure 5.5: Multiple magnetic field-shock crossings over a distance greater than the particle mean free path λ.

5.2.2 The momentum change after multiple magnetic field-shock crossings beyond the particle mean free path λ

At the nearly perpendicular shock, the distance between shock-field crossings can be greater than the particle mean free path λ since the number of crossings can be great as shown in Figure 5.5. We bunch the shock-field crossings that have a distance less than the particle scattering mean free path. In Figure 5.6, the squares are the bunches of shock-field crossings within the particle mean free path. The distance between the starting points of two bunches of crossings is greater than the particle mean free path, so the particle can go randomly back to the previous bunch of crossings or toward the next bunch of crossings. When the particle goes toward the next bunch of crossings or back to the previous bunch, the particle can be at the upstream region as well as downstream, so in an ensemble average sense we can randomly choose the region where the particle starts to cross the shock again. If there is a next bunch of shock-field crossings, the particle will never escape the shock since in our model the particle follows that magnetic field line. We have generated 5,000 magnetic field lines for each set of parameter values of the magnetic field to collect the number of crossings with a

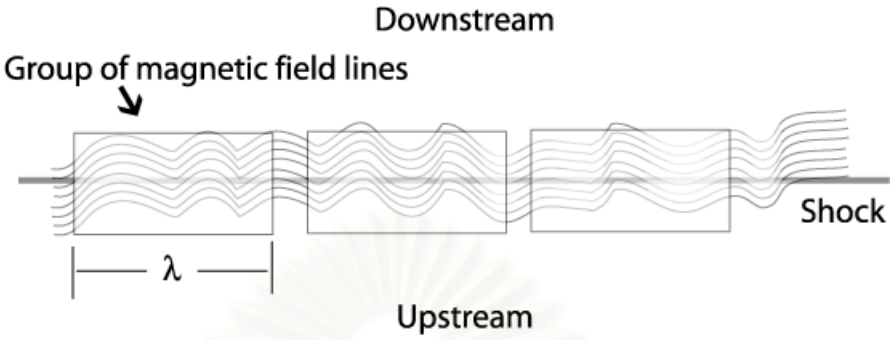

Figure 5.6: Groups of shock-field crossings within the particle mean free path (square boxes).

distance from the first crossing that is greater than λ and the number of crossings within λ. After that we can find the probability P that there is no next group of crossings, and the average number of crossings within one bunch, n_c. We vary the particle mean free path from 10 to 1000 au. The values of n_c and P for various parameters of the turbulent magnetic field are shown in Tables 5.2, 5.3, and 5.4 when the particle mean free path is 10, 100, and 1000 au, respectively.

Now we are going to find the momentum change in this case. We separate the approaching particles into 2 groups. The first group A is the group of particles approaching the shock from the right (the direction from downstream on a large scale) and the second group B is the group of particles approaching the shock from the left as shown in Figure 5.7. The particles in group A can return to the same bunch of shock-field crossings again or go back to the upstream region along the magnetic field line as shown in Figure 5.8. The particles in group B can go back to the same bunch of shock-field crossings again or go to the downstream region along the magnetic field line as shown in Figure 5.9. The particles in group A must encounter the shock again since the solar wind convects them to the shock,

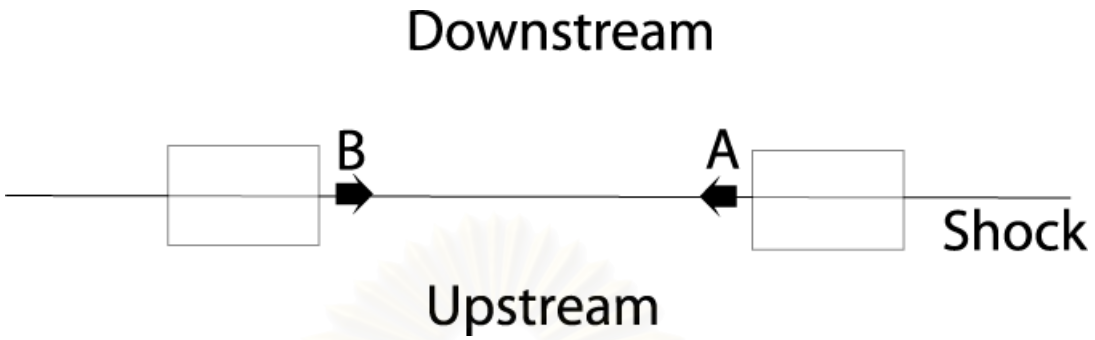

Figure 5.7: Two groups of particles to the next group of shock-field crossings are shown.

but those in group B can go to infinity downstream since some magnetic field lines in the downstream region never cross the shock again.

Now we find the momentum changes of each group of particles at the next bunch of crossings. If the particle is in the set A_3, it goes back to the shock again because of solar wind convection, and the momentum change is

$$\Delta p_4 = n_c \Delta p_2 + (B_2/B_1 - 1)\Delta p_1, \tag{5.19}$$

since it reflects at the shock $B_2/B_1 - 1$ times, from (5.17), and is then transmitted through the shock along the magnetic field that crosses the shock n_c times within a scattering mean free path. If a particle is in the set A_1, the momentum change after encountering the next bunch of crossings is $n_c \Delta p_2$. If the particle is in the set A_2, the momentum change is Δp_4, the same as that for A_3, since the particle may be reflected many times before it is finally transmitted through the shock. Figure 5.8 shows sets A_1, A_2, and A_3. If the particle is in the set B_3, there is no momentum change. If the particle is in the set B_1, the momentum change after encouter the next bunch of crossings is $n_c \Delta p_2$. If the particle is in the set B_2, the momentum change is Δp_4 as same as that for A_2 since the particle is reflected

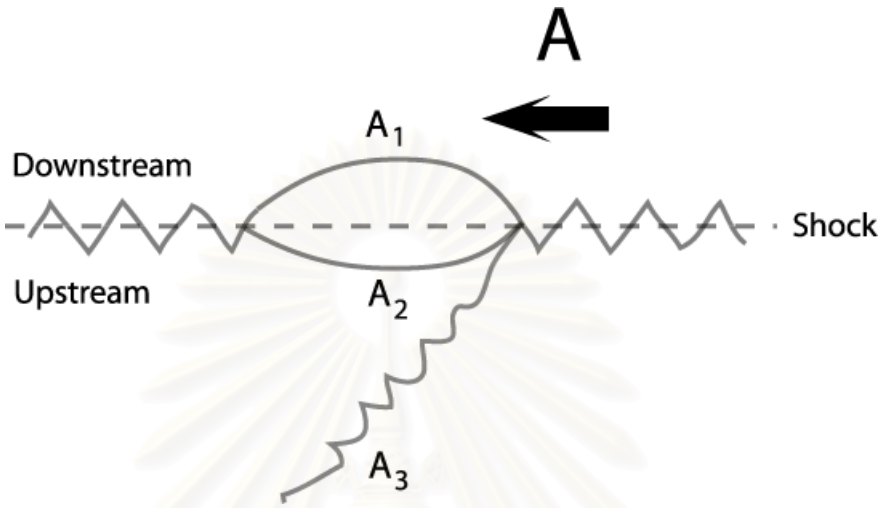

Figure 5.8: The sets of particles which come to the shock from the right, where the magnetic field line goes into the downstream region at the far right.

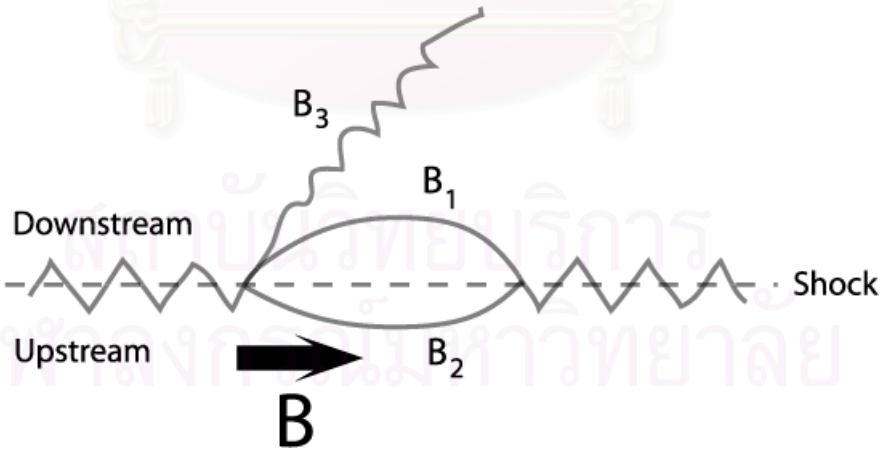

Figure 5.9: The sets of particles which come to the shock from the left, where the magnetic field line goes into the upstream region at the far left.

many times before it is transmitted through the shock finally. Figure 5.9 shows sets B_1, B_2, and B_3.

If the particle is in set A_1 or A_2, the probability to go right or left is no different. If the particle is in set A_3, the particle must go the shock again from the left (B) because of the solar wind convection. If the particle is in set B_1 or B_2, the probability to go right or left is no different. If the particle is in set B_3, the particle goes back to where it started downstream of the shock, and a full cycle has been completed. Let c_i be the probability that a particle in group A is in set A_i. Recalling that P is the probability that there is no next bunch of crossings, we have

$$\begin{aligned} c_1 &= \frac{1-P}{2} \\ c_2 &= \frac{1-P}{2} \\ c_3 &= P. \end{aligned} \tag{5.20}$$

Let d_i be the probability that a particle in group B is in set B_i. Therefore,

$$\begin{aligned} d_1 &= \frac{1-P}{2} \\ d_2 &= \frac{1-P}{2} \\ d_3 &= P. \end{aligned} \tag{5.21}$$

Let r_{ij} be the probability that a particle in group i will move to group j, where $i = A, B$ and $j = A, B$. Referring to the hollow arrows in Figure 5.8, we see that

$$\begin{aligned} r_{AA} &= \frac{c_1 + c_2}{2} = \frac{1-P}{2} \\ r_{AB} &= \frac{c_1 + c_2}{2} + c_3 = \frac{1+P}{2}. \end{aligned} \tag{5.22}$$

On the other hand, considering group B, the set B_3 is special. The escape or return of is particle is considered at the end of the entire process, just as in the theory of Drury(1983) (see§2.8), so we treat motion in set B_3 as the end of one "round" of acceleration:

$$\begin{aligned} r_{BA} &= \frac{d_1 + d_2}{2} = \frac{1-P}{2} \\ r_{BB} &= \frac{d_1 + d_2}{2} = \frac{1-P}{2}. \end{aligned} \tag{5.23}$$

Conceptually, we treat each bunch of crossings traversed in direction A or B as belonging to the same statistical ensemble and therefore treat them on equal footing. Let

$$\mathbf{R} = \begin{bmatrix} r_{AA} & r_{BA} \\ r_{AB} & r_{BB} \end{bmatrix}, \tag{5.24}$$

so that $\mathbf{R}$ is a transfer matrix, and let $\mathbf{F}_0$ be

$$\mathbf{F}_0 = \begin{bmatrix} n_A \\ n_B \end{bmatrix}, \tag{5.25}$$

where n_A is the initial number of particles in group A, and n_B is the intial number of particles in group B. Let $\mathbf{A}_i$ be the number of particles in each group after the particles pass a crossing bunch i times. Therefore

$$\mathbf{F}_i = \mathbf{R}^i \mathbf{F_0}. \tag{5.26}$$

The average momentum change when the particle was in group A and already passed the next bunch of crossings is

$$\begin{aligned} \Delta p_A &= c_1 \Delta p_{A_1} + c_2 \Delta p_{A_2} + c_3 \Delta p_{A_3} \\ &= \frac{1-P}{2} n_c \Delta p_2 + \frac{1-P}{2} n_c \Delta p_4 + P \Delta p_4 \\ &= \frac{1-P}{2} n_c \Delta p_2 + \frac{1+P}{2} \Delta p_4. \end{aligned} \tag{5.27}$$

The average momentum change when the particle was in group B and already passed the next bunch of crossings is

$$\begin{aligned}\Delta p_B &= d_1\Delta p_{B_1} + d_2\Delta p_{B_2} + d_3\Delta p_{B_3} \\ &= \frac{1-P}{2} n_c \Delta p_2 + \frac{1-P}{2}\Delta p_4. \end{aligned} \tag{5.28}$$

Then let $\mathbf{\Delta P}$ be

$$\mathbf{\Delta P} = \left[\begin{array}{cc} \Delta p_A & \Delta p_B \end{array} \right]. \tag{5.29}$$

Now $\mathbf{\Delta P F}_i$ is the average momentum gain at the $(i+1)$th bunch of shock-field crossings. The total average momentum gain from the first bunch to the final bunch is

$$\begin{aligned}\Delta p_m &= \mathbf{\Delta P}\left(\sum_{i=0}^{\infty} \mathbf{R}^i \mathbf{F}_0\right) \\ &= \mathbf{\Delta P}\left(\mathbf{1}-\mathbf{R}\right)^{-1}\mathbf{F}_0 \end{aligned} \tag{5.30}$$

We can show that

$$\left(\mathbf{1}-\mathbf{R}\right)^{-1} = \left[\begin{array}{cc} \frac{1}{P} & \frac{1-P}{P(1+P)} \\ \frac{1}{P} & \frac{1}{P} \end{array} \right]. \tag{5.31}$$

Now we will find where the initial particle for each round is. We first consider the where the round ends. The round ends when the escape probability is concerned, so the end of a round is in set B_3. In reality, the accelerated particle starts at the upstream region. Therefore the first round starts at set A_3 and ends at set B_3. For the next round, we start at set B_3, and end at set B_3. When the particles start at set A_3, all of them must be transmitted through the shock finally, and be in the group B. At this moment, the momentum gain is Δp_4, and the initial number of particles in each group can be written as

$$\mathbf{F}_{01} = \left[\begin{array}{c} 0 \\ 1 \end{array} \right]. \tag{5.32}$$

After all particles have been lost from the shock and gone into set B_3, the average momentum change is

$$\begin{aligned}
\Delta p_{m1} &= \Delta p_4 + \mathbf{\Delta P}\left(\mathbf{1}-\mathbf{R}\right)^{-1}\mathbf{F}_{01} \\
&= \Delta p_4 + \frac{1-P}{P(1+P)}\Delta p_A + \frac{1}{P}\Delta p_B \\
&= \frac{1-P}{P(1+P)} n_c \Delta p_2 + \left(1+\frac{1-P}{P}\right)\Delta p_4 \\
&= \frac{2}{P(1+P)} n_c \Delta p_2 + \frac{1}{P}\left(\frac{B_2}{B_1}-1\right)\Delta p_1
\end{aligned} \tag{5.33}$$

The above is the total momentum gain in going from the start (A_3) to the end of one round (B_3). These particles have not escaped yet, and then go back to the shock along the magnetic field line. All of these particles must be in the group A after the first crossing. Before the particles come to group A, they must be transmitted through the shock n_c times and their momentum change is $n_c\Delta p_2$. The initial number of particles in each group at the start of this round can be written as

$$\mathbf{F}_{02} = \begin{bmatrix} 1 \\ 0 \end{bmatrix}. \tag{5.34}$$

After that the averaged momentum change for this second round is

$$\begin{aligned}
\Delta p_{m2} &= n_c\Delta p_2 + \mathbf{\Delta P}\left(\mathbf{1}-\mathbf{R}\right)^{-1}\mathbf{F}_{02} \\
&= n_c\Delta p_2 + \frac{1-P}{P} n_c \Delta p_2 + \frac{1}{P}\Delta p_4 \\
&= \frac{2}{P} n_c \Delta p_2 + \frac{1}{P}\left(\frac{B_2}{B_1}-1\right)\Delta p_1
\end{aligned} \tag{5.35}$$

For all further rounds, the particles start at set B_3, so the average momentum change is Δp_{m2}. We can write Δp_{m1} as

$$\Delta p_{m1} = \frac{2}{P(1+P)} n_c \Delta p_2 + \frac{1}{P}\left(\frac{B_2}{B_1}-1\right)\Delta p_1$$

$$
\begin{aligned}
&= \frac{4mn_c}{3P(1+P)}\frac{B_2}{B_1}\left[U_1\sec\theta_1(1-\mu_m^3)-\frac{B_1}{B_2}U_2\sec\theta_2\right]+\frac{4m}{3P}\frac{B_2}{B_1}U_1\sec\theta_1\mu_m^3 \\
&= \frac{4mn_c}{3P(1+P)}\frac{B_2}{B_1}\left[U_1\sec\theta_1-\frac{B_1}{B_2}U_2\sec\theta_2\right] \\
&\quad +\frac{4m}{3P}\frac{B_2}{B_1}\left(1-\frac{n_c}{1+P}\right)U_1\sec\theta_1\mu_m^3 \qquad (5.36)
\end{aligned}
$$

and Δp_{m2} as

$$
\begin{aligned}
\Delta p_{m2} &= \frac{2}{P}n_c\Delta p_2+\frac{1}{P}\left(\frac{B_2}{B_1}-1\right)\Delta p_1 \\
&= \frac{4mn_c}{3P}\frac{B_2}{B_1}\left[U_1\sec\theta_1(1-\mu_m^3)-\frac{B_1}{B_2}U_2\sec\theta_2\right]+\frac{4m}{3P}\frac{B_2}{B_1}U_1\sec\theta_1\mu_m^3 \\
&= \frac{4m(1-n_c)}{3P}U_1\sec\theta_2\mu_m^3+\frac{4mn_c}{3P}\left[U_1\sec\theta_2-U_2\sec\theta_2\right]. \qquad (5.37)
\end{aligned}
$$

The momentum change for the case of one field-shock crossing is

$$\Delta p' = \frac{4m}{3}\left[U_1\sec\theta_2-U_2\sec\theta_2\right], \qquad (5.38)$$

where $\theta_1 \approx 89°$, $\sec\theta_2 = \sqrt{(r\tan\theta_1)^2+1}$, and $B_2/B_1 = \sec\theta_2/\sec\theta_1$. The average momentum change for the case of many field-shock crossings is

$$\Delta p_{m2} = \frac{4m(1-n_c)}{3P}U_1\langle\mu_m^3\sec\theta_2\rangle+\frac{4mn_c}{3P}U_1\langle\sec\theta_2\rangle-\frac{4mn_c}{3P}U_2\langle\sec\theta_2\rangle, \qquad (5.39)$$

where $\mu_m = \sqrt{1-\langle B_1\rangle/\langle B_2\rangle}$. Now we can use this momentum change to estimate the spectral index of accelerated particles. Since the crossing angle is not a constant for each crossing for the multiple crossings case, we use the average value of $\sec\theta_2$, B_1, and B_2. We know the distribution of the cosine of the crossing angle from Chapter 4, so we can find the average values of $\sec\theta_2$. We know $\langle B_1\rangle = B_0$, and then $\langle B_2\rangle = B_0\sqrt{(r\sin 89°)^2+\cos^2 89°}$, where r is the compression ratio. Table 5.1 shows $\langle\sec\theta_2\rangle$ vs. $\delta b/B_0$ for $r = 4$. This is derived from the distributions shown in Figures 4.21 to 4.40. Since Δp_{m1} is for the first round, but Δp_{m2} is for

Table 5.1: The values of $\langle \sec\theta_2 \rangle$ vs. $\delta b/B_0$ for $r = 4$ from the simulations.

$\delta b/B_0$	$\langle \sec\theta_2 \rangle$
0.5	15.5857
0.3	24.5353
0.1	69.2662

the other rounds, the cosmic ray spectrum index must be considered from Δp_{m2}, and Δp_{m1} has the effect of shifting the spectrum. We compare the momentum change for the case of multiple crossings to the momentum change after one crossing. The ratio of Δp_{m2} to Δp is

$$\frac{\Delta p_{m2}}{\Delta p'} = \frac{\frac{1-n_c}{P} U_1 \langle \mu_m^3 \sec\theta_2 \rangle + \frac{n_c}{P} U_1 \langle \sec\theta_2 \rangle - \frac{n_c}{P} U_2 \langle \sec\theta_2 \rangle}{U_1 \sec\theta_2 - U_2 \sec\theta_2}, \tag{5.40}$$

If we assume that the particle mean free path does not depend on the momentum of the particle, we have the power law of the cosmic ray spectrum. The power law index of the differential spectrum is $\gamma = (3mU_2 \sec\theta_2/\Delta p') + 1$ for the case of one field-shock crossing, and that for many field-shock crossings is

$$\begin{aligned} \gamma_m &= \frac{3mU_2 \sec\theta_2}{\Delta p_m} \\ &= \frac{\Delta p'}{\Delta p_m}(\gamma - 1) + 1. \end{aligned} \tag{5.41}$$

The values of $\Delta p_m/\Delta p'$ and γ_m are shown in Tables 5.2, 5.3, and 5.4 when the particle mean free path is 10, 100, or 1000 au, respectively.

The distribution of crossing angles has a great effect on the momentum gain. The average crossing angle is small when the crossing angle distribution is highly spread or $\delta b/B_0$ is high. The small crossing angle tends to cause a small momentum gain. From Tables 5.2, 5.3, and 5.4, the spectral index of accelerated particles is higher than that from the non-turbulent magnetic field. The number

Table 5.2: The values of n_c, P, $\Delta p_m/\Delta p'$, and γ_m for each case of the turbulent magnetic field with $\lambda = 10$ and the compression ratio $r = 4$.

$\delta b/B_0$	E_{slab}	l_z	$l_\perp$	n_c	P	$\Delta p_m/\Delta p'$	γ_m
0.5	1.0	1.0	-	2.43	0.13	0.57	2.72
0.5	1.0	0.5	-	3.03	0.16	0.50	2.99
0.5	0.8	1.0	1.0	2.27	0.12	0.63	2.57
0.5	0.5	1.0	1.0	2.16	0.11	0.68	2.45
0.5	0.5	0.5	1.0	2.34	0.11	0.69	2.43
0.5	0.5	1.0	0.2	2.63	0.15	0.51	2.95
0.5	0.2	1.0	1.0	2.11	0.10	0.73	2.36
0.5	0.2	0.5	1.0	2.15	0.11	0.66	2.50
0.5	0.2	1.0	0.2	2.90	0.17	0.48	3.06
0.3	1.0	1.0	-	2.39	0.22	0.55	2.80
0.3	0.8	1.0	1.0	2.19	0.17	0.68	2.45
0.3	0.5	1.0	1.0	1.96	0.15	0.74	2.34
0.3	0.2	1.0	1.0	1.87	0.14	0.80	2.24
0.1	1.0	1.0	-	2.28	0.54	0.63	2.57
0.1	0.8	1.0	1.0	2.03	0.38	0.87	2.13
0.1	0.5	1.0	1.0	1.74	0.32	0.98	2.01
0.1	0.2	1.0	1.0	1.50	0.30	1.01	1.98

Table 5.3: The values of n_c, P, $\Delta p_m/\Delta p'$, and γ_m for each case of the turbulent magnetic field with $\lambda = 100$ and the compression ratio $r = 4$.

$\delta b/B_0$	E_{slab}	l_z	$l_\perp$	n_c	P	$\Delta p_m/\Delta p'$	γ_m
0.5	1.0	1.0	-	5.72	0.33	0.32	4.05
0.5	1.0	0.5	-	7.52	0.43	0.28	4.52
0.5	0.8	1.0	1.0	5.08	0.28	0.35	3.79
0.5	0.5	1.0	1.0	4.66	0.26	0.37	3.63
0.5	0.5	0.5	1.0	5.13	0.27	0.37	3.64
0.5	0.5	1.0	0.2	6.37	0.38	0.29	4.37
0.5	0.2	1.0	1.0	4.83	0.25	0.38	3.58
0.5	0.2	0.5	1.0	5.08	0.27	0.37	3.67
0.5	0.2	1.0	0.2	7.02	0.43	0.27	4.63
0.3	1.0	1.0	-	5.51	0.51	0.32	4.08
0.3	0.8	1.0	1.0	4.59	0.39	0.38	3.56
0.3	0.5	1.0	1.0	4.13	0.36	0.40	3.46
0.3	0.2	1.0	1.0	4.10	0.35	0.41	3.38
0.1	1.0	1.0	-	3.85	0.95	0.42	3.34
0.1	0.8	1.0	1.0	3.58	0.69	0.56	2.76
0.1	0.5	1.0	1.0	2.96	0.62	0.59	2.68
0.1	0.2	1.0	1.0	2.52	0.62	0.57	2.75

Table 5.4: The values of n_c, P, $\Delta p_m/\Delta p'$, and γ_m for each case of the turbulent magnetic field with $\lambda = 1,000$ and the compression ratio $r = 4$.

$\delta b/B_0$	E_{slab}	l_z	$l_\perp$	n_c	P	$\Delta p_m/\Delta p'$	γ_m
0.5	1.0	1.0	-	13.55	0.79	0.22	5.46
0.5	1.0	0.5	-	15.47	0.91	0.21	5.70
0.5	0.8	1.0	1.0	12.08	0.68	0.24	5.15
0.5	0.5	1.0	1.0	11.28	0.64	0.24	5.07
0.5	0.5	0.5	1.0	12.03	0.66	0.24	5.02
0.5	0.5	1.0	0.2	14.14	0.85	0.21	5.66
0.5	0.2	1.0	1.0	11.44	0.65	0.24	5.11
0.5	0.2	0.5	1.0	11.86	0.67	0.24	5.13
0.5	0.2	1.0	0.2	14.74	0.89	0.20	5.77
0.3	1.0	1.0	-	10.01	0.96	0.23	5.18
0.3	0.8	1.0	1.0	9.49	0.84	0.26	4.80
0.3	0.5	1.0	1.0	8.67	0.80	0.26	4.78
0.3	0.2	1.0	1.0	8.66	0.78	0.26	4.72
0.1	1.0	1.0	-	4.03	1.00	0.41	3.41
0.1	0.8	1.0	1.0	4.89	0.99	0.45	3.21
0.1	0.5	1.0	1.0	4.37	0.98	0.43	3.30
0.1	0.2	1.0	1.0	2.52	0.62	0.57	2.75

of shock-field crossings within the particle mean free path, n_c, and the probability P that there is no further bunch of magnetic field-shock crossings also affect the cosmic ray spectral index. Roughly speaking, if n_c is large, the number of field-shock crossings beyond λ is small, so P is high. A particle can stay at the shock longer if P is smaller, so the particle can be accelerated many times and gain more momentum. Therefore, the lower crossing angle and the higher P cause the lower momentum gain. From chapter 4, the number of field-shock crossings along a field line only depends on $\delta b/B_0$, so n_c depends on $\delta b/B_0$.

A higher λ causes larger bunches of field-shock crossings, since there is much space to fill many field-shock crossings. The scale length of the magnetic field also affects the distance between crossings. Over the same distance, if the scale of magnetic field is small, n_c is high. Therefore, if $\delta b/B_0$ and λ are higher, n_c and P are higher, while if the scale of the magnetic field is greater, n_c and P are lower. Figure 5.10 shows the relation between $\bar{d}$, related to the scale of magnetic field lines, and γ_m for $\delta b/B_0 = 0.5$ and $\lambda = 100$ au.

Now we consider the effect of magnetic field parameters on the spectral index. In reality, λ is roughly proportional to $B^2/\delta B^2$. A higher $\delta b/B_0$ (increased turbulence) causes smaller crossing angles and smaller λ, so the higher $\delta b/B_0$ has two effects on the acceleration. The first effect is to increase momentum gain because the smaller λ causes a smaller P, while the second is to decrease momentum gain because of the smaller crossing angle. We find that the second effect dominates, and there is a higher spectral index (see Table 5.2-5.4), which implies fewer high energy particles. The spectral index also depends on the ratio of the scales, l_z and $l_\perp$, of the magnetic field to λ. If the scales are higher, n_c and P are small, and then the spectral index is again greater.

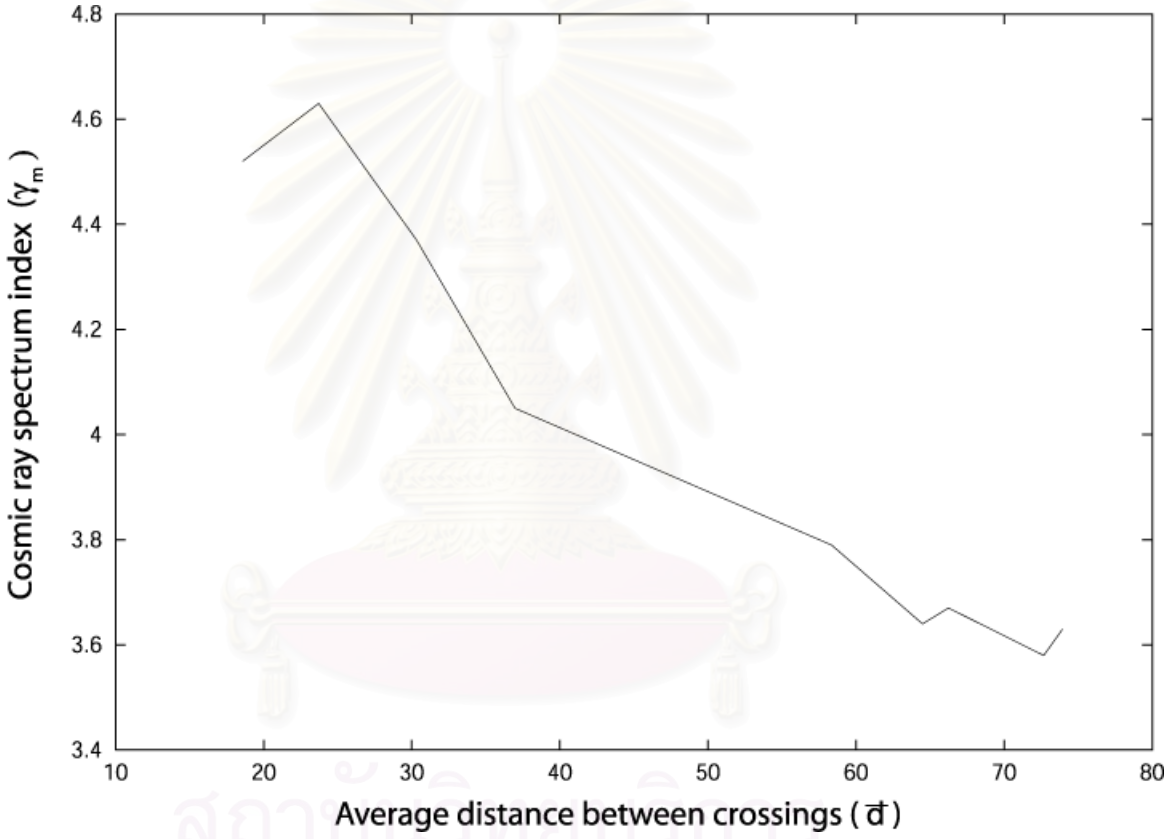

Figure 5.10: Plot of γ_m vs. $\bar{d}$ for $\delta b/B_0 = 0.5$ and $\lambda = 100$.

Chapter 6
Conclusions

We have simulated turbulent magnetic field lines for various values of the parameters $\delta b/B_0$, E_{slab}, l_z, and $l_\perp$. We collected the statistics of the number of field-shock crossings, the crossing angle, and the distance between crossings. These statistics are useful for the sawtooth mechanism of particle acceleration because the charged particles basically move along the magnetic field line. The change in the shape of the magnetic field line must affect the particle acceleration. We set the angle between the average magnetic field and the shock normal to be 89° since we already approximate it in Chapter 2. We also developed a new theoretical framework for taking multiple magnetic field-shock crossings into account.

6.1 Statistics of magnetic field lines

The number of crossings and the crossing angle only depend on $\delta b/B_0$, but the distance between crossings depends on all parameters. If $\delta b/B_0$ is greater, the number of crossings is greater, and the distribution of the crossing angle is spread more. The distance between crossings is scaled by l_z and $l_\perp$. A large/small l_z and $l_\perp$ give a large/small distance between crossings. If E_{slab}, l_z and $l_\perp$ are fixed, the distance between crossings is further as $\delta b/B_0$ is greater. If E_{slab} is lower, the 2D part dominates, and the magnetic field line forms more loops per unit length. If there are more loops per unit length, the distance between crossings is shorter. Therefore, if E_{slab} is greater, the distance between crossings is

greater. The distributions of the number of crossings, the crossing angle, and the distance between crossings are used to develop the sawtooth mechanism of particle acceleration.

6.2 Sawtooth mechanism of particle acceleration

The particles are accelerated less if we consider the effect of multiple field-shock crossings. The average shock-field crossing angle is smaller, which causes a smaller momentum gain, but that magnetic field line can cross the shock more than one time, which causes a greater momentum. The effect of the smaller shock-field crossing angle dominates the effect of many shock-field crossings. The ratio of the scale of the turbulent magnetic field to the particle mean free path also has an effect on the particle acceleration. If this ratio is high, the particle can diffuse but is contained along the magnetic field line at the shock, so the particle is accelerated more but still less than the acceleration at one shock-field crossing with a high crossing angle.

References

Bieber, J. W., Matthaeus, W. H., Smith, C. W., Wanner, W., Kallenrode, M. -B., and Wibberenz, G. Proton and Electron Mean Free Paths: The Palmer Consensus Revisited. Astrophys. J. **420** (1994): 294.

Bieber, J. W., Wanner, W., and Matthaeus, W. H. Dominant two-dimensional solar wind turbulence with implications for cosmic ray transport. J. Geophys. Res. **101** (1996): 2511.

de Hoffmann, F., and Teller, E. Magneto-hydrodynamic shocks Phys. Rev. **80** (1950): 692.

Drury, L. O'C. An introduction to the theory of diffusive shock acceleration of energetic particles in tenuous plasmas shocks Rep. Prog. Phys. **46** (1983): 973.

Fermi, E. On the origin of the cosmic radiation Phys. Rev. **75** (1949): 8.

Fermi, E. Galactic magnetic fields and the origin of cosmic radiation. Astrophys. J. **119** (1954): 1.

Jackson, J. D. Classical electrodynamics, 2nd ed.. John Wiley, 1975.

Malakit, K. Magnetic mirroring effect on the motion of energetic particles in plasma compressions. M.Sc. Thesis. Chulalongkorn University, 2002.

Matthaeus, W. H., Goldstein, M. L., and Roberts, D. A. Evidence for the presence of quasi-two-dimensional nearly incompressible fluctuations in the solar wind. J. Geophys. Res. **95** (1990): 20,673.

Matthaeus, W. H., Gray, P. C., Pontius, D. H., and Bieber, J. W. Spatial Structure and Field-line Diffusion in Transverse Magnetic Turbulence. Phys. Rev. Lett. **75** (1995): 2136.

Meechai, J.Trapping boundary of turbulent magnetic field lines. Senior Project. Chulalongkorn University, 2004.

Parker, E. N. Origin and dynamics of cosmic rays. Phys. Rev. **109** (1958): 4.

Parks, G. K. Physics of space plasmas: An introduction. Washington: Addison-Wesley Publishing Company, 1991.

Press, W. H., Flannery, B. P., Teukolsky, S. A., and Vetterling, W. T. Numerical Recipes. in C. Cambridge University Press, 1988.

Ruffolo, D., Matthaeus, W. H., and Chuychai, P. Trapping of Solar Energetic Particles by Small-Scale Topology of Solar Wind Turbulence. Astrophys. J. Lett. **597** (2003): 169.

Ruffolo, D., Matthaeus, W. H., and Chuychai, P. Seperation of magnetic field lines in two-component turbulence. Astrophys. J. Lett. **614** (2004): 420-434.

Terasawa, T. Energy spectrum and pitch angle distribution of particles reflected by MHD shock waves of fast mode. Planet. Space Sci. **27** (1979): 193-201.

Vitae

Name: Mr. Peera Pongkitiwanichkul

Born: August 28th, 1980 in Bangkok, Thailand

Farther: Mr. Sakol Pongkitiwanichkul

Mother: Mrs. Sansanee Pongkitiwanichkul

Education:

2002 Bachelor of Science (Physics),
Mahidol University, Thailand

Conference Presentations:

2004 Pongkitiwanichkul, P. and Ruffolo, D. "Effects of a turbulent magnetic field on the shock drift acceleration of particles at a nearly perpendicular shock." *Proc. 8th Ann. Symp. Computational Sci. and Eng. (Nakornratchasima)* (July 2004): 137.